

Exploring the antimicrobial  
efficacy of silver acetate  
against *Acinetobacter*  
*baumannii* and development of  
an *in vitro* biofilm model

Eden Mannix-Fisher



A thesis submitted in partial fulfilment of the requirements of Nottingham Trent  
University for the degree of Doctor of Philosophy.

August 2021

This work is the intellectual property of the author. You may copy up to 5% of this work for private study, or personal, non-commercial research. Any re-use of the information contained within this document should be fully referenced, quoting the author, title, university, degree level and pagination. Queries or requests for any other use, or if a more substantial copy is required, should be directed in the owner(s) of the Intellectual Property Rights.

## Acknowledgments

This thesis has been a labour of love for not just myself but many other people close to me and I'd like to say thank you here.

Firstly, I'd like to say thank you to my supervisory team, Dr Samantha McLean, Dr Verderio Edwards and Dr Winter, with a special thank you to Sam because she has been a literal pillar of support and guidance. There aren't really words for how grateful I am to her for everything she has helped me with over the past four years, she's been a supervisor, mentor and friend and I look forwards to working with her again.

Secondly I'd like to thank the entirety of the AROM group at NTU who have all in some way helped me to be a better scientist, better presenter, and most often been a listening ear as I struggled and occasionally swore through some portions of my PhD. I'd like to specifically mention Dr Jonathan Thomas for his help with the genome sequencing, Professor Lesley Hoyles for her guidance with presentations and papers and Adam Varney for his nanopore sequencing of my strains.

Special thanks to Hannah Southam for her training in the *Galleria mellonella* model at Sheffield University.

My final word of thanks is to my family, friends and my partner who have all been my rocks. There aren't really words for how much I've appreciated their support over the past four years. All I can say is thank you!

And to my Grandma... I did it

It's the words that count  
(S. Mclean 2017-2021)

# Table of Contents

Acknowledgments.....	3
List of Figures .....	vi
List of Tables .....	viii
List of Abbreviations .....	ix
List of Publications and Presentations .....	x
Abstract .....	xi
1 Introduction.....	1
1.1 The emergence and importance of <i>Acinetobacter baumannii</i> .....	1
1.1.1 The history of <i>Acinetobacter baumannii</i> taxonomy and its importance as a nosocomial pathogen.....	1
1.1.2 Antibiotic resistance in <i>Acinetobacter baumannii</i> .....	2
1.1.2.1 Enzymatic modifications and antibiotic resistance .....	2
1.1.2.2 Alterations to membrane permeability and efflux proteins.....	4
1.1.2.3 Target site alterations that provide antibiotic resistance.....	5
1.2 Biofilm formation in medical settings and methods to research.....	6
1.2.1 Biofilm formation in <i>Acinetobacter baumannii</i> .....	7
1.2.1.1 The role of Csu pili in biofilm formation in <i>Acinetobacter baumannii</i> ..	7
1.2.1.2 The role of biofilm associated protein (Bap) in biofilm formation in <i>Acinetobacter baumannii</i> .....	8
1.2.1.3 The role of outer membrane protein A (OmpA) in biofilm formation in <i>Acinetobacter baumannii</i> .....	8
1.2.1.4 The role of Poly- $\beta$ -(1,6)- <i>N</i> -acetylglucosamine (PNAG) in biofilm formation in <i>Acinetobacter baumannii</i> . .....	9
1.3 The activity and use of silver as an antimicrobial .....	10
1.3.1 The use of silver as an antimicrobial throughout history.....	10
1.3.2 The antimicrobial mechanisms of silver .....	12
1.3.3 Bacterial resistance to silver .....	13
1.4 A critical evaluation of <i>in vitro</i> assays and models used to study biofilm formation on artificial surfaces.....	17

1.4.1	Microtiter plate assays .....	18
1.4.1.1	The 96-well microtiter plate biofilm assay .....	18
1.4.1.2	The Minimum Biofilm Eradication Concentration (MBEC) Device (formerly known as the Calgary Biofilm Device) .....	19
1.4.2	The Modified Robbins Device (MRD).....	22
1.4.3	The Drip Flow Biofilm Reactor®.....	23
1.4.4	Flow cell biofilm models.....	26
1.4.5	The Centre for Disease Control biofilm model .....	28
1.5	Aims of this thesis.....	30
2	Materials and methods .....	31
2.1	Media and compound preparation .....	31
2.1.1	Muller-Hinton agar and broth .....	31
2.1.2	M9 minimal media .....	31
2.1.3	Silver acetate.....	32
2.1.4	Modified Artificial Urine Media .....	32
<b>2.1</b>	.....	<b>33</b>
2.2	Bacterial strains and culture methods of <i>Acinetobacter baumannii</i> .....	33
2.3	Determining colony forming units per millilitre (CFU ml <sup>-1</sup> ) of a culture .....	33
2.4	Growth and viability .....	34
2.4.1	Growth curves in flasks.....	34
2.4.2	Growth curves in the presence of silver acetate.....	34
2.4.3	Viability assays.....	34
2.5	Colony biofilm assay.....	35
2.6	96- and 24- well biofilm assays.....	35
2.6.1	96-well biofilm assay .....	35
2.6.2	24-well biofilm assay in the presence of silver acetate.....	36
2.7	Identification of oxacillinase genes in <i>Acinetobacter baumannii</i> .....	36
2.8	Genome sequencing of <i>Acinetobacter baumannii</i> NCTC 13302 .....	37
2.9	Minimum inhibitory/bactericidal concentration assays.....	38

2.10	<i>Galleria mellonella</i> treatment efficacy experiments .....	40
2.10.1	Inoculum testing of <i>Acinetobacter baumannii</i> .....	40
2.10.2	Toxicity testing of silver acetate .....	43
2.10.3	Treatment of an <i>Acinetobacter baumannii</i> infection with silver acetate ..	43
2.11	Drip Flow Biofilm Reactor Model.....	44
2.11.1	Production of an <i>A. baumannii</i> biofilm.....	44
2.11.2	Analysis of mDFR biofilms .....	45
2.11.2.1	Determination of viability of biofilms grown in the modified Drip Flow Reactor	45
2.11.2.2	Scanning electron microscopy .....	46
3	Biofilm formation capabilities, growth and antibiotic resistance of <i>Acinetobacter baumannii</i> strains resistant to carbapenems .....	48
3.1	Introduction.....	48
3.2	Results .....	51
3.2.1	PCR analysis of the OXA genes .....	51
3.2.2	Growth of <i>Acinetobacter baumannii</i> in different media demonstrates the biosynthetic capacity of this species .....	52
3.2.3	Colony biofilm formation assays show no significant difference in biofilm formation between strains.....	54
3.2.4	96-well biofilm formation assay reveals <i>Acinetobacter baumannii</i> NCTC 13302, 13305 and 12156 are the strongest biofilm producers.....	57
3.2.5	EUCAST disk diffusion assays show that the carbapenem resistant strains have resistance to antibiotics that are effective against type strains .....	58
3.2.6	Genome sequencing of NCTC 13302 .....	60
3.3	Discussion .....	62
4	The <i>in vitro</i> and <i>in vivo</i> antimicrobial activity of silver acetate against <i>Acinetobacter baumannii</i> .....	66
4.1	Introduction.....	66
4.2	Results .....	69
4.2.1	Silver acetate minimum inhibitory/bactericidal concentration assays for several <i>A. baumannii</i> strains shows silver acetate is bactericidal.....	69

4.2.2	Biofilm formation of NCTC 13302 is significantly reduced when exposed to the minimum inhibitory concentration of silver acetate .....	70
4.2.3	The permanence of silver acetate toxicity against exponentially growing <i>Acinetobacter baumannii</i> is concentration dependent.....	72
4.2.4	The <i>Galleria mellonella in vivo</i> model is an excellent model to study the pathogenicity of <i>Acinetobacter baumannii</i> and test the toxicity of silver acetate ...	75
4.2.4.1	<i>Galleria mellonella</i> infected with <i>Acinetobacter baumannii</i> NCTC 13302 at a concentration of $1.7 \times 10^6$ cells per larvae provides a survival rate of 20%	75
4.2.4.2	A range of silver acetate concentrations commonly used in antibiotic therapy shows minimal toxicity to <i>Galleria mellonella</i> .....	77
4.2.4.3	Treatment of <i>Galleria mellonella</i> larvae infected with <i>Acinetobacter baumannii</i> NCTC 13302 with silver acetate increased the survival and health of the larvae	79
4.3	Discussion .....	81
5	The development of a catheter-associated urinary tract infection model with a modified drip flow biofilm reactor® .....	84
5.1	Introduction.....	84
5.2	Results .....	87
5.2.1	Development of a biofilm tubing model .....	87
5.2.2	Preparation of biofilms obtained from the mDFR for characterisation studies	92
5.2.3	Development and testing of clinically relevant media for a urinary catheter infection model .....	94
5.2.3.1	<i>A. baumannii</i> growth in modified Artificial Urine media show significantly lower growth than in Mueller Hinton Broth.....	95
5.2.3.2	<i>A. baumannii</i> biofilm formation is not significantly altered by growth medium	95
5.2.3.3	Minimum inhibitory / bactericidal concentration assays reveal silver acetate to be more effective against <i>A. baumannii</i> grown in modified artificial urine medium compared with Mueller-Hinton broth .....	97

5.2.3.4	Exponentially growing <i>A. baumannii</i> is inhibited by the presence of silver acetate at close to or above the MIC for silver acetate in mAUM .....	98
5.2.3.5	Less biofilm is formed in mAUM than in MHB in response to the presence of silver acetate .....	101
5.2.4	Infection of silicone tubing with <i>Acinetobacter baumannii</i> within the modified Drip Flow Biofilm Reactor .....	103
5.2.4.1	Scanning electron microscopy images of biofilms obtained from mDFR show that biofilms grown in MHB are thicker and more mature than biofilms grown in mAUM	103
5.2.4.2	Live / dead staining and fluorescent imaging indicates that biofilms formed in mAUM may contain more dead cells than those formed in MHB ....	106
5.2.4.3	Viability counts of biofilms obtained from the mDFR reveal there is no significant difference between cells grown in MHB versus mAUM.....	109
5.3	Discussion .....	110
6	Discussion .....	115
7	References .....	118

## List of Figures

Figure 1.1: A timeline for the use of silver between the years 0 – 1800 A.D.....	10
Figure 1.2: The resistance mechanisms of the Sil system found on the plasmid pMGI101 .....	15
Figure 1.3: Minimum Biofilm Eradication Concentration assay plates .....	20
Figure 1.4: Bio-inLine® Biofilm Reactor a version of the Modified Robbins Device .....	22
Figure 1.5: The Drip Flow Biofilm Reactor®.....	24
Figure 1.6: A flow cell biofilm model.....	26
Figure 1.7: The CDC biofilm reactor as available from BioSurface Technologies Corporation.....	28
Figure 2.1: Schematic diagram for layout of 10 µl spots from MIC assay to set up the MBC assay .....	39
Figure 2.2: A healthy <i>Galleria mellonella</i> larva .....	40
Figure 2.3: <i>Galleria mellonella</i> injection methods.....	42
Figure 2.4: Six channel modified Drip Flow Reactor® set up to run with two channels.	44
Figure 3.1 Structure of the β-lactam nuclei of carbapenems versus penicillins (penams). .....	49
Figure 3.2: Growth curves of <i>Acinetobacter baumannii</i> strains in MHB, M9c and M9d show M9d produces the lowest turbidity while MHB produces the highest.....	53
Figure 3.3: Viable counts from colony biofilms show no significant difference between strains.....	56
Figure 3.4: 96-well plate biofilm assays showed variable biofilm formation between strains.....	57
Figure 3.5: Genome comparison between Query Sequence and the Reference Sequence .....	61
Figure 4.1: Melanisation of <i>G. mellonella</i> larvae upon infection.....	68
Figure 4.2: Crystal violet staining and viability of biofilms is reduced in the presence of silver acetate at the MIC indicating less biofilm production .....	71
Figure 4.3: The inhibition of exponentially growing <i>Acinetobacter baumannii</i> is dependent on the concentration of silver acetate.....	73
Figure 4.4: The bactericidal effect of silver acetate on <i>Acinetobacter baumannii</i> is concentration dependent .....	74
Figure 4.5: Exposure of <i>Galleria mellonella</i> larvae to a different concentrations of <i>Acinetobacter baumannii</i> NCTC 13302 causes differing levels of immune response and lethality .....	76

Figure 4.6: A range of medically relevant silver acetate concentrations shows minimal toxicity to <i>Galleria mellonella</i> .....	78
Figure 4.7: Treatment of <i>Galleria mellonella</i> larvae infected with <i>A. baumannii</i> NCTC 13302 with silver acetate reduced lethality and improved overall health of the larvae .	80
Figure 5.1: The glass bladder used to study catheter associated urinary tract infections <i>in vitro</i> .....	85
Figure 5.2: Schematic diagrams of the Drip Flow Biofilm Reactor® .....	87
Figure 5.3: Schematic diagram of modified Drip Flow Biofilm Reactor®.....	88
Figure 5.4: Six channel modified Drip Flow Biofilm Reactor® set up with only one channel .....	89
Figure 5.5: False colour SEM image of <i>Acinetobacter baumannii</i> biofilm .....	90
Figure 5.6: Growth curve in MHB for <i>Acinetobacter baumannii</i> NCTC 13302 .....	92
Figure 5.7: Silicone tubing used for growth of biofilms. ....	93
Figure 5.8: Slicing the silicone tube into 1 mm discs for SEM. ....	94
Figure 5.9: Growth of <i>A. baumannii</i> is reduced in modified Artificial Urine Medium compared with growth in Mueller-Hinton Broth.....	95
Figure 5.10: The inhibition of exponentially growing <i>Acinetobacter baumannii</i> is dependent on the concentration of silver acetate in mAUM .....	99
Figure 5.11: The bactericidal effect of silver acetate on <i>Acinetobacter baumannii</i> in mAUM is concentration dependent .....	100
Figure 5.12: Crystal violet staining, and biofilm viability is reduced in the presence of silver acetate regardless of concentration .....	101
Figure 5.13: Comparison of crystal violet staining and biofilm viability suggests biofilm formation is negatively impacted to a greater degree by silver acetate in mAUM .....	102
Figure 5.14: SEM images of biofilm surface taken at 15 kV .....	104
Figure 5.15: SEM images of biofilm thickness taken at 15 kV .....	105
Figure 5.16: Biofilms formed in MHB and AUM have no statistically significant differences in the percentages of live to dead cells .....	107
Figure 5.17: Live/Dead staining fluorescent microscopy images of <i>A. baumannii</i> recovered from mDFR biofilms grown in MHB (A) and mAUM (B) .....	108
Figure 5.18: Schematic diagram of proposed mDFR CAUTI biofilm model .....	113

## List of Tables

Table 2.1: Components of M9 minimal media from Sigma-Aldrich before the addition of casamino acids/MEM (50X) amino acids. ....	31
Table 2.2: Components of the modified Artificial Urine Media as stated in Liang <i>et. al.</i> (2020) <sup>184</sup> . ....	32
Table 2.3: <i>Acinetobacter baumannii</i> strains used in this study .....	33
Table 2.4: PCR primers used to identify the presence of oxacillinase genes in <i>A. baumannii</i> strains.....	37
Table 2.5: Conversion table of CFU ml <sup>1</sup> to CFU 10 $\mu$ l <sup>-1</sup> .....	41
Table 2.6: Description of physical appearance and therefore, melanisation of larvae for health scoring .....	43
Table 2.7: Fixing procedure for Scanning Electron Microscopy.....	46
Table 3.1: Confirmation of the presence or absence of OXA genes from genomic DNA. ....	51
Table 3.2: Colony biofilm size and appearance after 48-hour incubation on MHA.....	55
Table 3.3: Antibiotic resistance profiles of <i>A. baumannii</i> strains using EUCAST disk diffusions. Red = <i>resistant</i> , green = <i>sensitive</i> , yellow = <i>intermediate sensitivity</i> . ....	59
Table 3.4: Origins of annotated genomes for comparison of biofilm formation genes..	64
Table 4.1 Minimum inhibitory and bactericidal concentrations for silver acetate against a range of <i>A. baumannii</i> strains demonstrates significant antimicrobial activity.....	69
Table 5.1: MIC and MBC results for silver acetate tested in mAUM are lower than MIC and MBC results for MHB .....	97

## List of Abbreviations

Ag <sup>+</sup>	Silver ion
AgNO <sub>3</sub>	Silver nitrate
ANOVA	Analysis of Variance
ATCC	American Type Culture Collection
BAP	Biofilm Associated Protein
CAUTI	Catheter-Associated Urinary Tract Infections
CDC	Centre for Disease Control
CFU mL <sup>-1</sup>	Colony Forming Units Per Millilitre
CLSM	Confocal Laser Scanning Microscopy
DFR	Drip Flow Biofilm Reactor
DNA	Deoxyribonucleic Acid
ESKAPE	<i>Enterococcus faecalis</i> ; <i>Staphylococcus aureus</i> ; <i>Klebsiella pneumoniae</i> ; <i>Acinetobacter baumannii</i> ; <i>Pseudomonas aeruginosa</i> ; <i>Enterobacter</i> sp.
M9c	M9 minimal media with casamino acids
M9d	M9 minimal media with defined amino acids
mAUM	Modified Artificial Urine Media
MBC	Minimum Bactericidal Concentration
MBEC	Minimum Biofilm Eradication Concentration
mDFR	Modified Drip Flow Biofilm Reactor
MDR	Multi-drug Resistant
MFS	Major Facilitator Superfamily
MHA	Mueller-Hinton Agar
MHB	Mueller-Hinton Broth
MIC	Minimum Inhibitory Concentration
MRD	Modified Robbins Device
NCTC	National Collection of Type Cultures
OD	Optical Density
OMP	Outer Membrane Proteins
PBS	Phosphate Buffered Saline
PCR	Polymerase Chain Reaction
RNA	Ribonucleic Acid
RND	Resistance-Nodulation-
rpm	Revolutions Per Minute
SEM	Scanning Electron Microscopy

## List of Publications and Presentations

### Publications

Mannix-Fisher, E and McLean, S. 2021. '**The antimicrobial activity of silver acetate against *Acinetobacter baumannii* in a *Galleria mellonella* infection model**'. PeerJ. DOI 10.7717/peerj.11196

### Conferences and Talks

#### **Microbiology Society Annual Conference 2020: Poster**

'The efficacy of silver acetate as an antimicrobial against carbapenemase producing *Acinetobacter baumannii*'  
(cancelled due to COVID)

#### **6<sup>th</sup> Midlands Molecular Microbiology Meeting 2019: Poster and flash presentation**

'Silver Acetate Treatment of an *Acinetobacter baumannii* infection in the *Galleria mellonella* model'

#### **Science and Technology Annual Research Conference 2018: Poster and Presentation**

'Application of the *Galleria mellonella* model in silver acetate treatment of *Acinetobacter baumannii*'

## Abstract

*Acinetobacter baumannii* is a nosocomial pathogen with a remarkable capacity for antimicrobial resistance. This bacterial species possesses the ability to form biofilms and survive on abiotic surfaces within hospitals, which makes it a common cause of ventilator associated pneumonia, bacteraemia, catheter associated urinary tract infections, and wound and burn infections. As *A. baumannii* can cause catheter associated urinary tract infections via biofilm formation on catheters and silver acetate coated catheters are used commercially for prevention of infection, this thesis aimed to explore first the efficacy of silver acetate as an antimicrobial, and then to develop a modified Drip Flow Biofilm Reactor® tubing model to mimic biofilm formation within a catheter.

*A. baumannii* NCTC 13302 was first determined to be the best biofilm forming strain out of the five isolates in the study, and it contained the OXA-24-like gene that provides carbapenem resistance. This strain was then utilised to test the minimum inhibitory concentration of silver acetate, its biofilm prevention capabilities, and its growth inhibitory effects. This provided raw data which did not exist for silver acetate against *A. baumannii* as there were no other studies stating the antimicrobial activity of silver acetate against this species. A further test of *in vivo* toxicity of silver acetate was carried out using *Galleria mellonella* larvae which validated the low toxicity of the silver salt. A further test where the larvae were infected with *A. baumannii* and then treated with silver acetate showed a significant increase in the survival of the larvae, showing the effectiveness of silver acetate as a treatment.

The modified Drip Flow Biofilm Reactor® tubing model was developed first with *A. baumannii* NCTC 13302 in Mueller-Hinton Broth and subsequently with a modified Artificial Urine Media to move the model towards an imitation of a catheter associated urinary tract infection. During development, it was found that the most efficient way to assess biofilms grown within silicone tubing for five days was to run two samples in parallel and assess viability with cell counts and live/dead staining and to image with Scanning Electron Microscopy. The model developed herein will allow the study of *A. baumannii* biofilm formation on catheter tubing in conditions that begin to mimic the clinical environment. Future developments will focus on testing the antimicrobial activity of silver acetate coated catheter tubing against *A. baumannii*, and adaptation of the model to imitate bladder mechanics with a catheter fitted, which would provide a novel model to better study prevention of catheter associated urinary tract infections.

# 1 Introduction

## 1.1 The emergence and importance of *Acinetobacter baumannii*

### 1.1.1 The history of *Acinetobacter baumannii* taxonomy and its importance as a nosocomial pathogen

*Acinetobacter baumannii* is a Gram negative, aerobic bacterium that commonly causes nosocomial infections<sup>1,2</sup> and can acquire resistance mechanisms via horizontal gene transfer and survive on surfaces in hospital environments<sup>2,3</sup>. *A. baumannii* was first defined as a separate taxonomic group in 1986 when DNA relatedness and biochemical tests determined it to be too dissimilar to *Acinetobacter calcoaceticus* to remain part of this species and therefore a new species within the *Acinetobacter* genus was proposed<sup>4</sup>. Since then, *A. baumannii* has rapidly grown in importance due to its multidrug resistant nature and its common occurrence in hospital infections<sup>5</sup>.

One of the most well-known causes of an *A. baumannii* infection outside of a hospital situation, is war conflict<sup>6</sup>. In 2003 the Operation Iraqi Freedom conflict began, and following this there was an increase in *A. baumannii* infections<sup>7</sup>. The incidence and multi-drug resistant (MDR) nature of these infections earned *A. baumannii* the nickname 'Iraqibacter'<sup>6</sup>, but there are other examples of *A. baumannii* infections facilitated by war trauma which allows the justification that war trauma is a risk factor. The East Timorese conflict in 2006 saw 19 *Acinetobacter* sp. isolated from gunshot wounds<sup>8</sup> and there is a description of *A. baumannii* infections during the Vietnam war where *A. baumannii* is listed under a previous name as part of the *Mimeae-Herellae-Bacterium-Alcaligenes* group<sup>9,10</sup>. In all examples, the majority of the infections caused are skin and soft tissue infections, facilitated by the fact that the majority of patients are severely wounded military personnel and civilians with open wounds<sup>7,8,10,11</sup>.

*A. baumannii* is now listed as part of the "ESKAPE" pathogens group. "ESKAPE" is the acronym given to the group of six MDR pathogens that are the main causes of nosocomial infections across the globe, *Enterococcus faecalis*, *Staphylococcus aureus*, *Klebsiella pneumoniae*, *Acinetobacter baumannii*, *Pseudomonas aeruginosa* and the *Enterobacter* species<sup>12,13</sup>. *A. baumannii* most commonly causes pneumonia, bacteraemia, infection of wounds and urinary tract infections<sup>2,14,15</sup>, and due to the MDR

nature, with some strains resistant to carbapenems, some strains have been classed as Category 1 critical by the World Health Organisation determining their urgent need for antibiotic research<sup>16</sup>.

For a bacterium to be a successful pathogen it must possess a series of virulence factors that allow it to survive its environment within and outside of a host. As well as survival, it must be able to acquire nutrients for growth and protect itself from external threats such as antibiotics, other organisms, and the host immune system. *A. baumannii* possesses a wide range of virulence factors that allow it to cause infections in nosocomial environments<sup>17-19</sup>. These virulence factors include the presence of efflux pumps, siderophores for iron acquisition, lipopolysaccharides, haemolytic factors and desiccation resistance, but two of the most important factors in nosocomial environments would be antimicrobial resistance and biofilm formation as these allow *A. baumannii* to cause persistent and difficult to treat infections<sup>18,20,21</sup>.

### **1.1.2 Antibiotic resistance in *Acinetobacter baumannii***

*A. baumannii* is commonly said to have a remarkable capacity for genetic plasticity due to the ability of the bacteria to undergo genetic recombination and rearrangements along with a high number of insertion sequences<sup>2,22</sup>. Due to this ability, *A. baumannii* is known to easily acquire resistance to antibiotics<sup>2</sup>. Resistance mechanisms can be broadly broken down into five major categories, prevention of uptake, modification of the target, modification of the drug, efflux and metabolic by-pass<sup>23</sup>. The following sections will provide a brief overview of some of these mechanisms, focusing on the enzymatic modifications of the drug, alterations to membrane permeability / efflux, and genetic modification of the drug target with some examples, however this topic is vast and several reviews are available to explore this topic in depth.<sup>2,12,23</sup>

#### **1.1.2.1 Enzymatic modifications and antibiotic resistance**

One of the methods that *A. baumannii* uses to thwart antibiotic activity is via the production of enzymes that can modify or destroy the antibiotic<sup>2,23,24</sup>. Of all the enzymatic reactions that modify antibiotics,  $\beta$ -lactamases are the most widely researched in terms of antimicrobial resistance<sup>12</sup>. These enzymes provide resistance to  $\beta$ -lactam antibiotics, which mimic the shape of peptidoglycan and disrupt the synthesis of the bacterial cell wall<sup>25</sup>, by hydrolysing the  $\beta$ -lactam ring present in the antibiotic<sup>12,23</sup>.  $\beta$ -lactamase

enzymes provide resistance to penicillins, cephalosporins, monobactams and carbapenems<sup>12,23,26</sup> and are most commonly classified by the Ambler classification scheme based on their amino acid similarity, into one of four classes: A-D.<sup>12</sup>

*A. baumannii*, a very genetically mobile strain<sup>2</sup>, can readily acquire Class A extended-spectrum  $\beta$ -lactamases and Class B metallo- $\beta$ -lactamases which are often encoded on mobile genetic elements such as plasmids, transposons and integrons<sup>26,27</sup>, however *A. baumannii* contains chromosomally encoded Class C cephalosporinases<sup>28</sup>. The Class D oxacillinases are of high importance in *A. baumannii* and can be intrinsically encoded on the chromosome<sup>29</sup> or exist on plasmids providing plasmid-mediated resistance<sup>30</sup>. These enzymes provide carbapenem resistance in *A. baumannii*<sup>29-31</sup> which is a critical issue for tackling antibiotic resistance<sup>16</sup> and will be further discussed in chapter three.

Aminoglycoside modifying enzymes are another set of enzymes common in *A. baumannii*<sup>2,23</sup>. These enzymes can be divided into three categories, *N*-acetyltransferases (AAC enzymes), *O*-phosphotransferases (APH enzymes) and *O*-nucleotidyltransferases (ANT enzymes), based on the modification carried out on the antibiotic<sup>23,32,33</sup>. Aminoglycosides inhibit protein synthesis by interfering with the 30s ribosomal subunit and consequently interrupting protein elongation<sup>23</sup>. The acylation, phosphorylation or adenylation of these antibiotics reduces the affinity of the antibiotic to its ribosomal target<sup>23,32-34</sup>. There are a large number of aminoglycoside modifying enzymes within each class, reviewed in Kyriakidis *et. al.* (2021)<sup>23</sup> and the nomenclature usually denotes the position on the antibiotic where the enzyme exerts its effect<sup>33</sup> and their genes are easily passed amongst bacterial species via their presence on mobile genetic elements<sup>23,35</sup>.

$\beta$ -lactamases and aminoglycoside modifying enzymes are two examples of antibiotic modifications by enzymes that cause antibiotic resistance, however more genes can be found in *A. baumannii* that confer resistance to several other antibiotics including tetracyclines, amphenicols, fosfomycin and sulphonamides<sup>2,23</sup>. The most alarming aspect of enzyme mediated resistance is that many of these genes are transferable and modification of an antibiotic will render it ineffective.

### 1.1.2.2 Alterations to membrane permeability and efflux proteins

Antibiotics can only work if they reach the target molecule. In response to antibiotic pressure, downregulation of membrane porins and over expression of efflux proteins can reduce the concentration of antibiotic accumulated within the cell<sup>36</sup>. In Gram negative bacteria, outer membrane proteins (OMPs) are proteins that form a channel from the cytoplasm, through the periplasmic space and to the outside of the cell<sup>36</sup>. OmpA is the major porin in *A. baumannii* and has many functions including slow, non-specific transport of molecules across the cell membrane<sup>5,37</sup>. OmpA, along with CarO, the carbapenem resistance associated OMP, have both been demonstrated to have roles in antibiotic resistance, as loss of these porins can bring about resistance phenotypes<sup>36,38,39</sup>. The importance of porins can be emphasised by the fact that there have been outbreaks caused by carbapenem resistant *A. baumannii*, which have become resistant due to loss of porins from the cell<sup>2</sup>.

In tandem with decreased import, efflux proteins work to remove antibiotics and other molecules from the cell and periplasmic space as they accumulate<sup>2,23,36</sup>. There are two types of efflux pumps, ATP-dependent efflux pumps and proton-motive force efflux pumps<sup>32,36,40</sup>. The proton motive force group can be further divided into the Major Facilitator Superfamily (MFS), Resistance-Nodulation-Division (RND), Small Multidrug Resistance, Multidrug and Toxic Compound Extrusion and Drug/Metabolite Transporter superfamilies<sup>32,36,41</sup>.

In *A. baumannii* the main efflux pumps for antibiotic resistance fall into the proton motive force superfamilies MFS and RND<sup>32,36</sup>. MFS pumps are typically functional against specific types of antibiotic<sup>36</sup>, for example Tet(A). Tet(A) is an MFS pump that facilitates the movement of tetracycline out of the cytoplasm and into the periplasmic space where non-specific RND pumps can facilitate movement of the antibiotic out of the cell, providing *A. baumannii* with tetracycline resistance<sup>2,23,42</sup>. This MFS pump and others like it such as Tet(B), are concerning due to the potential to spread resistance, as these MFS genes can be shared via horizontal gene transfer on mobile genetic elements<sup>42</sup>.

RND pumps are potentially the most concerning efflux pump family in *A. baumannii* as they can be broad spectrum and provide bacteria with resistance to multiple types of antibiotic<sup>36</sup>. An example of one such efflux pump is the AdeABC complex, which is the most studied RND pump in *A. baumannii*<sup>43</sup>. This pump is composed of three parts, AdeA, a membrane facilitator protein, AdeB, a multidrug transporter and AdeC, an outer

membrane protein and the whole system is regulated by the two-component system AdeRS<sup>32,44</sup>. Overexpression of this pump can be caused by point mutations (single or multiple) within the *adeR* and *adeS* genes<sup>44</sup>, and this overexpression can cause resistance to  $\beta$ -lactams<sup>45</sup>, fluoroquinolones<sup>44</sup>, aminoglycosides<sup>32</sup>, and other classes of antibiotics<sup>23,36,45</sup>.

There are a wide array of porins and efflux pumps that provide antibiotic resistance in *A. baumannii*, and they have been reviewed many times throughout the literature such as in Vila, Martí and Sánchez-Céspedes (2007)<sup>36</sup>, Almasaudi (2018)<sup>43</sup> and Kyriakidis (2021)<sup>23</sup>. Often, the presence of an efflux pump and downregulation of a porin is not enough to provide high-level resistance, however this can be provided with the addition of other mechanisms such as enzymatic modifications of the antibiotic or alteration of the drug target<sup>2,23</sup>.

### 1.1.2.3 Target site alterations that provide antibiotic resistance

Antibiotic effects are carried out by binding to and/or blocking the activity of a specific molecule<sup>2,23</sup>. A third method of resistance against antibiotics is changing of the target molecule, often by mutation, but also by the production of enzymes and proteins<sup>2,23</sup>. Resistance to quinolones and polymyxins are good examples of this method of antibiotic resistance in *A. baumannii* as for both of these, the main method relies on mutation<sup>46-48</sup>.

Quinolone antibiotics target DNA gyrase and topoisomerase IV and halt DNA replication by altering the enzymes so they cannot carry out their tension relieving functions during DNA replication, this causes DNA strand breakage as a result of the strain<sup>49</sup>. The main mechanism that *A. baumannii* uses to resist quinolone activity is via direct mutations to the antibiotic targets<sup>49</sup>. In this case there are specific substitutions in the Quinolone Resistance-Determining Regions of *gyrA* (encoding DNA gyrase) and *parC* (encoding topoisomerase IV), which prevents the binding of quinolones to these enzymes<sup>23,46</sup>.

Another example of a target site alteration is the mechanism of polymyxin resistance. Polymyxin resistance and therefore colistin resistance in *A. baumannii* is extremely concerning as colistin is a last resort antibiotic to treat MDR *A. baumannii* infections<sup>48</sup>. To cause resistance to colistin, a mutation in the *pmrA-pmrB* two-component system has been implicated in causing the bacterial membrane to become more positively charged<sup>47,48</sup>. A mutation in *pmrB* (the sensor kinase) causes its overexpression which

leads to the production of phosphoethanolamine<sup>48</sup> and the overexpression of *naxD* which leads to the production of galactosamine<sup>47</sup>. Phosphoethanolamine and galactosamine are positively charged molecules that bind to the Lipid A component of the lipopolysaccharide and change the surface charge of the membrane to positive, causing the repulsion of cationic polymyxins<sup>47,48</sup>.

As target changing mutations are usually spontaneous, the scope for resistance is vast. This is due to the fact that these changes can cause overexpression, downregulation and amino acid substitutions that change the binding site of the molecule<sup>23</sup> and if the mutation is favourable, the bacteria will not correct it.

*A. baumannii* can carry multiple mechanisms of resistance to antibiotics and this has given rise to multi-drug resistant as well as pan- and extensively-drug resistant strains<sup>50,51</sup>. Extensively-drug resistant is the term given to strains that are resistant to all standard antibiotics excluding colistin or tigecycline, while pan-drug resistant strains are resistant to all known antibiotics<sup>50</sup>. Many of these mechanisms of resistance are present on mobile genetic elements and this is a particular concern with regards to biofilms, which not only provide bacteria with protection from external toxins, but also provide a breeding ground for the spread of antibiotic resistance.

## **1.2 Biofilm formation in medical settings and methods to research**

Bacteria were initially thought to exist predominantly as single-celled, free-floating, 'planktonic' cells, but this is not the case. The first published observation of a biofilm was recorded in 1933 referencing the growth of bacteria as a community underwater<sup>52</sup>. Nowadays, it is common knowledge within the scientific community that bacteria exist as planktonic cells and as sessile cells, where the bacteria are aggregated and connected together within a biofilm and protected via an extracellular matrix<sup>21,53</sup>. Biofilms can be formed when bacteria adhere to a surface in favourable conditions, and this surface can be abiotic or biotic in origin<sup>54</sup>. However, bacteria may not need a surface to form a biofilm and have been known to form biofilms at air-liquid interfaces<sup>55</sup>.

The formation of a stable biofilm has several stages, adhesion to a surface, aggregation of bacteria, maturation and maintenance of a the biofilm and finally dispersion<sup>53</sup>. Within a mature biofilm, bacteria will differentiate to carry out particular functions determined by

the number of cells around them<sup>53</sup>. To understand the volume of cells, bacteria carry out quorum-sensing, which is a form of intercellular communication based on recognising the amount of autoinducer molecules in the surrounding environment<sup>56,57</sup>. Autoinducers are molecules produced by bacteria that can freely leave and enter the cell and bind to receptors within the cytoplasm and membrane to trigger the production of more autoinducer in a positive feedback loop<sup>57</sup>. In *A. baumannii*, the quorum-sensing molecule produced is an acyl homoserine lactone, 3-hydroxy-C<sub>12</sub>-homoserine lactone<sup>58</sup> and it is required for biofilm formation and virulence of the organism<sup>58,59</sup>.

Biofilms are responsible for approximately 65-80% of human clinical infections, particularly respiratory infections or infections caused by the presence of an indwelling medical devices<sup>52,53,60</sup>. *A. baumannii* readily forms biofilms on abiotic and biotic surfaces<sup>55</sup>, and this ability is now recognised as a virulence factor<sup>1,18-20</sup>. The formation of biofilm on abiotic surfaces allows *A. baumannii* to cause device associated infections and persist in place<sup>18</sup>. Examples of infections relating to medical devices include ventilator associated pneumonia, which can be caused by the presence of an endotracheal tube<sup>53,60,61</sup>, and catheter associated urinary tract infections, which are caused by the presence of an indwelling urinary catheter<sup>15,62-64</sup>.

### **1.2.1 Biofilm formation in *Acinetobacter baumannii***

Biofilm formation in *A. baumannii* is a controlled process relying on various genes, the most important of which being those that control the production of the Csu pili, biofilm associated protein (BAP), outer membrane protein A (OmpA) and Poly- $\beta$ -(1,6)-N-acetylglucosamine (PNAG)<sup>20</sup>. Without these mechanisms, biofilm production tends to be severely diminished or cease altogether, affecting the virulence of *A. baumannii* strains<sup>65-68</sup>.

#### **1.2.1.1 The role of Csu pili in biofilm formation in *Acinetobacter baumannii***

Biofilm formation on medical devices by *A. baumannii* is a troublesome complication in nosocomial environments, but to form a biofilm, bacterial cells must first adhere to the surface of the device<sup>69</sup>. To facilitate adhesion to abiotic surfaces, *A. baumannii* have cell-surface appendages known as pili<sup>18,65,70</sup>.

The most important pili for biofilm formation on abiotic surfaces is a long cell extension that acts as an anchor to other cells and surfaces<sup>70,71</sup>. Multiple studies in the early 2000s identified this cell appendage as being a pili encoded by the *csuA/BABCDE* gene locus and then proved the importance of the Csu pili by producing mutants with defects within the gene locus<sup>55,72</sup>. These mutants had significantly reduced or no attachment capabilities on abiotic surfaces such as glass, and intracellular attachment was significantly reduced, reducing biofilm formation<sup>55,65,72</sup>. Despite reduced attachment on abiotic surfaces, removal of the *csu* operon did not affect attachment to biotic cells as biotic attachment is facilitated by different mechanisms such as the presence of OmpA and other pili<sup>64,65,70</sup>. Therefore, although biotic attachment is not affected, the virulence of *A. baumannii* lacking this gene locus, is likely to be reduced as these cells will poorly adhere to abiotic materials such as plastic and glass within a nosocomial environment and are more likely to be removed.

#### **1.2.1.2 The role of biofilm associated protein (Bap) in biofilm formation in *Acinetobacter baumannii***

The biofilm associated protein (Bap) is a largely conserved, cell-surface, protein in *A. baumannii* that is also present in other organisms<sup>66,71,73,74</sup>. This protein was initially found in *Staphylococcus aureus* and was shown to be involved in adhesion between, and accumulation of cells as well as having a role in the attachment of bacteria to abiotic surfaces<sup>75</sup>. A homologue of Bap was found in *A. baumannii* and the 854 kDa protein had similar characteristics, such as the repeating molecules, large size and role in adhesion and biofilm formation<sup>66</sup>. Bap has proven to be highly important to biofilm formation in both dynamic and static conditions, as biofilms formed by Bap negative strains are thinner and have less biovolume than Bap positive strains<sup>66,74</sup>. Bap does not, however, appear to be involved in primary attachment to abiotic surfaces, which leads to the conclusion that the major role of Bap in biofilm formation is intercellular attachment between cells, potentially facilitated by protein-protein binding of Bap to aid in the maturation of the biofilm<sup>66,76</sup>.

#### **1.2.1.3 The role of outer membrane protein A (OmpA) in biofilm formation in *Acinetobacter baumannii***

*A. baumannii* cannot form biofilms on abiotic surfaces without the presence of the Csu pili, but these cell appendages are not required for attachment to biotic surfaces<sup>71,72</sup>.

Attachment to, and therefore biofilm formation on biotic surfaces such as human lung epithelial cells relies upon the presence of the outer membrane protein A (OmpA)<sup>20,67</sup>. OmpA is one of the many outer membrane protein channels present in *A. baumannii* but it is one of the most important as it is the main porin responsible for the non-specific transport of molecules across the membrane<sup>37</sup>, and as such the *ompA* gene is highly conserved in *A. baumannii*<sup>77</sup>.

While the main role of OmpA is slow, non-specific diffusion of molecules across the cell membrane, it also has adherence capabilities that affect biofilm formation<sup>5,37</sup>. OmpA plays a critical role in attachment to biotic surfaces as it binds to fibronectin present in the extracellular matrix of human epithelial cells. When OmpA is not present, or fibronectin is blocked by antibodies, bacterial attachment to epithelial cells is negligible<sup>67,78</sup>. Yet biotic attachment is not the only function OmpA has a role in with regards to biofilm formation. It has been observed that OmpA deficient mutants have reduced biofilm forming ability on plastic and electron microscopy revealed that these cells were lacking in the long filamentous Csu pili the parental and OmpA complemented strains had. The filaments were present, but detached from the cell and clustered on the plastic<sup>67</sup>. This was most likely due to the lack of OmpA causing membrane destabilisation, as amino acids present in OmpA, non-covalently bind to components of peptidoglycan in the cell membrane. OmpA is not essential for bacterial survival but without it, the bacterial surface loses its integrity and its ability to correctly anchor the Csu pili essential for biofilm formation on plastic<sup>67,79</sup>.

#### **1.2.1.4 The role of Poly- $\beta$ -(1,6)-*N*-acetylglucosamine (PNAG) in biofilm formation in *Acinetobacter baumannii*.**

Within a biofilm, bacteria are bound to each other and the surface via various surface molecules and a polysaccharide matrix. This polymeric matrix binds the biofilm together as well as protecting bacteria from harsh environmental conditions such as desiccation as it may aid the bacteria in keeping water inside the cell<sup>18,21</sup>. A key component of the extracellular matrix is poly- $\beta$ -(1,6)-*N*-acetylglucosamine (PNAG), which has been found in both Gram negative and Gram positive bacterial species with roles in adherence and biofilm formation<sup>68,80,81</sup>. In *A. baumannii*, PNAG is encoded by the *pgaABCD* locus and has crucial roles in biofilm formation and attachment to cells and surfaces<sup>68,82</sup>. The importance of PNAG in biofilm formation was highlighted when strains deficient in the *pgaABCD* locus produced biofilms that had significantly less biomass and thickness in

comparison to the parental or *pgaABCD* complemented strains<sup>68</sup>. It is thought that PNAG aids *A. baumannii* in the presentation of other surface molecules and the maintenance of biofilm integrity under shear forces, as PNAG is highly adhered to the cell surface, but is not readily accessible to other molecules<sup>82</sup>

### 1.3 The activity and use of silver as an antimicrobial

#### 1.3.1 The use of silver as an antimicrobial throughout history

Silver has been known since around 4000 B.C., but the first medical use was reported around 1000 B.C.<sup>83,84</sup>. Initially, silver was forged into vessels that prevented the spoilage of liquids for consumption, but its use progressed over time to the treatment of ulcers and wounds by topical application and ingestion<sup>83</sup>. The use of silver both medically and otherwise increased throughout the *Anno Domini* period especially with the discovery of silver nitrate ( $\text{AgNO}_3$ ) in the early 700s<sup>83-85</sup>, which was perhaps due to its liquid state making it easier to utilise (Figure 1.1).

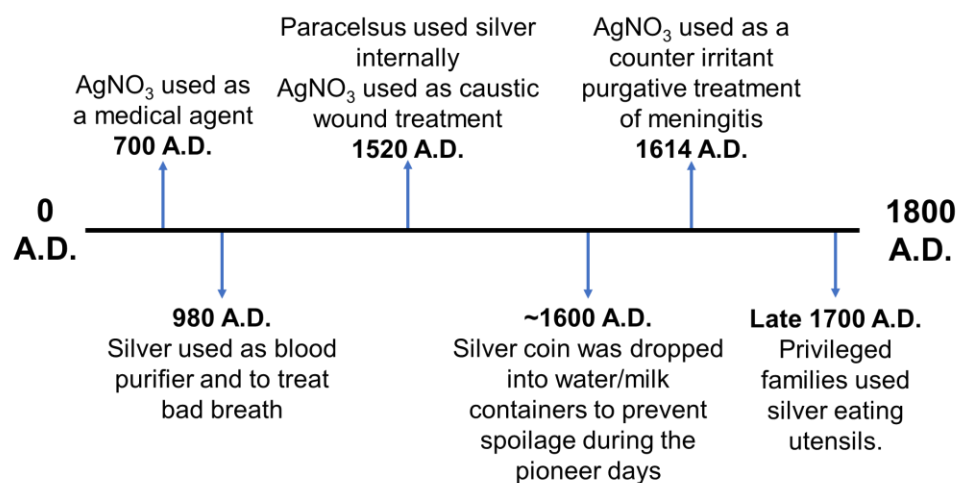


**Figure 1.1: A timeline for the use of silver between the years 0 – 1800 A.D.**

Silver has been used in different formats over time and for various purposes, from the treatment of wounds to use as a spoon or fork.<sup>83</sup>

By the 1800's silver and silver nitrate were accepted for use in the preservation of drinks and treatment of wounds, ulcers and a wide variety of maladies<sup>83,85</sup>. In the mid 1800's,

several pioneering scientists increased the number of ways silver was used<sup>83</sup>. Doctor J. Marion Sims, utilised silver wire to repair vesico-vaginal fistulas in the 1850's<sup>86</sup> and Doctor C.S.F. Crede applied 2% solutions of AgNO<sub>3</sub> to the eyes of new-borns to treat gonorrhoeal ophthalmia neonatorum, a practice that continued well into the 1980's<sup>84,87</sup>. In the late 1800's to early 1900's, W.S. Halsted used silver foil to improve post-operative healing<sup>83,85,88</sup>, and A.L. Roe used colloidal silver to treat many different infections of the eyes, including ulcers<sup>89</sup>.

With more doctors and scientists advocating the use of silver medically, thousands of people either ingested, or were injected with silver between 1900 and 1940, despite the fact that high doses of silver could cause convulsions, gastrointestinal problems and even death<sup>83</sup>. Silver ions have a low toxicity to humans<sup>90</sup>, however, repeated exposure and prolonged use will cause a build-up of silver deposits in the skin, nails, kidney, liver, eyes, mucosal membranes and the gums<sup>83-85,91</sup>. The deposition of silver in these areas will cause a blue/grey, irreversible discoloration to appear in the area, and it was this condition that brought about the term 'blue bloods' when referring to wealthy individuals, as privileged families that used silver utensils would commonly develop argyria<sup>83</sup>.

In the early 1900's modern antimicrobial chemotherapy began when Paul Ehrlich proposed the concept of selective toxicity where agents would cause minimal damage to the patient while still remaining effective against the causative organism of the infection<sup>92</sup>. This then led to the discovery and use of sulphonamides and penicillin<sup>85</sup>. The discovery of sulphonamides led to the production of silver sulphadiazine which was created in the 1960's by reacting sulphadiazine, a weak acid, with silver nitrate<sup>93</sup>. Silver sulphadiazine was found to be an effective treatment of burn wounds infected with *Pseudomonas aeruginosa* and was also a safer alternative to silver nitrate due to the insoluble nature of silver sulphadiazine versus silver nitrate<sup>93</sup>. Further studies against a wider range of Gram negative and Gram positive species proved the efficacy of silver sulphadiazine and it remains as a burns treatment to this day<sup>94-96</sup>. As medicine progressed and less harmful antimicrobials were discovered, the use of silver decreased over the latter half of the 20<sup>th</sup> century. The threat of antimicrobial resistance has brought a resurgence of silver antimicrobials back to the forefront of medicine, however, with the advancement of technology, silver nanoparticles are now being created that appear to be more effective in healing burns<sup>96,97</sup>.

Silver nanoparticles are silver clusters ranging from 1 – 100 nm and the interest in their use and efficacy has increased during the 21<sup>st</sup> century due to antibiotic resistance<sup>98</sup>.

There are multiple ways to synthesise silver nanoparticles using physical, chemical and biological methods. Of these three, biological methods using plant extracts, bacterial cell supernatants and microorganisms extracted from soil containing heavy metals are more favourable as they are cheap and eco-friendly. Siddiqi *et. al.* (2018)<sup>99</sup> provides a comprehensive review of the methods of synthesis and characteristics of silver nanoparticles available at that time. Due to size of silver nanoparticles, they have a large surface area to volume ratio which improves efficacy, making them potent antimicrobials with lower toxicity than silver salts<sup>98</sup>

The particles were first used as a slow release coating and were found to be effective against *Escherichia coli* in the early 2000's<sup>100,101</sup>. However, while silver nanoparticles are used in many consumer products, including toys, toothpaste and deodorants<sup>102</sup>, and are also available as wound dressings<sup>98</sup>, silver nanoparticles are not universally used in medicine<sup>99</sup>. The mixed reception to silver nanoparticles is due their extreme variation<sup>99</sup>, from their shape, size, stability and toxicity due to the many ways they can be made and the long term effects are still largely unknown<sup>97-99</sup>. Multiple reports state the toxicity of silver nanoparticles on cell lines and animal models, as they can cause the generation of reactive oxygen species and have cytotoxic and genotoxic effects on cells at high concentrations<sup>103,104</sup>. Due to the variation in the nanoparticles, the testing methods and the lack of human studies, it is impossible to form a definitive conclusion about the safety of nanoparticles in medicine, and their continued use in commercial products could cause problems such as silver resistance in bacteria before these particles are approved for medicinal use<sup>98,103,104</sup>.

### **1.3.2 The antimicrobial mechanisms of silver**

Silver has been used in many forms throughout history, but it is inert in its solid, elemental form, only having an antimicrobial effect after it dissociates into silver ions ( $\text{Ag}^+$ ) within fluids<sup>90</sup>. In its ionic form, silver has a strong affinity for electron donor groups that contain sulphur, nitrogen and oxygen and binding to sulphhydryl groups within bacterial cells is a critical part of its antimicrobial activity<sup>90,105</sup>.

To have an antimicrobial effect,  $\text{Ag}^+$  must first bind to the bacterial cytosolic membrane of Gram-positive and Gram-negative bacteria and enter the cell.  $\text{Ag}^+$  will bind to disulphide, amino, imidazole, carbonyl and phosphate residues present in cell surface receptors and cross the cell membrane via endocytosis. However, binding to certain cell

receptors and enzymes will cause denaturation of the cell membrane, impairing the bacterial ability to transport key metabolites and nutrients across it<sup>90</sup>. Once within the cell, Ag<sup>+</sup> will bind to proteins, polysaccharides, DNA and RNA, impairing bacterial cell metabolism and replication<sup>90,106,107</sup>. The effects on cell metabolism are highly dependent on the interaction of silver ions with thiol groups within enzymes<sup>84,105</sup>.

One example of Ag<sup>+</sup> action on metabolism is the interaction of the ion with enzymes within the dehydratase family. This family of enzymes have key anabolic and catabolic roles in metabolism, but also contain iron-sulphur clusters. Ag<sup>+</sup> targets these Fe-S clusters and will displace the iron, degrading the catalytic cluster past the point of repair via reduction or replacement of the metal, which will block metabolism at various points due to non-functional enzymes<sup>108</sup>. The release of iron from the Fe-S clusters causes an increase in free iron, affecting iron homeostasis within the cell and increasing the concentration of hydroxyl radicals. Ag<sup>+</sup> can also cause an increase in superoxides via interaction with cytochrome *bd* an enzyme within the electron transport chain<sup>109</sup>. The production of free radicals will increase the production of reactive oxygen species within the cell which can cause further damage to cellular components and genetic material<sup>105,109</sup>.

Whilst production of reactive oxygen species will damage the genetic material of the bacterial cell, Ag<sup>+</sup> can also interact directly with DNA and RNA to block replication and therefore growth of bacterial cells<sup>90</sup>. The interaction of Ag<sup>+</sup> with DNA and RNA is due to the silver's affinity with nitrogen and oxygen as Ag<sup>+</sup> will bind to the N7 atoms of guanine and adenine, and therefore the GC and AT base pairs of DNA. In RNA, Ag<sup>+</sup> does not bind to adenine and will bind to only the N7 and then O6 atoms of guanine<sup>110</sup>.

Given all the above antimicrobial mechanisms of silver, the metal can correctly be described as oligodynamic and resistance to silver is uncommon<sup>105</sup>. Due to the wide ranging effects of silver within the bacterial cell, resistance mechanisms would need to revolve around excluding or removing silver from the cells<sup>111</sup>.

### **1.3.3 Bacterial resistance to silver**

Silver is known as a biocide due to its oligodynamic nature, which means that bacterial resistance is rare<sup>105,112</sup> however, resistance to silver in bacteria has been known since the 1970's when a strain of *Salmonella enterica* subspecies Typhimurium killed three

people and closed down a burns unit in Massachusetts<sup>113</sup>. The strain was resistant to multiple antibiotics as well as silver and mercuric chloride and was found to contain a conjugative plasmid pMG101 that could be transferred to other bacteria, causing spread of the resistance phenotype<sup>113,114</sup>. Following on from this, another study isolated strains of *Klebsiella pneumoniae*, *Enterobacter cloacae*, *E. coli*, *Proteus mirabilis* and *Citrobacter freundii* that were resistant to silver after being treated with silver sulphadiazine<sup>115</sup>.

Silver resistance was not only found in clinical strains but also strains isolated from the environment such as *Pseudomonas stutzeri* AG259 and *A. baumannii* BL88, which are both environmental isolates discovered in the 1980's and 1990's<sup>116,117</sup>. In both strains, the resistance to silver was caused by a plasmid (pKK1 in *P. stutzeri* and pUPI199 in *A. baumannii*) that resulted in the accumulation of silver ions within the bacterial cell, but conferred resistance<sup>116–118</sup>. The *A. baumannii* pUPI199 plasmid could be transferred via conjugation to *E. coli* and it caused the appearance of a silver resistance phenotype, although the growth of these cells was significantly slowed due to the new metabolic burden<sup>117</sup>. With the appearance of silver resistance, studies were then carried out to determine how the resistance occurred and what the mechanisms were.

Bacteria have the ability to gain resistance phenotypes via endogenous (mutational changes) and exogenous (transfer of genetic material) means<sup>112</sup>. The most common endogenous method for acquisition of silver resistance has been shown to be a loss of outer membrane porins<sup>119</sup>, however *A. baumannii* is not currently known to have any endogenous mechanisms of resistance to silver<sup>120</sup>. In *E. coli* the loss of some outer membrane porins has been shown to reduce the membrane permeability of the cell and reduce the amount of silver than can reach its targets<sup>119</sup>. This mechanism may be aided by efflux proteins that actively pump silver out of the cell, but the system could still be overwhelmed if the concentration of silver ions in the environment remains high for a prolonged period<sup>119</sup>. In contrast plasmid mediated resistance gained by the transfer of genetic material can offer a far more robust mechanism of resistance<sup>114,121</sup>.

A silver resistance plasmid that is most noteworthy is the plasmid pMG101, which was isolated from the first *S. Typhimurium* strain with silver resistance<sup>113,122</sup>. This plasmid contains a *sil* cassette that codes for heavy metal efflux proteins and periplasmic sequestration proteins<sup>121–123</sup>. The *sil* cassette contains *silE*, *silS*, *silR*, *silC*, *silF*, *silB*, *silA*, an open reading frame ORF105 that could be renamed as *silG* due to its homology to *cusG*, a gene in the copper resistance cassette, and *silP* (Figure 1.2)<sup>121,122</sup>.

**This image has been removed due to third party copyright.**

**Figure 1.2: The resistance mechanisms of the Sil system found on the plasmid pMGI101**

Along the top of the figure is the order in which the genes are found within the plasmid and their orientation. Below shows a schematic of the proteins produced by the *sil* genes. SilE is a periplasmic protein that binds silver ions and accumulates them within the periplasmic space. SilCBA is a three-component protein complex that spans the membranes of the bacterium and is responsible for direct efflux of silver ions from the cell. SilF is another periplasmic protein which chaperones silver ions to SilCBA and SilS and SilR are a two-component sensor kinase/regulator protein pair. SilP is an ATPase heavy metal transporter that is responsible for transporting silver ions out of the cytoplasm and into the periplasm to be chaperoned by the periplasmic proteins<sup>121,122</sup>. Figure is adapted from Randall *et. al.* (2015)<sup>121</sup>

The silver genes are not always found as complete sets, which allows for varied resistance but *silE* appears to be the gene with highest importance<sup>114,124</sup>. SilE is a protein that binds specifically to silver ions within the periplasmic space and packages them into clusters. This stops the ions from travelling further into the cell and causing damage<sup>121,122</sup>. Without SilE, bacteria were found to lose their resistance phenotype<sup>121</sup>. Similarly, the loss of the SilCBA efflux protein complex can cause a loss of resistance<sup>121</sup> as this protein is a three-part cation/proton efflux protein that removes silver ions collected within the cell and periplasm<sup>122</sup>. SilSR is a two component sensor kinase and response regulator pair and SilP is an ATPase heavy metal efflux protein<sup>122</sup>. ORF105 is homologous to CusG, a copper transport chaperone in the *cus* operon, which has led to the hypothesis that ORF105 may be a silver chaperone and SilG may be an appropriate name for the protein<sup>121</sup>. Deletions of *silSR*, *silP* or *silG*, have no effect on silver resistance, but *silF* is interesting. SilF has been identified as a chaperone protein transporting silver ions to SilCBA, but pMG1101 also contains a *cus* operon for copper resistance<sup>121</sup>. The *sil* operon contains homologues of all the *cus* operon genes, except for *silE*, and the *cus* operon can compensate for losses of certain Sil proteins. When the *cus* operon is removed along with *silF*, there is a loss of the resistance phenotype proving the importance of SilF as a chaperone protein<sup>121</sup>.

Overall, both mutational and plasmid mediated resistance mechanisms result in a reduction of the concentration of silver ions entering the cell cytoplasm, but plasmid mediated resistance is of greater concern in medicine as most burns and wounds are polymicrobial and therefore can result in transfer of resistance between species<sup>125</sup>. Recently there has been an increase in the number of studies exploring silver resistance in clinical settings, and multiple groups have found evidence of multi-drug resistant bacteria carrying *sil* genes and/or plasmids identical or homologous to pMG1101<sup>114,123,125-127</sup>. This is a cause for concern despite the apparent rarity of silver ion resistance as multiple papers have stated that the use of silver may cause selection of silver resistant strains with antibiotic resistances<sup>112,123,126</sup>. As well as potential selection for MDR strains, silver resistance that develops from a genetic mutation causing a reduction of porins, may decrease antibiotic susceptibilities as the bacteria are less permeable<sup>112,127</sup>.

Overall, silver resistance appears to be rare, however it is still an area that requires exploration and silver sensitivities should be tested prior to use<sup>128</sup>. With the increasing commercial use of silver containing products, such as the recently introduced silver containing trolley handles used by some supermarket chains, it is highly possible that

selective pressure could induce the appearance of silver resistant strains and reduce the effectivity of a sorely needed antimicrobial therapy.

#### **1.4 A critical evaluation of *in vitro* assays and models used to study biofilm formation on artificial surfaces**

While many biofilms form on living tissue such as in burns and other skin wounds, a large proportion of human infections in clinical environments are caused by biofilm formation on devices such as catheters, endotracheal tubes, feeding tubes, central venous catheters and implants<sup>60</sup>. Silver compounds can be used to prophylactically treat infections caused by bacterial biofilms, by preventing the attachment of bacteria to the abiotic material used in the device. However, to effectively treat these infections and elucidate appropriate treatments and preventions there is a need to understand how biofilms are formed *in situ*, as bacteria within biofilms are much more resistant to antibiotics than planktonic bacteria<sup>129</sup>.

Our understanding of biofilms is largely from research using *in vitro* methods, most often the *in vitro* microtiter plate assay and the Calgary Biofilm device as they are relatively cheap, high throughput and easy to use<sup>129</sup>. However, these models, while useful, are simple and do not mimic the natural environments of biofilms well. Biofilms in clinical infections are better mimicked by *in vivo* biofilm models due to the manner in which the host cells and defences interact with bacterial biofilms<sup>129–131</sup>. Many *in vivo* models exist that utilise small animals such as insects, mice, rats, rabbits and guinea pigs but larger mammals are also used<sup>130</sup>. However, *in vivo* models are costly both financially and ethically<sup>130</sup>, so the use of *in vivo* animal models should only be considered when an *in vitro* system is unable to answer the research question effectively<sup>130</sup>.

As *in vivo* models are unfavourable without due cause, many *in vitro* models have been developed to explore aspects of biofilm formation, gene expression and treatment methods<sup>130,132,133</sup>. The main aim when developing *in vitro* biofilm models, or modifying ones that already exist, is to create a model with an environment that is as representative of the natural conditions as possible, to produce biofilms that better mimic those in nature<sup>132,134</sup>. The development of more clinically relevant *in vitro* biofilm models will reduce the frequency with which *in vivo* animal models are needed. *In vitro* models that better represent naturally occurring biofilms will be available for testing of biofilm

intervention strategies with only the most promising leads being taken forward for animal studies. The following section explores some of the most common biofilm models; their main uses, strengths, and limitations.

## **1.4.1 Microtiter plate assays**

### **1.4.1.1 The 96-well microtiter plate biofilm assay**

One of the most commonly used methods to evaluate the biofilm forming capabilities of a bacterial strain is the 96-well microtiter plate assay<sup>132,133,135</sup>. The assay was developed by Madilyn Fletcher in 1977 and since then it has been adapted many times for growth of many organisms and the testing of antimicrobial compounds<sup>135–138</sup>. To create a biofilm with this assay, bacteria are incubated in a 96-well microtiter plate with media incubated to allow biofilm formation. After a period, commonly around 24 hours, the wells of the plate are washed to remove loosely bound cells. The biofilm is then stained and biofilm biomass is quantified via absorbance readings of resuspended dye or viability assays performed to determine viable cell numbers<sup>132,135,139</sup>. The popularity of this method can be attributed to its low cost, simplicity and ease of use along with the speed of the experiment<sup>138</sup>, and the assay can be automated to improve reproducibility of the results<sup>137</sup>. However, this method is not without limitations.

The 96-well microtiter assay is an endpoint assay, which means that the only way to measure biofilm formation over time is to set up multiple biofilms and sample at different time points. Measuring biofilm formation in this way requires the experiment to be highly reproducible, however no information can be gained pertaining to a single biofilm over time.<sup>132</sup> It is also carried out in 'batch culture' which means there is no influx of fresh media and nutrients which can lead to bacterial exhaustion and starvation, limiting the size and properties of the biofilm formed<sup>132,133,138</sup>. Another set of limitations surrounds the integrity of the biofilm formed in the wells and the methods of quantification.

The most common method for quantification of the biofilm is staining with crystal violet after washing to remove unbound cells<sup>135,137,139</sup>. Washing of biofilms in wells can potentially disrupt the biofilm formed, which may give false or non-reproducible results<sup>135</sup>, although automating this process can make the results more reproducible<sup>137</sup>. However, even with an automated washing process, crystal violet stains not just live cells, but dead cells and the extracellular matrix<sup>139</sup>. This means there is no information gained about the

viability of the biofilm without extra steps where the biofilm is scraped and resuspended for cell counting, allowing for the introduction of contamination and a decrease in the reproducibility of results. There are other stains and dyes which can be used to identify live and dead cells within the biofilm however these are expensive and so crystal violet is the most commonly used as it is a cheap and easy to use non-differentiating stain<sup>139</sup>. A final issue with the integrity of the biofilm, is caused by the fact this assay is usually conducted in static conditions and therefore, there is a potential for sedimentation, which allows planktonic cells to become part of the biofilm more easily than they would in nature<sup>132</sup>. The microtiter plate method is an easy-to-use model that can give basic information about whether biofilm formation is possible, and it is a high throughput method. However, it is not representative of the natural environments where biofilms are formed therefore, biofilms in this assay will not have the same structural properties as naturally occurring biofilms.

#### **1.4.1.2 The Minimum Biofilm Eradication Concentration (MBEC) Device (formerly known as the Calgary Biofilm Device)**

The Minimum Biofilm Eradication Concentration (MBEC) device (Figure 1.3), formerly known as the Calgary Biofilm Device (CBD) was developed by Ceri *et. al.* in 1999 as a method for rapid antibiotic susceptibility screening of biofilms<sup>140</sup>. The device is composed of two-parts, a lid with 96 pegs attached that can be broken off, and a base which can be a trough or a 96-well microtiter plate<sup>140</sup>.

**A**

This image has been removed due to  
third party copyright.

**B**

This image has been removed due to  
third party copyright.

**Figure 1.3: Minimum Biofilm Eradication Concentration assay plates**

The MBEC assay plates consist of a lid with 96 pegs which protrude down into A) wells or B) a trough. Biofilm can then grow on the surface of the pegs while static, or under movement provided by shaking or rocking. Images from Innovotech<sup>141</sup>.

In the standard MBEC Assay<sup>®</sup>, biofilms are grown on the pegs when immersed in the media and the planktonic cells remain in the broth<sup>132,138,142–144</sup>. After the biofilm has been established, the lid can be transferred to a second plate containing antibiotic. The biofilms are incubated in the antibiotic, usually overnight and are then removed to sterile media and resuspended via centrifugation and sonication<sup>140,141,143</sup>. The biofilm is usually quantified via viable counts or absorbance readings<sup>143</sup>, however as individual pegs can be snapped off, the biofilms present on the pegs can be qualitatively analysed by Scanning Electron Microscopy (SEM) or Confocal Laser Scanning Microscopy (CLSM)<sup>142</sup>. When analysing biofilm biomass in this way the position of the microscope must be precise because biofilm growth tends to be the highest at the air-liquid interface point on the peg<sup>142</sup>.

As the morphology of a biofilm is influenced by the flow of media, it is important to be able to test the antibiotic susceptibilities of the biofilms under shear stress<sup>145</sup>. Flow can be introduced to the MBEC device via placement on a rotary shaker (96-well microtiter plate) or a rocker (trough)<sup>143,145</sup>. However, while this will provide some shear stress, it will not be high and it may not match the direction of flow *in situ*<sup>131</sup>.

The MBEC device, although a good device for testing antibiotic susceptibilities of biofilms, is still a microtiter plate model. As such, it is an endpoint assay, providing no information about biofilm formation over time, and it is also a batch culture assay, meaning the biofilm may be prone to nutrient exhaustion<sup>132</sup>. The experiment can be lengthened and bacterial biofilms can be grown for days with daily rinsing and replenishment of media<sup>144</sup>. However, this will increase the risk of contamination due to continuous changes of the bottom trough or plate<sup>138</sup> and also force the biofilm to pass through the air-liquid interface at every change, potentially disrupting morphology<sup>132</sup>.

Despite the risk of contamination with the standard method, the MBEC Assay<sup>®</sup> is still a common method for testing of antimicrobial compounds on biofilms<sup>133</sup>, as it is a cheap and high throughput method that does not require expensive, advanced equipment other than a spectrophotometer<sup>131,132</sup>. However, data obtained from this device about the effectiveness of an antimicrobial compound, may not translate to active biofilms *in situ*, as the model is not an accurate reflection of the human body, nor device infections, as the growth conditions, media available and ultimately the structure of the biofilm formed will be very different<sup>131</sup>.

### 1.4.2 The Modified Robbins Device (MRD)

The Robbins device was developed in 1981 and was initially used to evaluate the effects of biofilm formation in industrial situations such as waste water transport<sup>146</sup>. The device consisted of a pipe with several evenly spaced plugs that could be removed and tested without the need to drain the entire system<sup>146</sup>. This device was later adapted for laboratory use and named the Modified Robbins Device (Figure 1.4) and consists of a 41.5 cm long acrylic block with up to 25 sample plugs that can be attached to catheter material in such a way that the surface of the material is flush with the inner surface of the lumen<sup>147</sup>.

**This image has been removed due to third party copyright.**

#### **Figure 1.4: Bio-inLine® Biofilm Reactor a version of the Modified Robbins Device**

The Modified Robbins Device above is the Bio-inLine® Biofilm reactor produced by BioSurface Technologies Corporation that has been altered slightly to allow for ease of sampling. This model contains 12 sample plug holders, the coupons can be of any material and can be readily changed. The device contains switches at either end (yellow handles) that can contain the fluid within the MRD at any point in time. Image from BioSurface Technologies Corporation<sup>148</sup>

To form a biofilm, the MRD is sterilised, primed with sterile growth medium, then inoculated by passing bacterial culture in the exponential growth phases through the lumen of the device for a set time, followed by a flow of sterile media<sup>146,147,149–152</sup>. Bacterial starter cultures are usually grown up in batch culture, however the device can be connected to a bioreactor which will give reproducible concentrations of bacteria in a consistent growth phase<sup>153</sup>.

As the MRD has a high number of sampling ports, the device is of particular use when analysing biofilm formation on multiple types of substrate in the exact same conditions<sup>150,153,154</sup>. It has been used to analyse the efficacy of biocides and antibiotics and their capability to halt biofilm formation<sup>149,150</sup>, and it can also be used to grow

multispecies biofilms<sup>154</sup>. The MRD operates under flow conditions and as such is a more accurate method of testing biofilm formation on oral devices and catheter materials than static models<sup>151,152,155</sup>.

Unfortunately, the MRD is not designed for direct observation of biofilm formation, but the plugs can be removed over the course of the experiment and can be viewed via microscopy such as SEM and CLSM without significant manipulation<sup>132,146</sup>. However, removal of the plugs may introduce artefacts and contamination to the device<sup>132</sup>. Another limitation for the MRD is due to its size and run time, even though these characteristics can generally be considered advantages, as the MRD can then provide a high number of samples and can be operated for weeks. Extended run times will require large amounts of media, especially under high flow rates, and the device itself is too large to fit into a standard incubator with the media and pump attached in experiments where a constant temperature is necessary across the whole system, therefore a larger incubator or constant temperature room would be required.

The MRD is a good starting point for the testing of material and antimicrobial compounds, however it is likely to be a much more accurate representation of biofilms formed in industrial situations<sup>146</sup> than biofilms formed in human disease. This is due to the incredibly complex nature of living systems and how they interact with bacterial biofilms<sup>131</sup>.

### **1.4.3 The Drip Flow Biofilm Reactor®.**

The Drip Flow Biofilm Reactor® (Figure 1.5) was developed by Goeres and colleagues at Montana State University as a model for biofilm formation under low-shear, at the air-liquid interface<sup>134</sup>. Commercially available models consist of a polyethylene terephthalate, polysulfone or anodised aluminium block with four or six individual channels that can be sealed with air-tight lids. Inflow of fluid is usually via a needle port set in the lid and a second port allows for the attachment of an air filter. An effluent port is placed in on end of each chamber and the DFR is usually operated at a 10° angle to allow the run off to leave the chamber<sup>134,156</sup>.

**This image has been removed due to third party copyright.**

**Figure 1.5: The Drip Flow Biofilm Reactor<sup>®</sup>**

The Drip Flow Biofilm Reactor<sup>®</sup> as available through BioSurface Technologies Corporation can contain four to six channels and the non-modified version is as above, with a needle port for influent and an effluent port at the end of the chamber. The slide coupon in this image is a glass microscope slide, but this can be interchanged with other coupon materials for testing. Image from BioSurface Technologies Corporation<sup>156</sup>

In the standard method of operation, biofilms are established in batch culture on a coupon, which is often a microscope slide, that rests in the chamber and is covered by inoculum while the DFR is rested flat. After a period, inoculum is drained away and the DFR is returned to its original 10° angle and sterile media is dripped over the coupon surface via the needle port<sup>134</sup>. The biofilm will begin to grow on the surface of the coupon under low shear, loosely mimicking biofilms formed on teeth and catheters, and in lungs and wounds<sup>133,134</sup>

The biofilm is formed on the surface of the coupon in the standard method of operation, biofilms are easily accessible for analysis<sup>132,133</sup>, as they can be aseptically removed with sterile forceps<sup>157</sup>. After removal of the coupon, biofilms can be analysed for viability with viable counts<sup>134,157,158</sup> and live/dead fluorescent staining of recovered and homogenised biofilm<sup>158</sup>. Biofilm can also be analysed *in situ* via SEM and CLSM<sup>134,157,158</sup>, or simple photography for surface area analysis<sup>159</sup>.

The reactor was developed to be versatile<sup>134</sup>, and therefore, has been used in its original form in various studies testing biofilm formation on different surfaces, with and without antimicrobial intervention<sup>133,157–159</sup>. However, these are not the only uses for the model, as it can be modified to suit the needs of the researcher<sup>134</sup>. This capability for modification gave rise to the modified Drip Flow Biofilm Reactor models, where the modification is not always the same for different researchers<sup>133</sup>. Curtin and Donlan<sup>160</sup> and Fu *et. al.*<sup>161</sup> used an mDFR where the modification allows for the attachment of antimicrobial coated catheter tubing within the reactor chambers and biofilm is formed inside the catheter

segments via the flow of inoculum and then sterile media. Ionescu *et.al.*<sup>162</sup> modified the DFR to hold specimen trays in the base of each chamber. These trays could hold multiple specimens made of coated material and were submerged in media under flow to replicate the flow conditions of an oral biofilm<sup>162</sup>.

Unlike with biofilms formed on coupons or material surfaces, the biofilms are formed on the inner surface of tubing and are more complicated to access and analyse. To do so, samples can be cut into 1 mm sections and analysed via SEM<sup>160</sup>, or they can be left whole and the biofilm is removed via cutting the tube and then recovering the biofilm via sonication and vortex mixing<sup>161</sup>. The recovered biofilm cells can then be quantified by viability assays<sup>161</sup> or via live/dead fluorescent staining that will provide an estimation of the health of the biofilm by providing the percentage of live to dead cells present in the produced biomass<sup>158,163</sup>.

The main advantage of using the DFR is its capacity to be modified and adapted to the researchers needs. Unlike the MRD, the DFR is small<sup>132</sup> and does not require a lot of space to operate while also being small enough to fit inside benchtop autoclaves. Like the MRD, temperature control for long term experiments may be difficult as the reactor may not fit within a small incubator alongside the media and waste containers. Unfortunately, due to the size of the reactor, only four to six samples can be acquired with one run<sup>132,133</sup>. So, while multiple samples can be tested in parallel, for repeat experiments, the reactor would need to be set up from scratch, which is a timely disadvantage for experiments that last for multiple days.

The DFR is a good model for testing antimicrobial intervention strategies on surfaces, however biofilms grown on coupons are unlikely to be truly representative of biofilms formed in clinical infections. The mDFR models have the potential to be more representative of true infections of implanted devices, for instance, by the utilisation of an artificial urine media in a catheter infection model to test antimicrobial compounds could be highly representative of the clinical biofilms formed within catheter tubing.

#### 1.4.4 Flow cell biofilm models

Flow cell models have been used to analyse biofilm formation under flow conditions since the 1980's<sup>164</sup>, however, these models usually consisted of single channels<sup>164,165</sup>. In 1994, Wolfaardt *et. al.*<sup>166</sup> designed a four chamber, flow channel model that allowed for multiple biofilms to be formed, in parallel (Figure 1.6). Building on this model, there are now more recently published protocols for creating similar, modern flow cells from polycarbonate and stainless steel<sup>167-169</sup>.

**This image has been removed due to third party copyright.**

#### Figure 1.6: A flow cell biofilm model

A schematic diagram of the system required to form a biofilm within the flow cell biofilm model. Image adapted from Tolker-Nielson and Sternberg (2014)<sup>168</sup>

The main use of these models is to directly analyse biofilm formation under laminar flow<sup>166-170</sup>. This is easily achieved in this model as the chambers are often closed with a glass coverslip which allows for direct microscopy<sup>132</sup>. After inoculation of the system via injection of bacteria directly into the inflow tube<sup>168</sup> or into an injection port<sup>169</sup>, the flow cell is flipped upside down to allow bacterial attachment to the substrate without flow<sup>168,170,171</sup>. The flow cell is then flipped back over and sterile media is pumped through at a low flow rate<sup>167-171</sup>. Once established, the system can run without intervention for weeks<sup>168</sup>.

Biofilms are formed on the surface of the substrate, often a glass coverslip, and due to the size of the flow cell microscopic analysis is easily performed without halting the model<sup>132</sup>. The most common way to analyse biofilm formation in this model is by CLSM<sup>167-169</sup> and fluorescent tagging can allow for analysis of gene expression during biofilm growth<sup>170,171</sup>. The easy analysis that can be carried out in a non-invasive and non-destructive manner is one of the main strengths of this model as this allows real-time analysis of biofilm growth and the effects of stressors such as antimicrobials<sup>132,171</sup>. The continuous flow of media for a long period is also a strength of this model because, as with the MRD and the DFR, this allows for the formation of biofilms with a larger biomass and biovolume similar to those in nature<sup>171</sup>.

Limitations to this model are that it is low-throughput<sup>132</sup> and has a complex set up<sup>167,168</sup>, while direct sampling is impossible<sup>132</sup>. As well as this, biofilms formed in flow cells also risk being damaged and detached via the formation and passing of air bubbles<sup>172</sup>. However, air bubbles can easily be removed from the system via the addition of bubble traps at the inflow end of the device<sup>167,168</sup>.

Something to consider with flow cell models, is that most flow cells are custom made and require a peristaltic pump, which can be a costly endeavour<sup>169</sup>, however commercial models are available through BioSurface Technologies Corporation<sup>173</sup>. When considering clinical representation, these models may be of low similarity to clinical biofilms, however, a wealth of information on biofilm formation can be gathered *in situ* and these biofilms are more representative than those formed in microtiter plates as they are under flow.

### 1.4.5 The Centre for Disease Control biofilm model

Rotary biofilm models were first created in the early 2000's<sup>174,175</sup>, with the Centre for Disease Control (CDC) reactor (Figure 1.7) developed by Donlan *et. al.*<sup>175</sup> to imitate biofilms formed in potable water supplies. The initial purpose of the reactor was to create a mixed culture biofilm that imitated biofilms formed in hospital water systems, to test the efficacy of disinfectants<sup>175</sup>.

**This image has been removed due to third party copyright.**

#### **Figure 1.7: The CDC biofilm reactor as available from BioSurface Technologies Corporation**

The CDC reactor enables the sampling of 24 coupons under shear stress that can be altered independently of the flow rate of media into the vessel. Image from BioSurface Technologies Corporation<sup>176</sup>

The reactor consists of a large glass vessel which holds approximately 1 L of liquid, with an effluent port set in the side and a lid<sup>133,177</sup>. The height of the effluent port can vary between reactors and determines the maximum volume that can be held in the reactor<sup>177</sup>. The lid for the reactor is constructed to hold eight removable rods that hold three coupons each, with four inlet ports for inoculum, media and gases<sup>130,133,175,178</sup>. This allows for a large number of samples to be gathered during a single run<sup>130,132,133</sup>.

For biofilms to form on the coupons set in the holders, inoculum is added directly to the vessel containing media and then bacteria are grown in batch phase for a period before continuous flow of media is started<sup>175,177-179</sup>. Batch phase conditions in this reactor allow for the attachment of bacteria to the coupons while they are under shear stress caused by the rotation of the magnetic stirrer bar<sup>133,175,177,179</sup>. Analysis of these biofilms is simple as the coupons are attached to removable holders and can therefore be removed at any point throughout the experiment, which allows for biofilm analysis over time<sup>130,175</sup>. The most common methods of analysis are viability assays of biofilms homogenised by vortex mixing and sonication<sup>177,179,180</sup>. Other methods include fluorescent staining, SEM and CLSM which can give insights into the structure, gene expression and cell viability of biofilms<sup>133,178,180,181</sup>.

The CDC reactor is a very useful model for testing and creating repeatable biofilms under high shear stress and is an ideal model for testing potable water systems<sup>132,179,182</sup>. The intensity of the shear stress that biofilms are exposed to can vary widely<sup>179</sup> as the rotation frequency of the magnetic stirrer bar can be altered independently of the flow rate, which makes the model more flexible with regards to the type of flow environments it can imitate<sup>132</sup>. Another strength of this model is the number of replicates that can be gained in one run due to the presence of 24 removable coupons<sup>130,175,178</sup>. The presence of so many coupons makes it possible to test multiple surfaces and coatings in one run<sup>130</sup>, however for experiments comparing biofilm formation between strains, only one individual strain per reactor can be tested, and removal of coupons for testing of biofilm formation over time can introduce contamination<sup>132</sup>.

The CDC reactor is commercially available through BioSurface Technologies Corporation<sup>176</sup> and has an ASTM standard procedure<sup>133</sup>. It has been used to test a variety of experiments such as quorum sensing, cell viability on materials and coatings, antibiotic and disinfectant screening and it can also be modified in multiple different ways as reviewed in Gomes *et. al.* (2018)<sup>133</sup>, Azeredo *et. al.* (2017)<sup>132</sup>, and Coenye and Nelis (2010)<sup>130</sup>. This reactor is also a good tool to confirm screening of antimicrobial compounds that have been deemed effective in microtiter plate biofilms as the CDC reactor tests inhibition of established biofilms as opposed to inhibition of biofilm formation<sup>177</sup>. Unfortunately testing antibiotics in the CDC reactor can be expensive due to the mass of compound required to reach therapeutic levels in such a large volume<sup>130</sup>.

Rotary biofilm models such as the CDC reactor have been effectively used to imitate biofilms in water systems<sup>133,175</sup>, however, for clinical biofilms such as those in urinary catheters, the flow dynamics are likely to be completely different, so the CDC reactor may produce different biofilms to those in a clinical environment and remains best suited for biofilm formation in industrial settings.

## 1.5 Aims of this thesis

The first aim of this thesis was to test the efficacy of silver acetate as an antimicrobial against a carbapenem-resistant strain of *A. baumannii*. *A. baumannii* is a bacterium that has only been acknowledged as a concerning pathogen in the last 40 years, while silver is an ancient therapy that has been shown to be effective against many bacteria due to its oligodynamic effects.

The use of silver salts as an antimicrobial therapy declined with the production of antibiotics, but with the current issue of antimicrobial resistance, the use of silver salts such as silver acetate, to prevent infection is increasing. This creates a gap in the knowledge that allows infections caused by *A. baumannii* to be exposed to a therapy that has not yet been tested against the bacterial species.

Silver acetate is currently available as a catheter coating to prevent infections. *A. baumannii*, while not the most common cause of catheter associated urinary tract infections (CAUTIs) is a worrying uropathogen due to the MDR nature of the bacteria. So after the establishment of the antimicrobial activity of silver acetate against *A. baumannii*, the second aim of this thesis was to develop a biofilm model that better imitates a catheter associated urinary tract infection (CAUTI) using the modified Drip Flow Reactor® (mDFR) as the base.

To better understand biofilm infections and the efficacy of preventative treatments such as silver containing coatings, more representative models are needed in research. While *in vivo* models are the closest to human infections, they have a high ethical cost. With a more representative *in vitro* model, only the best antibiofilm strategies in this model will be taken to *in vivo* testing which will reduce the ethical cost.

## 2 Materials and methods

### 2.1 Media and compound preparation

#### 2.1.1 Muller-Hinton agar and broth

Mueller-Hinton agar (MHA) and broth (MHB) were used throughout the study as standard media to cultivate bacteria. Mueller-Hinton Agar and Broth powders were obtained from Sigma Aldrich and made up to standard specifications.

#### 2.1.2 M9 minimal media

Two types of M9 minimal media (Table 2.1) were tested in a growth curve as potential media that could be used in a situation where minimal media was required. The first media was a semi-defined M9 minimal media with casamino acids (M9c) and required the addition of 2 g L<sup>-1</sup> ThermoFisher Scientific casamino acids. The second media was a defined M9 minimal media (M9d) which required the addition of ThermoFisher Scientific Minimum Essential Medium (MEM) amino acids solution (50X) to a final concentration of 1X.

**Table 2.1: Components of M9 minimal media from Sigma-Aldrich before the addition of casamino acids/MEM (50X) amino acids.**

<b>Nutrient</b>	<b>Concentration</b>
5X M9 Salts	200 ml
Magnesium sulphate	0.002 M
Calcium chloride	0.0001M
Glucose	0.22

### 2.1.3 Silver acetate

Silver acetate was obtained from Sigma-Aldrich for the purpose of testing its antimicrobial activity against sessile and planktonic bacterial cells. Silver acetate in its solid form is a light sensitive powder stored in an opaque bottle. When needed, silver acetate was made up to 5 mg ml<sup>-1</sup> by dissolving in sterile distilled water and was stored for two weeks maximum in an opaque centrifuge tube or a dark box at room temperature.

### 2.1.4 Modified Artificial Urine Media

To develop the mDFR biofilm model further, an artificial urine media was used. The protocol used was first produced by Brooks and Keevil (1997)<sup>183</sup> and later adapted by Liang *et. al.* (2020)<sup>184</sup>, the components of which are listed in Table 2.2.

**Table 2.2: Components of the modified Artificial Urine Media as stated in Liang *et. al.* (2020)<sup>184</sup>.**

Nutrient	Manufacturer	Concentration
EDTA	Sigma-Aldrich	3 mM
Citric Acid	Sigma-Aldrich	2 mM
Calcium chloride	Sigma-Aldrich	2.5 mM
Sodium chloride	Sigma-Aldrich	80 mM
Sodium sulphate	Acros Organic	10 mM
Magnesium Chloride	Sigma-Aldrich	5 mM
Uric Acid	Sigma-Aldrich	0.23 mM
Sodium Bicarbonate	Sigma-Aldrich	37 mM
Bovine Peptone	Oxoid	1 (g L <sup>-1</sup> )
Yeast Extract	ThermoFisher Scientific	0.05 (g L <sup>-1</sup> )
Urea	Sigma-Aldrich	170 mM
Creatinine	Acros Organic	7 mM
Ammonium Chloride	Sigma-Aldrich	25 mM
Lactic Acid	SLS	1mM
Iron II sulphate	Sigma-Aldrich	3.5 µM
Potassium Phosphate (monobasic)	Sigma-Aldrich	50 mM
pH		6.5

## 2.2 Bacterial strains and culture methods of *Acinetobacter baumannii*

Strains were obtained from Public Health England and stored at -80°C as 20 % glycerol stocks and were grown up from the frozen stock on MHA at 37°C overnight. To create liquid overnight cultures a few morphologically similar colonies were touched with a loop and transferred to 5 ml MHB to be incubated overnight at 37°C shaking at 150 revolutions per minute (rpm). Strains in use are listed in Table 2.3.

**Table 2.3: *Acinetobacter baumannii* strains used in this study**

NCTC/ATCC number	Additional information
ATCC 17978	Isolated from fatal meningitis of 4-month old infant
NCTC 12156	Type Strain
NCTC 13301	Type D carbapenemase reference strain
NCTC 13302	Type D carbapenemase reference strain
NCTC 13305	Type D carbapenemase reference strain

## 2.3 Determining colony forming units per millilitre (CFU ml<sup>-1</sup>) of a culture

Strains were incubated for 18 hours in 5 ml MHB, shaking at 150 rpm at 37°C. The overnight cultures were then diluted to a turbidity of optical density (OD)<sub>600nm</sub> 0.8, 0.6, 0.4, 0.2 and 0.1, using sterile MHB as a blank. Using a 96-well plate each sample was serially diluted down to 10<sup>-10</sup> in the relevant media.

Two MHA plates were divided into four and a Miles and Misra experiment was carried out where 5 x 10 µl spots of dilutions 10<sup>-10</sup> to 10<sup>-3</sup> were spotted in each section before the plate was left to dry<sup>185</sup>. After drying the plates were inverted and incubated for 18 hours at 37°C.

After incubation, single colonies were counted in the lowest dilution that gave 3-30 colonies per spot and averages of the five spots were taken. These averages were used to calculate CFU ml<sup>-1</sup> and were plotted onto a scatter graph against OD<sub>600nm</sub> with a line of best fit, allowing for estimation of the CFU ml<sup>-1</sup> of a culture at any given OD<sub>600nm</sub>.

## **2.4 Growth and viability**

### **2.4.1 Growth curves in flasks**

To analyse growth in different types of media, 21 ml of the test media was added to a 250 ml conical flask in triplicate for each strain. 1 ml was immediately taken before the addition of bacteria to calibrate the spectrophotometer to different media and the absorbance was read at OD<sub>600nm</sub> for the time zero reading.

Each flask was injected with a 1% inoculum of overnight culture, before flasks were incubated with shaking at 150 rpm at 37°C for 24 hours. Hourly readings were taken throughout the day for 7 hours with a final reading taken at 24 hours.

### **2.4.2 Growth curves in the presence of silver acetate.**

0.9 ml of MHB was added to each well of a 24-well plate with a further addition 0.1 ml of bacterial overnight culture diluted to 0.5 OD<sub>600nm</sub>. The plate was incubated with orbital shaking in a BioTek® Cytation™ imaging reader (4mm) at 37°C until an OD<sub>600nm</sub> of 0.3 was reached. Silver acetate was then added to wells to the required final concentration. Growth was monitored every 20 min for 24 h. Three biological repeats were carried out with the final row of the plate utilised as blanks for the silver concentrations.

### **2.4.3 Viability assays**

To measure viability of bacteria, columns 2-12 of a 96-well plate were filled with 90 µl sterile phosphate buffered saline (PBS). To the wells of column two, 100 µl of neat bacterial culture was added and serial dilutions of 10 µl were carried out across the entirety of the plate. 10 µl of each well was spotted onto an MHA plate with five repeats and the MHA plates were incubated overnight at 37°C. Single colonies were counted and multiplied by the dilution factor to calculate the CFU ml<sup>-1</sup>.

## **2.5 Colony biofilm assay**

The colony biofilm assay was carried out according to Merritt *et. al.* (2011)<sup>186</sup> and utilised 50 mm polycarbonate track-etched filters with a pore size of 0.2  $\mu\text{m}$  (Sartorius) placed on an MHA plate. Before commencing the experiment, the membranes were sterilised under an ultraviolet light on both sides for 10-15 minutes.

The membranes were placed on MHA plates and overnight cultures were diluted to  $\text{OD}_{600\text{nm}} \sim 0.05$ . A 5  $\mu\text{l}$  spot of these cultures was then placed on the centre of the membrane and the plates were left to dry before being incubated at 37°C for 24 hours. Subsequently the membranes were transferred to fresh MHA plates and incubated for a further 24 hours after which the membranes were removed and added to 50 ml centrifuge tubes containing 10 ml of sterile PBS. To remove the biofilm from the surface of the membrane, the tubes were vortex mixed for approximately 60 seconds and a 1 ml pipette was used to break up any clumps of biofilm. Viable counts were then determined (section 2.4.3).

## **2.6 96- and 24- well biofilm assays**

### **2.6.1 96-well biofilm assay**

Overnight cultures were diluted to  $\text{OD}_{600\text{nm}} \sim 0.5$  in sterile PBS. For each strain, 90  $\mu\text{l}$  of MHB was added to five wells followed by 10  $\mu\text{l}$  of diluted bacteria. Five wells of a final row were also filled with 90  $\mu\text{l}$  MHB only to act as blanks and sterility controls. The plate was then incubated, static, at 37°C for 18 hours.

After incubation, the media in the wells was removed by inversion and gentle blotting. The wells were then washed with 200  $\mu\text{l}$  of PBS and shaken at 100 rpm for five minutes, twice. After washing, 125  $\mu\text{l}$  of 0.1 % crystal violet was added to all wells and incubated on the bench at room temperature for 1 hour. To remove the crystal violet the plate was inverted, and the wells were washed with 200  $\mu\text{l}$  PBS until the eluate was clear. The plate was then allowed to dry.

To all wells 125  $\mu\text{l}$  ethanol was added and the plate was shaken at 100 rpm for two minutes. 100  $\mu\text{l}$  of the crystal violet-containing eluate was then added to a 96-well plate

and the absorbance read at OD<sub>540nm</sub> to quantify the amount of biofilm present via the bonded crystal violet.

### **2.6.2 24-well biofilm assay in the presence of silver acetate**

Silver acetate prepared as stated in section 0 and diluted in MHB to the desired concentration was added to each well in column one of two 24-well plates. A 2-fold serial dilution of the silver acetate was carried out down the plates, after which 100 µl of overnight bacterial culture diluted to OD<sub>600nm</sub> ~ 0.5 in PBS was added to all but the final wells of each row. The wells in the final row were left as blank and sterility controls. The 24-well plates were then incubated as in section 2.6.1. The first well plate was assayed as in section 2.6.1, while the biofilm was harvested from the second well plate for a viable count. To remove the biofilm, the wells were washed gently as in section 2.6.1 but instead of adding crystal violet, 500 µl PBS was added to the well and vigorously mixed to resuspend the biofilm. Viable counts were carried out on the resulting suspensions according to section 2.4.3.

### **2.7 Identification of oxacillinase genes in *Acinetobacter baumannii***

To identify the oxacillinase genes in the *A. baumannii* strains a polymerase chain reaction (PCR) assay was carried out with the primers listed in Woodford *et. al.* (2006)<sup>30</sup>. Single PCRs were carried out testing each strain for the OXA-genes listed in Table 2.4 with the OXA-51-like primers acting as positive controls for *A. baumannii*. The PCR was carried out using Taq 2X Master Mix (New England Biolabs<sup>®</sup>inc), diluted to 1X, and thermocycler conditions were set as follows: 95°C for 30 s for 1 cycle, 35 cycles of 95°C for 30 s, 53°C for 60 s, and 68°C for 45 s, and a final cycle at 68° for 5 mins.

After PCR, gel electrophoresis was carried out with a 1.5 % agarose gel at 120 V for 30-45 minutes. The amplified bands were visualised using a Biorad ChemiDoc™ MP Imaging System and compared to a GeneRule 100 bp DNA (ThermoFisher Scientific) ladder to clarify the size of the bands.

**Table 2.4: PCR primers used to identify the presence of oxacillinase genes in *A. baumannii* strains.**

Primer	Sequence	Target
OXA-51-likeF	5' -TAATGC TTT GAT CGG CCT TG- 3'	<i>bla</i> <sub>OXA-51-like</sub>
OXA-51-likeR	5' -TGG ATT GCA CTT CAT CTT GG- 3'	
OXA-23-likeF	5' -GAT CGG ATT GGA GAA CCA GA- 3'	<i>bla</i> <sub>OXA-23-like</sub>
OXA-23-likeR	5' -ATT TCT GAC CGC ATT TCC AT- 3'	
OXA-24-likeF	5' -GGT TAG TTG GCC CCC TTA AA- 3'	<i>bla</i> <sub>OXA-24-like</sub>
OXA-24-likeR	5' -AGT TGA GCG AAA AGG GGA TT- 3'	
OXA-58-likeF	5' -AAG TAT TGG GGC TTG TGC TG- 3'	<i>bla</i> <sub>OXA-58-like</sub>
OXA-58-likeR	5' -CCC CTC TGC GCT CTA CAT AC- 3'	

\*\*Primer sequence origin<sup>30</sup>

## 2.8 Genome sequencing of *Acinetobacter baumannii* NCTC 13302

Genomic DNA was isolated from overnight cultures of *A. baumannii* NCTC 13302 with the GenElute™ Bacterial Genomic DNA kit (Sigma Aldrich) and following the manufacturer's instructions. The extracted double-stranded DNA was then quantified for ds-DNA using the ds-DNA high sensitivity assay kit (ThermoFisher Scientific) on the Qubit fluorometric quantification platform (ThermoFisher Scientific) and then quality checked with a Nanodrop 2000 Spectrophotometer (ThermoFisher Scientific) by Adam Varney. Quality ratios considered acceptable were the  $A_{260}/A_{280}$  and  $A_{260}/A_{230}$  with a range of 1.8 - 1.9 and 1.9 - 2.2 respectively. Oxford Nanopore sequencing was carried out in house by Adam Varney. Illumina sequencing of the same strain was carried out by MicrobesNG (<http://microbesng.com>).

To assemble the genome from the Nanopore and Illumina sequencing reads, the barcodes on Nanopore reads were trimmed using porechop 0.2.4 in CLIMB-BIG-DATA and then the reads were assembled using the program canu 2.0. After initial assembly, the resulting contigs were polished using the programs racon 1.4.13, medaka 1.03 and then nanopolish 0.13.2 to improve the accuracy of the genome assembly. Following the polishing of the Nanopore reads the genome was mapped with the Illumina sequencing using the minimap 2.17 program and the resulting assembly was further polished using

the programs racon 1.4.13 and pilon 1.24. All programs used to assemble the genome in CLIMB-BIG-DATA used the pre-set parameters.

After assembly, the sequences for the chromosome and the largest plasmid (>151kbp) were compared to the published genome for *A. baumannii* NCTC 13302 (Accession number:NZ\_UIGA01000005) in BLAST and with EasyFig 2.2.2.

## **2.9 Minimum inhibitory/bactericidal concentration assays**

To the first row of a 96-well plate, 200 µl of antimicrobial compound dissolved in culture media was added in triplicate for each strain. To the remaining wells of the plate 100µl of MHB was added and the plate was serially diluted down to row 10 leaving rows 11 and 12 as sterility and growth controls. To all wells of the plate up to and including row 11, 10µl of overnight culture diluted to 0.1 OD<sub>600nm</sub> was added. The plate was wrapped in foil to protect light sensitive compounds and was incubated at 37°C for 18 hours. The minimum inhibitory concentration (MIC) was the well with the lowest concentration of compound which inhibited growth.

A minimum bactericidal concentration (MBC) assay was set up by plating 10µl of each well from the MIC assay onto an MHA plate as shown in Figure 2.1. The MBC is the well that contains the lowest concentration of antimicrobial, which does not show growth on the agar plate.

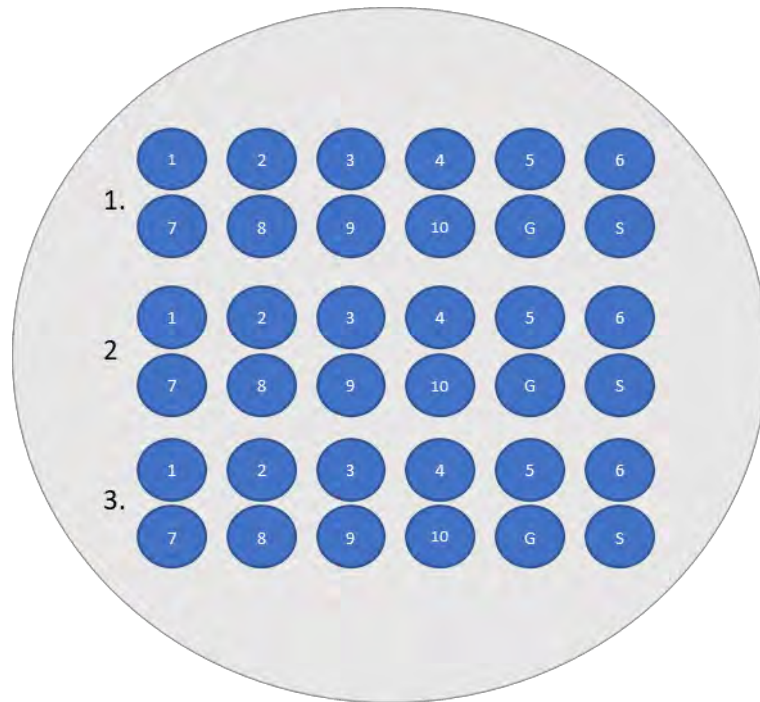


**Figure 2.1: Schematic diagram for layout of 10  $\mu$ l spots from MIC assay to set up the MBC assay**

This layout allows for easy visualisation of differences in MBCs between replicates. The numbers in each spot represent the well numbers going down the plate. i.e. 1 = the highest concentration of antimicrobial compound while G = Growth control and S = Sterility control.

## 2.10 *Galleria mellonella* treatment efficacy experiments

*G. mellonella* larvae were ordered from TruLarv, Bio Systems Technology in pots of 50 and were used immediately upon arrival. Only healthy larvae were selected for use, which is shown by their colouring as healthy larvae are a cream colour (Figure 2.2) with no brown discolouration or black spots (melanisation) that move freely without stimulation. Each *G. mellonella* test was carried out in temporally spaced triplicate for biological repeats.



**Figure 2.2: A healthy *Galleria mellonella* larva**

Healthy *Galleria mellonella* larvae from TruLarv Bio Systems Technology are cream in colour as above and approximately 2-3 cm length and 0.3 g in weight. There are very few outliers to these sizes due to the standardisation of handling and age of the larvae when they are packaged and sent.

### 2.10.1 Inoculum testing of *Acinetobacter baumannii*

The day before arrival of the larvae, an overnight culture of *A. baumannii* NCTC 13302 was prepared (section 2.2). When the larvae arrived, 80 healthy larvae were divided evenly between eight, inverted petri dishes with a 10 cm Whatman Filter paper fitted in the lid. The test plates (six petri dishes) were labelled according to the amount of bacteria the larvae would be exposed to, while the remaining two were labelled as unaffected (no injection control) and H<sub>2</sub>O control (injection control).

To prepare the inoculum for each sample, the turbidity of 1 ml of the 5 ml overnight culture of NCTC 13302 was measured at OD<sub>600nm</sub> and the remaining 4 ml was centrifuged at 5000 rpm for 10 minutes. After centrifugation the supernatant was discarded, and the

pellet was resuspended in the appropriate volume of H<sub>2</sub>O to produce 1 x 10<sup>9</sup> CFU ml<sup>-1</sup>. The 1 x 10<sup>9</sup> CFU ml<sup>-1</sup> aliquot was then serially diluted to ~1 x 10<sup>2</sup> CFU ml<sup>-1</sup> in ten-fold dilutions to provide the concentrations shown in . For the purpose of knowing how many bacteria each larva was exposed to, calculations were carried out to work out the colony forming units per 10 µl as 10 µl was the amount injected per larva ( ).

**Table 2.5: Conversion table of CFU ml<sup>-1</sup> to CFU 10µl<sup>-1</sup>**

CFU ml <sup>-1</sup>	CFU 10µl <sup>-1</sup>
1 x 10 <sup>4</sup>	1 x 10 <sup>2</sup>
1 x 10 <sup>5</sup>	1 x 10 <sup>3</sup>
1 x 10 <sup>6</sup>	1 x 10 <sup>4</sup>
1 x 10 <sup>7</sup>	1 x 10 <sup>5</sup>
1 x 10 <sup>8</sup>	1 x 10 <sup>6</sup>
1 x 10 <sup>9</sup>	1 x 10 <sup>7</sup>

To inject the *G. mellonella*, a 50 µl Hamilton syringe was washed via drawing up and expelling first sterile H<sub>2</sub>O, then 70% ethanol, then sterile H<sub>2</sub>O. After washing, 10µl of the inoculum was drawn into a 50 µl Hamilton syringe and the larva was either held between the fingertips or laid over a stage (an inverted petri dish with a 1000 µl pipette tip taped to the surface) as shown in Figure 2.3. The inoculum was then injected into last left proleg, and the larva was carried over to the petri dish with a filter paper in the lid while still on the needle to allow for circulation of the inoculum load. After a few seconds following removal of the needle, the larva would begin to move and would not excrete fluid if the injection was successful. The wash step of the syringe was repeated before injecting the next *G. mellonella*.

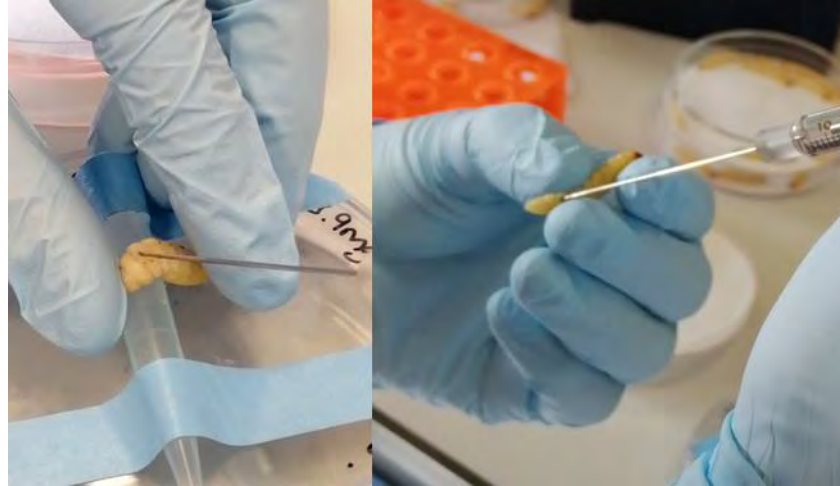


**Figure 2.3: *Galleria mellonella* injection methods**

Shown above are the two methods used to inject the larvae. Both methods show injection into the last left proleg of the larva.

After injecting all larvae, barring the no-injection control, with the correct concentration of bacteria, or H<sub>2</sub>O in the case of the vehicle control, the plates were lightly taped closed and incubated at 37°C. The larvae were scored for live, or dead and health (by melanisation score) at 0, 24, 48, 72 and 96 hours. Live/dead scoring was undertaken by gently prodding the larvae with blunt tweezers and watching for movement or by turning the larvae onto their back; healthy larvae will quickly turn themselves back over. Health scoring involved judging the melanisation (appearance of brown colouring) of the *G. mellonella* and scoring them according to Table 2.6.

**Table 2.6: Description of physical appearance and therefore, melanisation of larvae for health scoring**

Score	Description	
0	Completely black larvae	
1	Brown larvae with black spots	
2	Light brown/cream larvae with dark brown spots	
3	Cream larvae with brown line or spots on tail	
4	Cream larvae with no spots	

### 2.10.2 Toxicity testing of silver acetate

Following the same method as in section 2.10.1 the larvae were injected with concentrations of silver acetate that varied from 1.25 – 80 mg kg<sup>-1</sup>. As above, ten larvae were not injected to ensure nothing was wrong with the handling of the larvae and ten larvae were injected with H<sub>2</sub>O only and these 20 larvae acted as controls. The larvae were incubated for 96 hours at 37°C with live/dead and health scoring carried out every 24 hours.

### 2.10.3 Treatment of an *Acinetobacter baumannii* infection with silver acetate

20 larvae were injected with 10µl of 1.7 x10<sup>6</sup> CFU larvae<sup>-1</sup> and 20 larvae were injected with 1.7 x10<sup>5</sup> CFU larvae<sup>-1</sup> *A. baumannii* following the method outlined in 2.10.1 Following a 30-minute incubation at 37°C, ten larvae from each concentration were injected with 10 mg kg<sup>-1</sup> or 20 mg kg<sup>-1</sup> silver acetate into the last right proleg. The larvae were monitored for their survival and melanisation every 24 hours over the course of 96 hours.

## 2.11 Drip Flow Biofilm Reactor Model

A modified six-channel polyethylene terephthalate (PET) Drip Flow Biofilm Reactor® (mDFR) with catheter modification was purchased from BioSurface Technologies Corporation<sup>156</sup> and used to grow biofilms within silicone tubing.

### 2.11.1 Production of an *A. baumannii* biofilm

Two channels of a six-channel mDFR were used, with both corresponding to one biological repeat. (Figure 2.4). Each channel contained a 7.5 cm length of silicone tubing (internal diameter = 3 mm, external diameter = 5mm, wall thickness = 1 mm) that was connected to the influx and efflux ports at the ends of each channel.

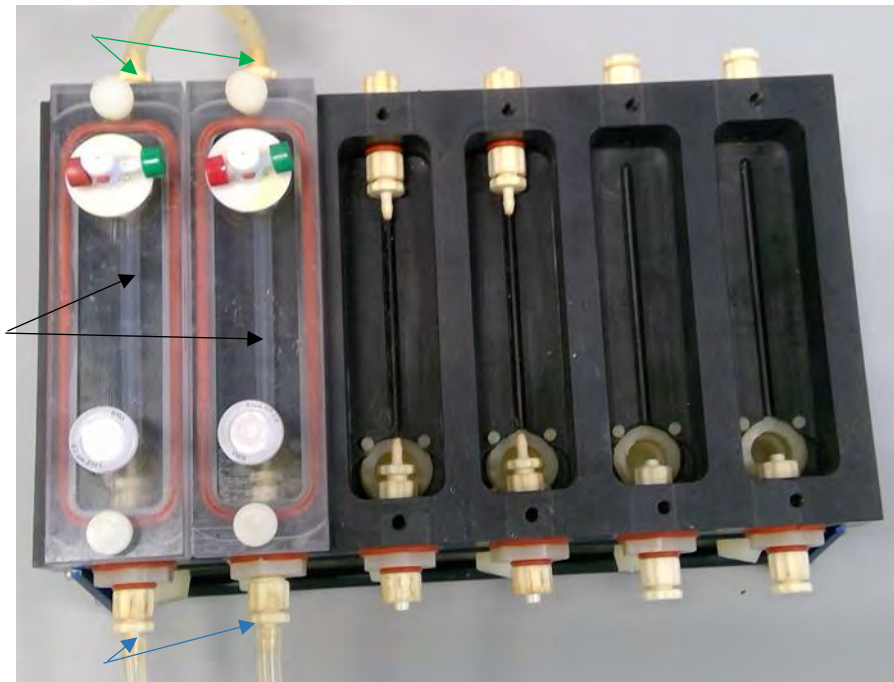


**Figure 2.4: Six channel modified Drip Flow Reactor® set up to run with two channels**

Above image shows the modified Drip Flow Reactor® set up to run for two channels only for one biological repeat after autoclaving. Black arrows indicate the silicone tubes for biofilm sampling. Influx ports are shown with green arrows and effluent ports are indicated with blue arrows.

To grow an *A. baumannii* biofilm, a 5 ml overnight culture of bacteria was added to 500 ml sterile MHB and stirred with a magnetic flea for 3 hours at 37°C until the bacteria reached early exponential growth phase. While the bacteria grew, half strength MHB was flushed through the mDFR removing any air bubbles and priming the tubing. After three hours, the exponential phase bacteria were run through the mDFR at a speed of  $0.5 \pm 0.067 \text{ ml min}^{-1}$  for two hours before the tubing from the bacteria was clamped off and sterile half strength MHB was set to flow through the system for five days at the same speed. The experiment was repeated three times to provide three biological repeats.

To analyse the biofilm formed when grown with modified artificial urine media (mAUM, section 2.1.4), 50% MHB was replaced with full strength mAUM and the method was carried out as described above.

### **2.11.2 Analysis of mDFR biofilms**

At the end of the five-day incubation the tubing was clamped off and the biofilm-containing tubes were disconnected from the influx ports under sterile conditions. The tubes from each channel were placed in sterile 15 ml centrifuge tubes and were washed by running 3 ml sterile PBS down the inside of the tube, to remove any unbound cells. The tube from channel one was placed in a sterile petri dish to be fixed for SEM, while the tube from channel two was placed into a fresh 15 ml centrifuge tube for viability assays.

#### **2.11.2.1 Determination of viability of biofilms grown in the modified Drip Flow Reactor**

To determine viability of mDFR biofilms, viability assays (section 2.4.3) and live/dead staining were performed.

To remove the biofilm from the inside of the silicone tubing, 10 ml sterile PBS was pipetted directly through the lumen of the silicone tubing and pipetted up and down vigorously for a minute. The centrifuge tube was then vortex mixed for 1 minute, sonicated at full power for 2 minutes using an Ultrawave Q Series sonicating machine before vortex mixing again for another minute. This process was repeated until all the biofilm was removed from the tube.

The bacterial suspension was centrifuged at 5000 rpm for 10 minutes and the supernatant discarded before resuspension of the cell pellet in 1 ml sterile PBS. 100 µl of this culture was stained with the LIVE/DEAD® BacLight™ Bacterial Viability Kit \*for microscopy\* by Invitrogen. This kit used two stains, SYTO 9 and propidium iodide to stain the membrane of the cells where 0.150 µl of each stain is added to the bacterial culture and incubated for ten minutes at room temperature. During the incubation 1 ml of molten 1 % agarose was spread evenly across the surface of a microscope slide and left to set before 10 µl of stained bacterial suspension was added to the surface. A coverslip was placed over the top of the spot and the slide is viewed at 100 X magnification on a Leica DMI8 fluorescent microscope under brightfield (BF), Green Fluorescent Protein and Texas red settings. The resulting images from four fields of view for each sample were counted using the cell counter in ImageJ, opened with Fiji. 100 µl of the remaining unstained suspension is serially diluted in sterile PBS in triplicate and plated out on an MHA plate for viability counts as described in section 2.4.3.

### 2.11.2.2 Scanning electron microscopy

After washing away any unbound cells with sterile PBS and transferring to a petri dish, the silicone tube from channel one of the mDFR for each biological repeat was sliced using a sterile scalpel into 1 mm thick sections. Of the final sections, four sections were chosen at random and the biofilm present was fixed according to the procedure shown in Table 2.7.

**Table 2.7: Fixing procedure for Scanning Electron Microscopy**

Chemical	Time (mins)
4 % Paraformaldehyde	30
50 % Ethanol	20
60 % Ethanol	20
70% Ethanol	20
80 % Ethanol	20
90 % Ethanol	20
100% Ethanol	40
1:2 HMDS/100 % Ethanol	20
2:1 HMDS/100 % Ethanol	20
100 % HMDS	Overnight

After fixing, each disc was sliced laterally, placed lumen side up and sputter coated with gold using a Quorum Q150R ES Sputter Coater creating a 5 nm layer of gold across the surface of the tube lumen. The samples were then viewed and secondary electron imaging was carried out with a scanning electron microscope (Jeol JSM-7100F LV FEG-SEM) with high vacuum at 15 kV.

### 3 Biofilm formation capabilities, growth and antibiotic resistance of *Acinetobacter baumannii* strains resistant to carbapenems

#### **3.1 Introduction**

*Acinetobacter baumannii* is a Gram negative, aerobic bacterium that commonly causes hospital infections such as ventilator associated pneumonia, bacteraemia, catheter-associated urinary tract infections and wound and burn infections<sup>1,2</sup>. The key factors that allow *A. baumannii* to be such a concerning pathogen are its abilities to form biofilms and resist antibiotic killing<sup>1,2,55</sup>. Biofilm formation, and particularly biofilm formation on abiotic surfaces, allows *A. baumannii* to cause device associated infections that persist<sup>18</sup>. The organism has a host of mechanisms such as the Csu pili, BAP, OmpA and PNAG which have important roles in biofilm formation abiotic surfaces and are covered in more depth in section 1.2.1.

*A. baumannii* infections are difficult to treat due to the pathogen's ability to resist antibiotics via innate and acquired mechanisms of resistance providing resistance to  $\beta$ -lactams, aminoglycosides, tetracyclines, quinolones and other classes of antibiotics<sup>2,23</sup>. The rapid acquisition of antibiotic resistance mechanisms has led to the appearance of multidrug, pan-drug and extremely-drug resistant strains<sup>50,51</sup> and last resort antibiotics such as the carbapenems are rapidly losing their effectivity<sup>187</sup>. There is currently a push for research into antimicrobial therapies to tackle *A. baumannii* strains resistant to carbapenems, as these strains have been classified as critical pathogens by the World Health Organisation<sup>16</sup>.

Carbapenems are  $\beta$ -lactam antibiotics that were used as 'last resort' antibiotics for *A. baumannii* infections until resistance appeared in the 1990's and began to spread<sup>187,188</sup>. These antibiotics are similar in structure to penicillin, but have a double bond between carbons 2 and 3 of the  $\beta$ -lactam ring, and they possess a carbon at Carbon 1 (Figure 3.1) instead of sulphur<sup>189,190</sup>.

**This image has been removed due to third party copyright.**

**Figure 3.1 Structure of the  $\beta$ -lactam nuclei of carbapenems versus penicillins (penams).**

The nuclei of penicillins and carbapenems differ in the presence of a carbon at C1 and a double bond between C2 and C3 and carbon alters the stability of the antibiotic along with its resistance to  $\beta$ -lactamase enzymes<sup>189</sup>. Image adapted from El-Gamal *et. al.* (2017).

These antibiotics are broad spectrum but due to the development of antibiotic resistance and the potency of these compounds, carbapenems are used as “last-line” or “last resort” antibiotics<sup>190</sup>. Carbapenems can be divided into groups based on their activity with Group 1 being chemicals with broad-spectrum but limited activity (ertapenem), Group 2 being carbapenems with broad-spectrum and high activity (imipenem, meropenem, doripenem), while Group 3 are carbapenems are under development but are aimed to be effective against Methicillin-resistant *Staphylococcus aureus* infections. One example is Razupenem, but this was discontinued for use due to a high number of undesirable effects during the clinical trials<sup>189</sup>.

In *A. baumannii*, carbapenem resistance is mainly conferred by the presence of oxacillinase genes (OXA-genes) which produce  $\beta$ -lactamase enzymes<sup>191</sup>. There are four main subgroups of OXA-genes, OXA-51-like, OXA-23-like, OXA-24-like and OXA-58-like and all except for the OXA-51-like genes are plasmid encoded<sup>187,191,192</sup>. The OXA-51-like gene is a chromosomally encoded gene that is intrinsic to all *A. baumannii* and can therefore be used as an identification mechanism for this species. The OXA-51-like gene can confer resistance when the genetic area surrounding the gene is favourable and contains an insertion sequence (ISAba1) directly upstream of the gene<sup>31,192</sup>. OXA-genes are globally distributed in *A. baumannii* with OXA-23 being the most widespread gene and the most common in hospital infections<sup>191–194</sup>. OXA-24-like genes are less well distributed and restricted largely to the United States and Asia while OXA-58-like genes are found mainly in southern European countries<sup>192</sup>.

This chapter aimed to phenotypically characterise several *A. baumannii* strains containing Type D carbapenemase genes and identify the strain with the highest level of biofilm formation for use in further chapters. After identification of the most appropriate strain, *de novo* whole genome sequencing was carried out and compared to the published sequence of the strain to ensure the full genome of the chosen strain was known and to check for any genomic changes between the published strain and that stocked within our laboratory.

## 3.2 Results

### 3.2.1 PCR analysis of the OXA genes

Carbapenem resistance is usually attributed to the gain of carbapenemase genes in *A. baumannii*. Three of the strains tested (NCTC 13301, NCTC 13302 and NCTC 13305) are Type D carbapenemase type strains obtained from Public Health England. PCR was used to confirm the presence of OXA-51-like genes in all strains used as expected for *A. baumannii*. The OXA-23-like gene present in NCTC 13301, the OXA-24-like gene present in NCTC 13302 and the OXA-58-like gene present in NCTC 13305 were also confirmed by PCR. The *A. baumannii* type strain (NCTC 12156) and the clinical reference strain ATCC 17978 did not contain any of the OXA genes tested except the OXA-51-like gene (Table 3.1).

**Table 3.1: Confirmation of the presence or absence of OXA genes from genomic DNA.**

Strain	OXA-51-like	OXA-23-like	OXA-24-like	OXA-58-like
NCTC 12156	+	-	-	-
ATCC 17978	+	-	-	-
NCTC 13301	+	+	-	-
NCTC 13302	+	-	+	-
NCTC 13305	+	-	-	+

### **3.2.2 Growth of *Acinetobacter baumannii* in different media demonstrates the biosynthetic capacity of this species**

Initial characterisation of five *A. baumannii* strains (Table 2.3) sought to determine how well the species grows in different nutrient conditions, including rich, defined (known amino acids) and semi-defined (amino acids supplemented in the form of hydrolysed casein) media. Strains were grown over 24 h with absorbance readings used to monitor growth stages of the bacteria.

Figure 3.2 depicts the growth curves of all the strains of bacteria in the three types of growth media. Every strain tested grew to the highest turbidity in MHB and on the graph it is possible to see the exponential curve that is stereotypical of bacterial growth in rich media. M9 minimal media supplemented with 2 g L<sup>-1</sup> hydrolysed casein allowed the strains to grow to turbidities reaching OD<sub>600</sub> ~ 1.5. Whilst M9 minimal medium supplemented with 1X ThermoFisher Scientific MEM amino acids solution (from a 50X stock) solution produced the lowest turbidity and slowest growth for most strains when compared to the other media. However, all strains were able to grow to turbidities approaching 1.0 OD<sub>600</sub> as a minimum in this medium.

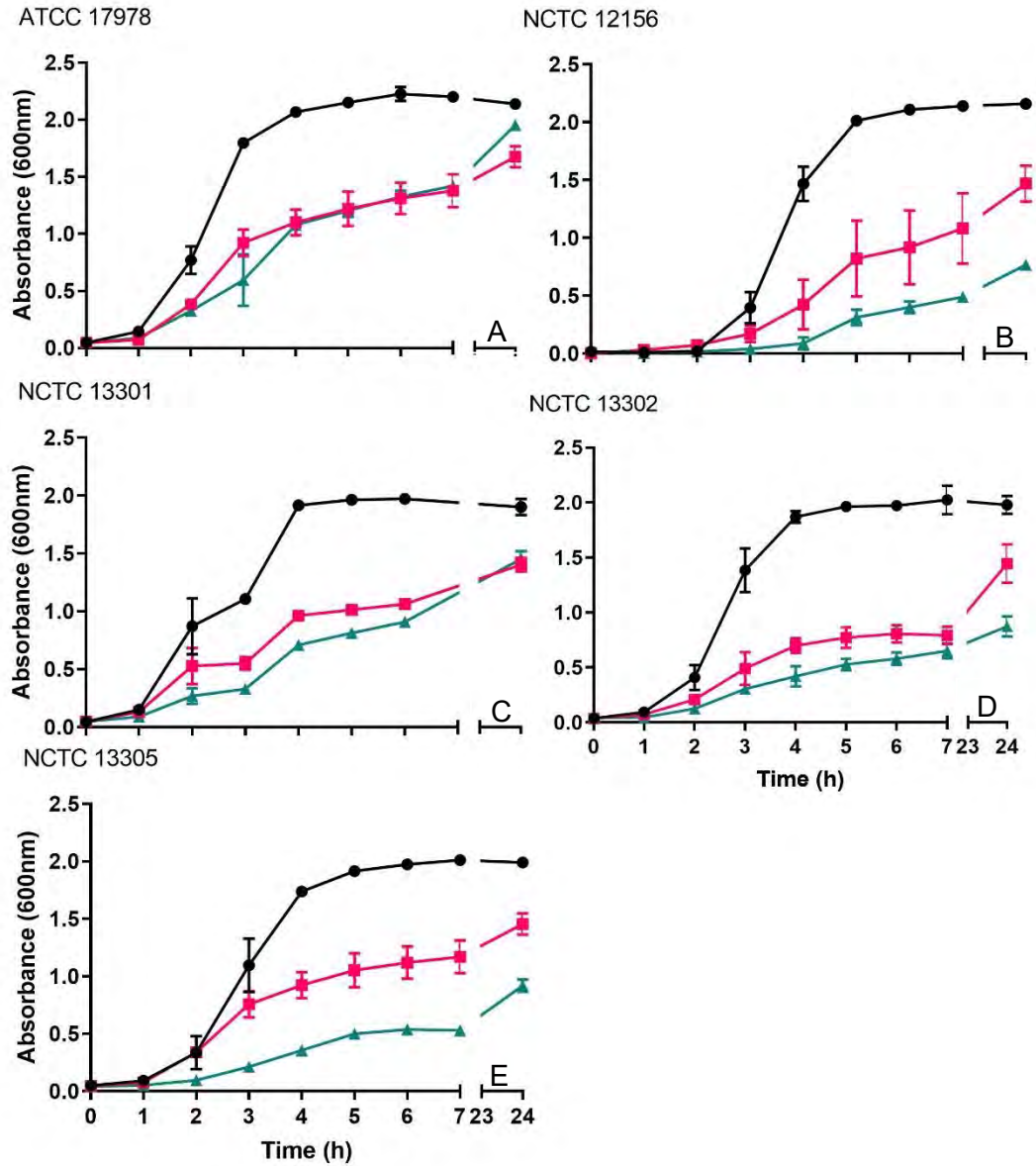


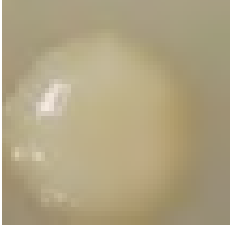
**Figure 3.2: Growth curves of *Acinetobacter baumannii* strains in MHB, M9c and M9d show M9d produces the lowest turbidity while MHB produces the highest**

Bacteria were incubated in MHB (black circle), M9c (pink square) and M9d (blue triangle) and absorbance readings were taken over the course of 24 hours. Graphs A-E show that MHB consistently produces the highest absorbance readings and therefore best growth while M9d produces the lowest absorbance readings. N=3  $\pm$ SD.

### **3.2.3 Colony biofilm formation assays show no significant difference in biofilm formation between strains**

The colony biofilm assay allows biofilms to form on semi-permeable membranes at the interface of nutrient supply and the air and allows for the study of static biofilm formation on solid surfaces<sup>186</sup>. The assay was used to determine which of the strains were proficient biofilm formers. Colonies were grown on semi-porous membranes that allowed nutrients to transfuse from the agar to the bacteria over time. Table 3.2 shows the sizes and appearances of the colony biofilms grown over this period. After 2 days of incubation, the colonies were washed and resuspended and viable counts were carried out to compare bacterial viability. There were no significant differences between the viable counts of the resuspended colony biofilms. Figure 3.3, ( $P = 0.7870$  with ANOVA).

**Table 3.2: Colony biofilm size and appearance after 48-hour incubation on MHA**

Strain	Colony biofilm image	Diameter of colony (mm)
NCTC 12156		6
ATCC 17978		6
NCTC 13301		5
NCTC 13302		6
NCTC 13305		8

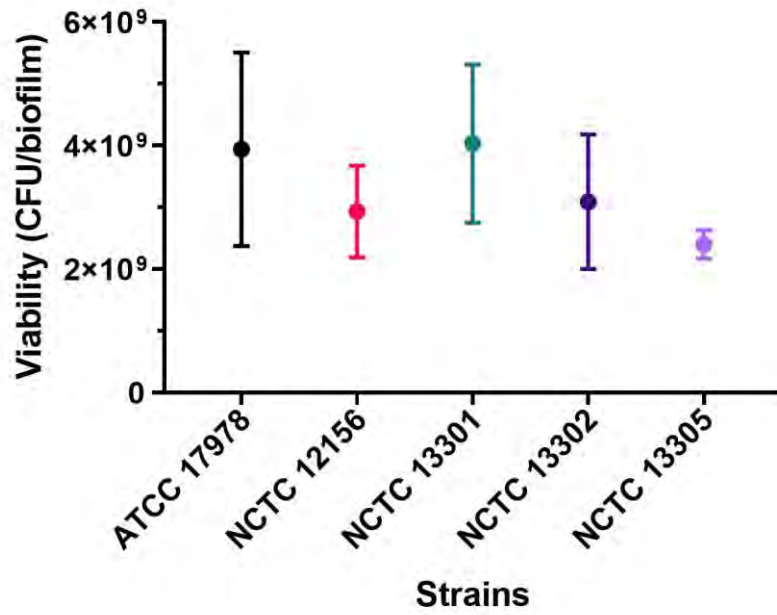


**Figure 3.3: Viable counts from colony biofilms show no significant difference between strains**

A 5  $\mu$ l spot of overnight bacterial culture diluted to  $\sim 0.5$   $OD_{600nm}$  was placed in the centre of a polycarbonate track-edged filter membrane resting on an MHA plate and incubated for 24 hours. After 24 hours the membrane still holding the growing colony biofilm was added to a fresh MHA plate and the plates were incubated for a further 24 hours. At the end of the time period, bacterial biofilms were imaged and subsequently washed from the membrane and viable counts were performed. All biofilms formed had viable counts of approximately  $3.09 \times 10^9 (\pm 1.63 \times 10^9)$  CFU/biofilm. (N=3  $\pm$  SEM, one-way ANOVA with Tukey's multiple comparison showed no significant difference between strains).

### 3.2.4 96-well biofilm formation assay reveals *Acinetobacter baumannii* NCTC 13302, 13305 and 12156 are the strongest biofilm producers

*A. baumannii* biofilms were assayed in MHB media in a 96-well plate to determine biofilm formation in a simple static biofilm assay with a solid – liquid interface. To evaluate the size of the biofilm formed crystal violet was added to biofilms and the absorbance was recorded. NCTC 12156 was the strongest biofilm former in MHB followed by NCTC 13302 and NCTC 13305 with NCTC 13301 producing the least amount of biofilm (Figure 3.4). A one-way ANOVA with Tukey's multiple comparisons test revealed that there were significant differences between ATCC 17978 and NCTC 12156 ( $P = 0.0017$ ), NCTC 12156 and NCTC 13301 ( $P = 0.0004$ ) and NCTC 13301 and NCTC 13302 ( $P = 0.0352$ ). NCTC 13302 consistently produced the largest amount of biofilm of the Type D Carbapenemase strains, making it suitable for further biofilm and antimicrobial studies.

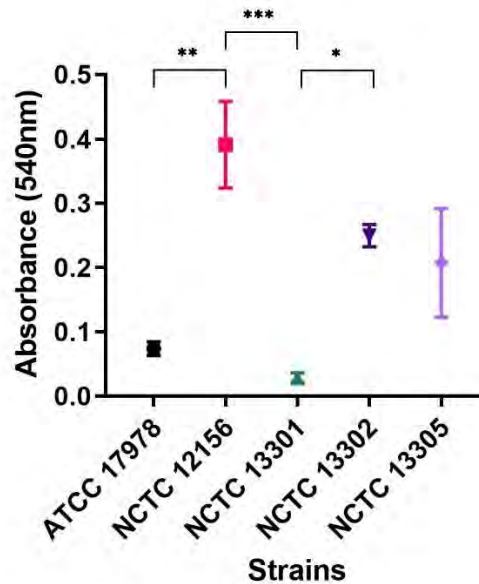


**Figure 3.4: 96-well plate biofilm assays showed variable biofilm formation between strains**

10  $\mu$ l of bacterial overnight culture diluted to 0.05  $OD_{600nm}$  was added to 90  $\mu$ l of MHB within a 24 well plate and plates were incubated overnight for 18 hours. After which the media was removed, and wells were washed to remove any unbound cells before remaining biofilms were stained with crystal violet. The resulting absorbance readings from the recovered crystal violet staining are shown above. P values: \*\*\* = 0.0004, \*\* = 0.0017, \* = 0.0352.  $N=5 \pm SEM$ .

### **3.2.5 EUCAST disk diffusion assays show that the carbapenem resistant strains have resistance to antibiotics that are effective against type strains**

To understand the antibiotic susceptibility profiles of the carbapenem resistant strains; disk diffusion assays were carried out according to the EUCAST method with the results shown in Table 3.3. As expected, the Type strain (NCTC 12156) and the clinical strain (ATCC 17978) generally showed the greatest sensitivity to the antibiotics tested. NCTC 13301 and NCTC 13302 had the highest resistance levels whilst NCTC 13305 was occasionally sensitive to antibiotics that the other carbapenemase producing strains were resistant to.

**Table 3.3: Antibiotic resistance profiles of *A. baumannii* strains using EUCAST disk diffusions. Red = resistant, green = sensitive, yellow = intermediate sensitivity.**

Class	Strain →	NCTC 12156	ATCC 17978	NCTC 13301	NCTC 13302	NCTC 13305	Breakpoints	
	Antibiotic ↓	Zone diameter (mm ±SD)	>S (mm)	≤R (mm)				
Carbapenems	Imipenem	33 (±0)	29.5 (±0.71)	11 (±0)	0 (±0)	18.5 (±0.71)	24	21
	Doripenem	27.5 (±0.71)	29 (±0)	12.5 (±0.71)	0 (±0)	20.5 (±0.71)	50	22
	Meropenem	30 (±0)	29 (±1.41)	11.5 (±0.71)	0 (±0)	18 (±0)	21	15**
Aminoglycosides	Amikacin	18 (±0)	17.5 (±0.71)	3.5 (±4.95)	8.5 (±0.71)	0 (±0)	19	19
	Gentamicin	12 (±0)	19 (±0)	0 (±0)	0 (±0)	0 (±0)	17	17
	Tobramycin	17 (±0)	19 (±0)	0 (±0)	12 (±0)	10 (±0)	17	17
Cephems, inc. Cephalosporins I, II, III and IV	Ceftazidime	23 (±1.41)	23 (±0)	0 (±0)	0 (±0)	20 (±0)	18	14
	Cefepime	20.5 (±0.71)	22.5 (±0.71)	12 (±0)	14 (±0)	25 (±0)	18	14
	Cefotaxime	18.5 (±0.71)	19.5 (±0.71)	0 (±0)	0 (±0)	9.5 (±0.71)	23	14
	Ceftriaxone	15.5 (±0.71)	19.5 (±0.71)	0 (±0)	0 (±0)	10 (±0)	21	13
Fluoroquinolones	Ciprofloxacin	26.5 (±0.71)	27.5 (±0.71)	0 (±0)	0 (±0)	26.5 (2.12)	50	21
	Levofloxacin	30 (±0)	29.5 (±0.71)	10.5 (±0.71)	13.5 (±0.71)	29 (±1.41)	23	20

\* Antibiotics highlighted in cream use the CLSI M100 (2020) breakpoints as no breakpoints were available through EUCAST (2021)

\*\* For meningitis, Meropenem resistance breakpoint is 21 mm

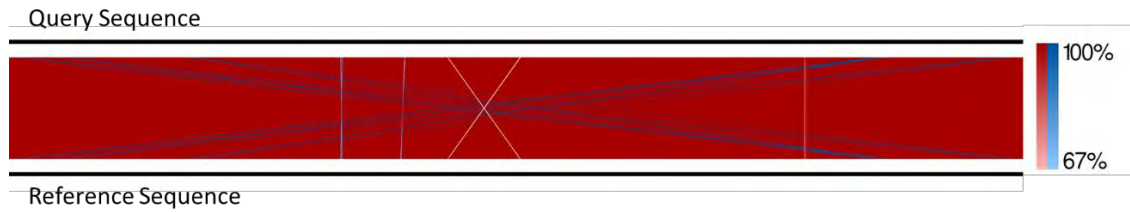
### 3.2.6 Genome sequencing of NCTC 13302

*A. baumannii* NCTC 13302 is a Type D carbapenemase reference strain available through Public Health England, with a published genome (Accession number: NZ\_UIGA01000001). As NCTC 13302 was the strain chosen for future chapters, it was important to check that the genome of the strain received matched the published genome. Hybrid *de novo* whole genome sequencing was carried out using both Oxford nanopore and Illumina reads. After completion, comparisons of the chromosome and the largest plasmid (>151443bp) to their counterparts in the reference sequence were performed using BLAST and EasyFig 2.2.2.

In both the chromosome (Figure 3.5A) and the plasmid (Figure 3.5B), there were no major insertions or deletions in comparison to the reference strain, however there were a few points where NCBI BLAST identified a sequence match in an alternate position on the reference sequence. In the chromosomal sequence, there were also a few inversions, where the gene sequence inversely matched another sequence in a different place. However, despite these extra matches, the dark red at these points indicates that the Query sequence matches the same point on the Reference sequence with a high percentage of accuracy.

An analysis in CLIMB-BIG-DATA with the program snippy, searched for single nucleotide polymorphisms, and one base pair insertion was found on the chromosome and no single nucleotide polymorphisms were identified on the plasmid. The chromosomal insertion caused a frameshift mutation due to the presence of a TG motif where in the reference strain it was only a T. A BLAST search revealed this frameshift mutation to be ~50 bp away from the end of a urea aminohydrolase subunit  $\alpha$  gene. This gene is duplicated immediately downstream of the gene containing the frameshift, but without the insertion suggesting that change will have little impact upon the strain phenotype.

**A.**



**B.**



**Figure 3.5: Genome comparison between Query Sequence and the Reference Sequence**

*De novo* whole genome sequencing was carried out on the lab *A. baumannii* NCTC 13302 query sequence and compared to the published reference genome (NZ\_UIGA01000001). The dark red colour indicates that for the A) chromosome and B) plasmid, the sequences matched with a high percentage in the forward direction. The thick black lines running horizontally along the top and bottom of the red colour block represent the genome sequences with the top sequence being the Query Sequence (from our laboratory strain) and the bottom line is the Reference Sequence for the published strain. Blue lines indicate where there are inverse matches while red lines indicate matches in the forward direction. The intensity of each colour corresponds to the percentage accuracy of the match. Images were generated in EasyFig 2.2.2.

### 3.3 Discussion

This chapter aimed to understand the phenotypic characteristics of strains containing Type D carbapenemases in comparison to a type strain (NCTC 12156) and a clinical strain (ATCC 17978) that do not contain these enzymes. A secondary aim of this chapter was to determine which strain to use for subsequent Drip flow biofilm reactor and the silver acetate studies.

While most work in the study utilised MHB as the growth media, the growth curves in rich, defined and semi-defined media, gave an idea of the biosynthetic capacity of the strains and how they would grow if an experiment required the use of a media where all the components could be controlled and were known. MHB is a rich medium containing beef infusion, starch, and casein hydrolysate. When bacteria grow in this media the precise components are not known and batch to batch variation can become an issue, use of defined and semi-defined media provides some control over the bacterial receipt of nutrients. In this case, it was found that the defined M9 minimal media, with defined amino acids caused less growth than the other two media types, while the M9 media supplemented with hydrolysed casein, provided higher final cell densities to be achieved. Casein hydrolysate supplies a higher concentration of amino acids<sup>195</sup> than MEM amino acids (Thermofisher Scientific) so M9 minimal media supplemented with hydrolysed casein was better able to meet the nutritional requirements of *A. baumannii* due to higher availability of nutrients.

The colony biofilm and 96-well plate biofilm assay were experiments carried out to understand how well the strains of *A. baumannii* formed biofilms on solid media and in liquid media. *A. baumannii* is a bacterial strain that forms biofilms well on abiotic surfaces such as catheters, endotracheal tubes and artificial heart valves due to the presence of biofilm formation factors such as the Csu pili which enable bacterial attachment to abiotic surfaces<sup>55,65</sup>. Biofilm formation is an important virulence factor for this pathogen and while there were no differences in the amount of biofilm formed on the solid media in the colony biofilm assay, there were differences in the amount of biofilm formed in liquid media in the 96-well plate biofilm assay.

The colony biofilm assay carried out in this way may not have been the most effective method to study biofilm formation on a surface because the colonies were only incubated for 48 hours. Due to the short incubation period, it was hard to distinguish between what

could have been a large colony and what was a biofilm, and biofilms may not have had the chance to form yet. A better alternative would have been to incubate the biofilms in duplicate for 7 days, measuring the thickness and diameter of the colony each day for one sample and analysing the viability with the second sample as done in Singla, Harjai and Chhibber (2014).

Nevertheless, as the biofilm model developed in Chapter 5 produces biofilms formed in liquid media, a strain was selected for further study that grew a sufficient biofilm at a solid-liquid interface. While there was no significant difference between the amount of biofilm formed by NCTC 13302 and NCTC 13305 in the plate biofilm assay, the amount of biofilm formed by NCTC 13305 was not significantly different from NCTC 13301, the strain with the lowest biofilm formation. The results for NCTC 13305 also contained the greatest variation. NCTC 13302 produced less variation and produced significantly more biofilm than NCTC 13301 and this result influenced the decision to carry NCTC 13302 into the work with the modified Drip Flow Reactor®.

Using the available annotated genomes (Table 3.4) it was possible to compare the presence of some of the key biofilm proteins, Bap, OmpA, PNAG and the Csu pili within the five strains. NCTC 12156, NCTC 13302 and NCTC 13305 all contained representations of Bap, OmpA, PNAG and the Csu pili. NCTC 13301 contained OmpA, the Csu pili and PNAG, but did not contain BAP, and ATCC 17978 only contained PNAG. Bap is the protein responsible for maturation of a biofilm and increased biovolume and thickness, PNAG is an important polysaccharide protein present in the biofilm, OmpA is the major porin in *A. baumannii* and has a role in membrane stability and anchoring of the Csu pili which is involved in adhesion of bacterial cells to abiotic surfaces<sup>65-68</sup>. The lack of these proteins in both strains is the likely cause of the reduced biofilm formation in the plate biofilm assay and with further time, it may have been possible to spot differences in biofilm formation in the colony biofilm assay.

**Table 3.4: Origins of annotated genomes for comparison of biofilm formation genes.**

Strain	Origin
NCTC 12156	GCA_900444725.1
NCTC 13301	GCA_900444735.1
NCTC 13302	GCA_900444745.1
NCTC 13305	GCA_900444775.1
ATCC 17978	American Type Culture Collection <sup>196</sup>

As previously stated, *A. baumannii* is a bacterium that is regularly multi-drug resistant, with some pan-drug resistant strains appearing across the globe<sup>191</sup>. To understand the resistance profiles of the strains, a series of disk diffusion assays were carried out with a range of antibiotics from different groups and with differing mechanisms of action. It was interesting to see here that while NCTC 13301 and NCTC 13302 were resistant to every antibiotic tested, NCTC 13305 was not and had some intermediate and sensitive resistances suggesting that NCTC 13301 and NCTC 13302 may hold additional mechanisms of resistance to other antibiotic classes which NCTC 13305 does not have.

NCTC 13301 had more resistance to antibiotics of other classes when compared to NCTC 13302, but NCTC 13302 contained more resistance to the carbapenems than NCTC 13301 which agrees with what is usually seen in isolates from hospitals<sup>192,197,198</sup>. NCTC 13305 was only resistant to imipenem and had intermediate sensitivity to meropenem and was sensitive to doripenem. The difference in the sensitivity to carbapenems between the strains is due to the OXA-genes that each strain holds. The OXA-23 and OXA-24 enzymes alone are able to confer resistance to carbapenems, while OXA-58 does not always confer resistance<sup>192</sup>. Héritier *et. al.* (2005) found that when the OXA-58 gene is transformed into a sensitive bacterial strain, only weak resistance is conferred and it is not enough to determine resistance<sup>45</sup>. However when they transformed the same gene into bacteria that over expressed an efflux pump, the resistance levels increased, highlighting that this gene may rely on other mechanisms to confer resistance<sup>45</sup>.

Despite the presence of a published genome for *Acinetobacter baumannii* NCTC 13302, *de novo* whole genome sequencing was carried out. This was done for two reasons, firstly to check that the genome matched the published version and didn't have any

insertions/deletions and secondly as a training exercise as bioinformatics and genome sequencing are highly important skills in modern microbiology research. There were no major gaps or insertions in the genome sequence of our strain obtained from Public Health England and the sequence matched the reference sequence with a high percentage accuracy. This meant that we could confidently proceed using this strain knowing that its identity was correct, and no significant mutations had occurred during handling and storage of the strain.

The single insertion, in the form of a TG motif where originally there was only a T, is potentially a source of interest, as this was found in a urea amidohydrolase subunit  $\alpha$  gene which codes for a urease responsible for the catalysis of ammonia<sup>199</sup>. However, the same gene was then repeated directly after in the sequence without the frameshift mutation. This reading could potentially be an error as sequencing errors are still possible with hybrid sequencing, or it could represent a true change in sequence. This would produce a protein with an unrecognisable C terminal region due to a frameshift mutation towards the end of the gene. To test this, the gene could be sequenced using Sanger sequencing to confirm the presence of the insertion.

In conclusion, this chapter provides preliminary data on the biofilm formation capabilities of the *A. baumannii* strains and justifies the use of NCTC 13302 as the Type D Carbapenemase strain chosen for further study. The reasoning for this is that the strain demonstrates an MDR phenotype and produces a significantly higher amount of biofilm than NCTC 13301 and was more consistent across repeats than NCTC 13305. The presence of the OXA-24 gene confers antibiotic resistance to carbapenems at a level greater than the more common OXA-23 gene. While the OXA-23 gene is more common than OXA-24 it is found increasingly in the united states and Asia<sup>192</sup> and in a recent study in Iran, 30% of the *A. baumannii* ventilator associated pneumonia isolates on an ICU ward contained the OXA-24 gene<sup>193</sup>.

## 4 The *in vitro* and *in vivo* antimicrobial activity of silver acetate against *Acinetobacter baumannii*

### 4.1 Introduction

The use of silver as an antimicrobial dates back as far as 4000 BC when silver was first discovered. In the years following, silver has had many uses including to preserve food and water after the realisation that food and drink lasted longer when kept in silver containers<sup>83</sup>. Silver was used in medicine from 1000 BC<sup>84</sup> and is still in use today as an antimicrobial<sup>90</sup>.

Currently silver is used in various applications including creams, wound dressings and coatings in the form of silver sulphadiazine and silver nitrate but in its inert state elemental silver has no antimicrobial effect<sup>90</sup>. When in liquid, silver dissociates to the silver cation  $\text{Ag}^+$  and it is this that is biologically active, many studies have found that there is a direct correlation between the concentration of silver ions in a solution and lethality to bacteria<sup>90,105</sup>. Silver ions have an oligodynamic effect on bacterial cells, to gain entry into cells,  $\text{Ag}^+$  ions must first bind to electron donor receptors on the bacterial membrane and once bound the ions are transported across the cell membrane via endocytic vacuoles<sup>90,105</sup>.

Inside the cell, silver ions are able to bind with numerous targets, they bind to sulphhydryl groups on amino acids, disrupting protein function<sup>84</sup>, they are thought to disrupt iron-sulphur clusters<sup>90</sup>, thiol groups and sulphhydryl-liganded metals<sup>109</sup>. They also bind to the bases of DNA and RNA<sup>110</sup>, which is thought to be responsible for mutation and issues with replication, however this has yet to be proven *in vivo*. There is also evidence of the role for silver in membrane disruption causing enhanced permeability<sup>109</sup>.

When silver enters the human body, the excretory system usually removes it without lasting effects<sup>90</sup> however at high quantities, silver can accumulate in the skin and cause a rare, greyish discoloration known as agyria, which was more common in the earlier uses of silver<sup>83</sup>. There have been only a few cases of agyria in recent years, due to prolonged exposure to the metal, either via ingestion, or via the use of wound dressings<sup>90,108,200</sup>.

There is currently significant interest in silver nanoparticles and their application as they have a large surface area to volume ratio and thus a higher potency<sup>98</sup>. However, these particles are not yet approved for use on humans in medicine due to questions surrounding their safety<sup>98,103,104</sup>, despite their use in commercial items such as toys, deodorants and toothpaste<sup>102</sup>. For medical applications, silver is usually administered as silver salts (e.g. silver sulphadiazine and silver nitrate) which can be irritants<sup>84</sup>. Silver acetate is a silver salt that is currently used as an antimicrobial coating in commercially available grafts<sup>201</sup>, however there is little data on the efficacy of silver acetate, and none surrounding the efficacy of silver acetate on *A. baumannii*.

As a therapeutic agent, it is important to understand the efficacy of silver acetate in living systems, to ensure that the silver salt can be administered in concentrations that are both safe to the host and toxic to the infecting pathogen. *G. mellonella* larvae are used as *in vivo* models to test toxicity of compounds and pathogenesis<sup>202–204</sup>, because the immune systems of *G. mellonella* larvae are comparable to those of mammalian systems in that they possess humoral and cellular immunity<sup>203,205,206</sup>. This immunity makes them a useful model for pathogenesis and antimicrobial testing<sup>203,207</sup>. *G. mellonella* larvae are increasingly used as a high-throughput ethically viable alternative to mammalian models for testing toxicity of compounds to the host<sup>208–211</sup>. One recent study compared the toxicity of exposure to eight different food preservatives in both *G. mellonella* and rat models, concluding that there was a strong correlation between the LD<sub>50</sub> values of those preservatives in *G. mellonella* larvae and rats providing evidence of the suitability of this model for preliminary toxicity testing<sup>212</sup>.

When exposed to a pathogen, the larvae undergo a series of responses including melanisation, which is a visible reaction to infection and an indicator of immune response within the larvae<sup>213</sup>, therefore melanisation can be used as an indicator of larval health. Upon recognition of a foreign body, the prophenoloxidase cascade is activated which results in melanin production<sup>214</sup>. Melanin aids clotting of the larval haemolymph which aids phagocytosis by plasmocytes and granulocytes<sup>204</sup> and is a good indicator of an active immune response. This melanisation of the larvae results in a brown discolouration of the skin (Figure 4.1).



**Figure 4.1: Melanisation of *G. mellonella* larvae upon infection**

*G. mellonella* larvae are shown to produce a brown discolouration (melanisation) upon the activation of the larval immune response. Melanisation can start off as small brown spots appearing around the tail or along a line across the back. As the infection continues and the larval health declines, this brown discolouration can completely cover the body of the larva.

The first aim of this chapter was to elucidate the efficacy of silver acetate as an antimicrobial agent against a carbapenem resistant strain of *A. baumannii* *in vitro*. The second aim was to determine the toxicity of silver acetate in an *in vivo* *G. mellonella* larvae model and to determine whether silver acetate would act as an effective treatment against an *A. baumannii* infection.

The data in this chapter has been published in: Mannix-Fisher, E and McLean, S. 2021. 'The antimicrobial activity of silver acetate against *Acinetobacter baumannii* in a *Galleria mellonella* infection model'. PeerJ. DOI 10.7717/peerj.11196

## 4.2 Results

### 4.2.1 Silver acetate minimum inhibitory/bactericidal concentration assays for several *A. baumannii* strains shows silver acetate is bactericidal

The antimicrobial activity of silver acetate has been demonstrated for several bacterial species but has yet to be determined for *A. baumannii*<sup>215-218</sup>. To determine the antimicrobial activity of silver acetate against *A. baumannii*, the five strains of *A. baumannii* described in Chapter 3 were tested against serially diluted concentrations of silver acetate in MIC and MBC assays, to determine whether the mechanism of action was bactericidal or growth inhibitory.

Silver acetate was shown to be a potent antimicrobial with the compound having an MIC of  $4.56 \pm 1.59$  mg L<sup>-1</sup> or less for all strains tested (Table 4.1). The strains ATCC 17978 and NCTC 13305 appeared to be more resistant to silver acetate, however the sensitivity levels for all strains do not vary significantly.

Silver acetate is suggested to be a bactericidal compound based on the MBC results shown in Table 4.1. For strains NCTC 12156, NCTC 13302 and NCTC 13305 a Wilcoxon matched-pairs signed rank test revealed there is a significant difference between the MIC and the MBC of silver acetate ( $P = 0.0313$ ). There is no significant difference between the inhibitory and bactericidal concentrations for strains NCTC 13305 and ATCC 17978.

**Table 4.1 Minimum inhibitory and bactericidal concentrations for silver acetate against a range of *A. baumannii* strains demonstrates significant antimicrobial activity**

Bacterial Strain	Type/Orgin	MIC mg L <sup>-1</sup> (±SD)	MBC mg L <sup>-1</sup> (±SD)
ATCC 17978	Clinical Isolate	4.56 (1.59)	9.11 (3.19)
NCTC 12156	Type strain	3.91 (0)	7.81 (0)
NCTC 13301	Type D carbapenemase reference strain OXA-23	3.91 (0)	6.64 (2.62)
NCTC 13302	Type D carbapenemase reference strain OXA-25	3.91 (0)	7.81 (0)
NCTC 13305	Type D carbapenemase reference strain OXA-58	4.56 (1.59)	13.03 (9.49)

\*N = 3 ± SD

#### **4.2.2 Biofilm formation of NCTC 13302 is significantly reduced when exposed to the minimum inhibitory concentration of silver acetate**

As biofilms are a major source of infection, it was necessary to elucidate the effectivity of silver acetate against *A. baumannii*, a bacterial species that readily forms biofilms. Bacteria grown overnight were incubated in a 24-well plate in Mueller-Hinton Broth containing varying concentrations of silver acetate from 0 to 7.81 mg L<sup>-1</sup> and using crystal violet staining, the amount of biofilm formed overnight was observed. (Figure 4.2:A). At concentrations below the MIC, there was no significant difference in the absorbance of crystal violet and therefore the amount of biofilm formed, in comparison to the negative control that contained no silver acetate. When the bacteria are incubated in the presence of silver acetate at the MIC (3.91 mg L<sup>-1</sup>), or two-fold higher (7.81 mg L<sup>-1</sup>) there was a low absorbance level of crystal violet and therefore a smaller amount of biomass in the well, potentially due sedimentation, but was significantly lower than in the absence of silver acetate (ANOVA and a Tukey's multiple comparison test,  $p < 0.0001$ ).

The biofilm growth assay was repeated as above and used to enumerate the viable cells in the biofilm after exposure to varying concentrations of silver acetate. Figure 4.2:B shows that there is no significant difference between the viability of cells when the biofilm is exposed to concentrations of silver acetate below the MIC compared to the no silver control. In the presence of silver acetate at the MIC there are few viable cells remaining, whilst at twice this concentration, no cells remain viable.

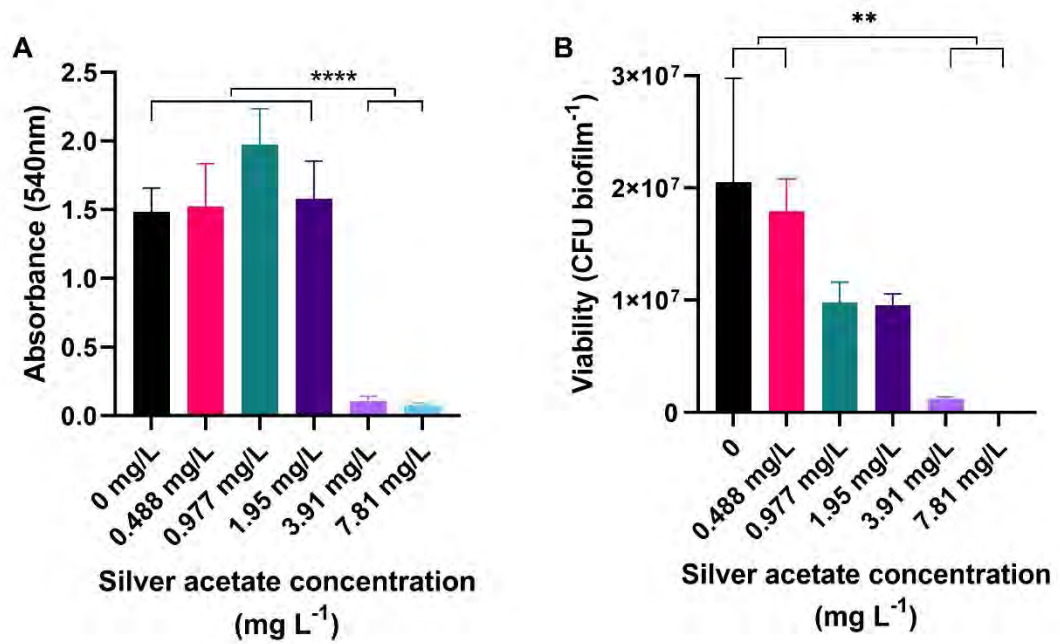


**Figure 4.2: Crystal violet staining and viability of biofilms is reduced in the presence of silver acetate at the MIC indicating less biofilm production**

*A. baumannii* cultures were incubated statically in Mueller-Hinton broth at 37 °C in 24-well plates in the presence of varying concentrations of silver acetate (0 - 7.8 mg L<sup>-1</sup>). (A) After incubation, the wells were washed and stained with crystal violet to determine the amount of biofilm formed (OD<sub>540</sub>). Differences in biofilm formed between the lower (0 – 1.95 mg L<sup>-1</sup>) and higher (3.9 - 7.8 mg L<sup>-1</sup>) concentrations of silver acetate were highly significant (ANOVA and Tukeys multiple comparison test, \*\*\*\*P < 0.0001). (B) After incubation, biofilms were disaggregated, and bacterial viability was determined. Significant differences in biofilm formation were observed between the lowest (0 – 0.49 mg L<sup>-1</sup>) and highest concentrations of silver acetate (3.9 - 7.8 mg L<sup>-1</sup>, ANOVA and Tukey’s multiple comparison, \*\*P = 0.0005 - 0.003) N = 3 ± SEM.

### **4.2.3 The permanence of silver acetate toxicity against exponentially growing *Acinetobacter baumannii* is concentration dependent**

In most infection situations, antimicrobial intervention occurs when the infection is established and at this point, the bacterial load will be high, and the pathogen will be actively growing. Therefore, after the identification of the minimum inhibitory concentrations of silver acetate against *A. baumannii* I sought to determine how exposure of exponentially growing bacteria to silver acetate at a range of concentrations impacted growth and viability.

At concentrations below the MIC for silver acetate (3.91 mg L<sup>-1</sup>) Figure 4.3 shows that there is no effect on the growth of the bacteria, a two-way ANOVA with Tukey's multiple comparison stated there was no significant difference between these concentrations and the no silver control at 0, 8, 16 and 24 hours. At 7.8 and 15.6 mg L<sup>-1</sup> bacterial growth was inhibited and significantly different ( $P < 0.0001$ ) from the concentrations lower than the MIC for the duration of the experiment. Figure 4.4 shows that bacteria were killed at these concentrations. Surprisingly, bacteria exposed to 3.91 mg L<sup>-1</sup> silver acetate initially showed a decrease in absorbance (Figure 4.3:C), however at 10 hours the absorbance began to recover. This recovery was also observed in the viability data (Figure 4.4) where at 8 hours there was a significant difference ( $P < 0.05$ ) in the viability of bacteria exposed to 3.91 mg L<sup>-1</sup> versus bacteria exposed to 1.95 mg L<sup>-1</sup>. At 24 hours the viability of bacteria at these two concentrations was no longer significantly different as bacterial growth at the MIC had increased.

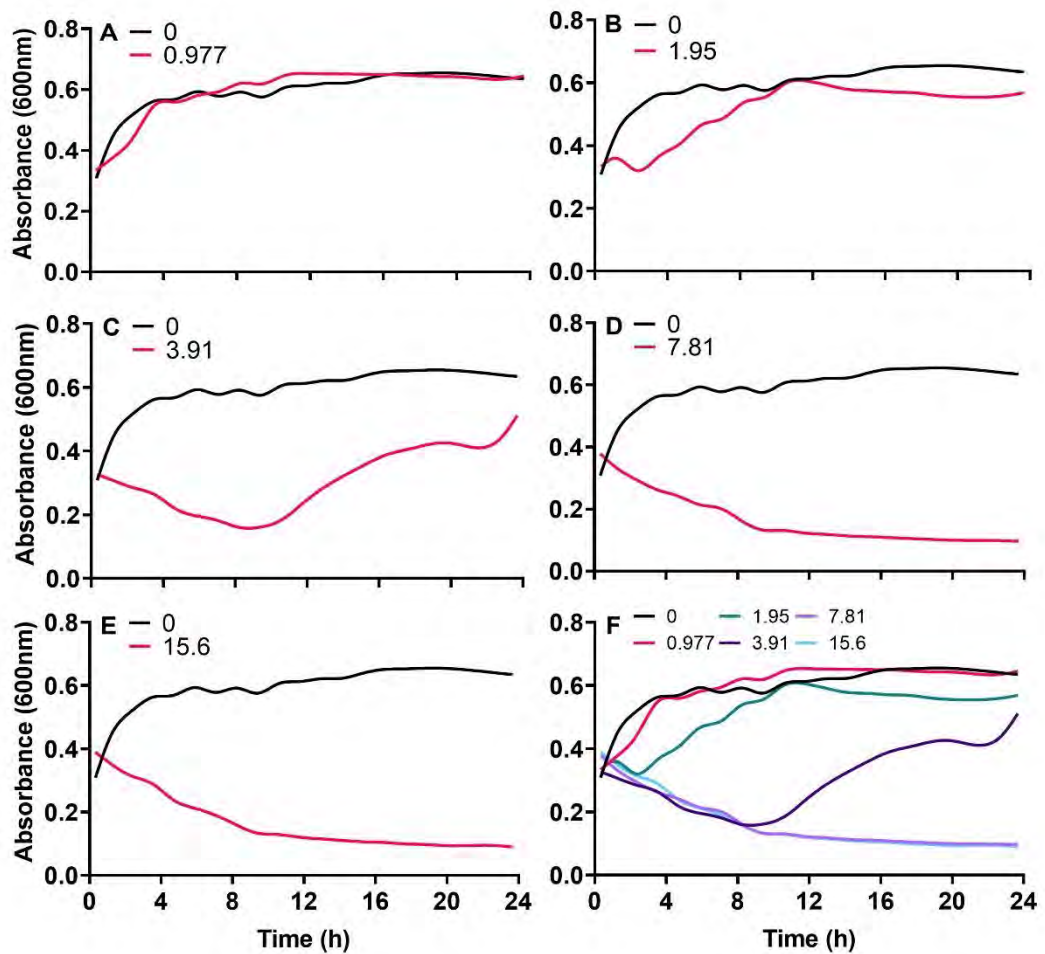


**Figure 4.3: The inhibition of exponentially growing *Acinetobacter baumannii* is dependent on the concentration of silver acetate**

Silver acetate was added to exponentially growing cultures at final concentrations of (A) 0.98, (B) 1.95, (C) 3.91, (D) 7.81 and (E) 15.60 mg L<sup>-1</sup>. Cultures were incubated at 37 °C with shaking and growth monitored via absorbance (OD<sub>600</sub>) every 20 min for 24 h. (F) Panel shows growth in the presence of all concentrations of silver acetate for comparison. N = 3, error bars are omitted for clarity, but standard deviations were all within the range 0.0006 – 0.1664.

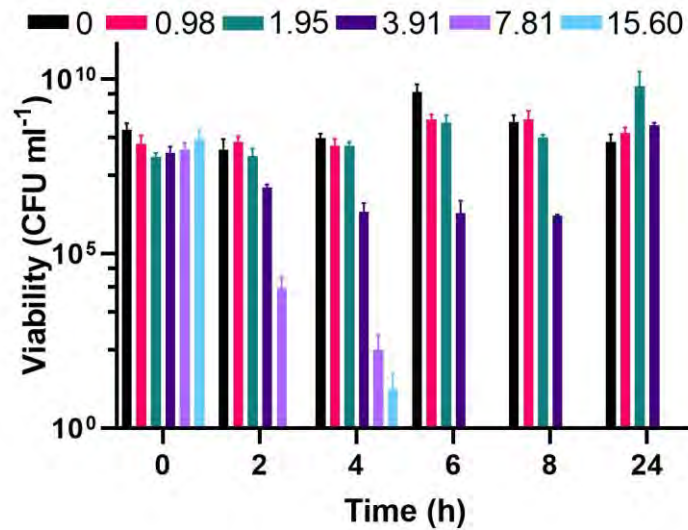


**Figure 4.4: The bactericidal effect of silver acetate on *Acinetobacter baumannii* is concentration dependent**

Batch cultures of *A. baumannii* were grown at 37 °C with shaking to early exponential phase when silver acetate was added at final concentrations of 0, 0.98, 1.95, 3.91, 7.81 or 15.60 mg L<sup>-1</sup> (t = 0 h). Cultures were incubated for a further 24 h with viability determined at two-hour intervals to eight hours post-exposure (t = 2 - 8 h) and at 24 h. N = 3 ± SEM.

#### **4.2.4 The *Galleria mellonella* *in vivo* model is an excellent model to study the pathogenicity of *Acinetobacter baumannii* and test the toxicity of silver acetate**

*Galleria mellonella* larvae are insects within the order lepidoptera that have recently gained popularity as useful models to study bacterial pathogenesis and compound toxicity. The following experiments utilised these models to test first for a concentration of *A. baumannii* cells that causes a significant decrease in larval survival and then the toxicity of silver acetate to the *G. mellonella* larvae. The final experiment determined whether silver acetate at levels non-toxic to the host could increase the survival of larvae infected with concentrations of *A. baumannii* that caused significant larval death, providing data on how well silver acetate could work as a treatment of such infections.

##### **4.2.4.1 *Galleria mellonella* infected with *Acinetobacter baumannii* NCTC 13302 at a concentration of $1.7 \times 10^6$ cells per larvae provides a survival rate of 20%**

Initial testing in this study sought to determine the virulence of NCTC 13302 using a *G. mellonella* infection model and determine the concentration of bacteria that provided 20% survival. Figure 4.5:A shows survival of the larvae over 96 hours, with the lowest concentration of bacteria injected ( $1.7 \times 10^2$  bacteria per larva) showing no significant difference in larval death compared to the negative controls. The highest concentration of bacteria ( $1.7 \times 10^7$  bacteria per larva) killed all larvae within 24 - 48 hours and intermediate concentrations killed varying numbers of larvae over the four-day incubation. Melanisation (Figure 4.5:B) was monitored as an indicator of health of the larvae with a score of four being completely healthy larvae. This data supported the survival data with decreased health observed with increased bacterial load.

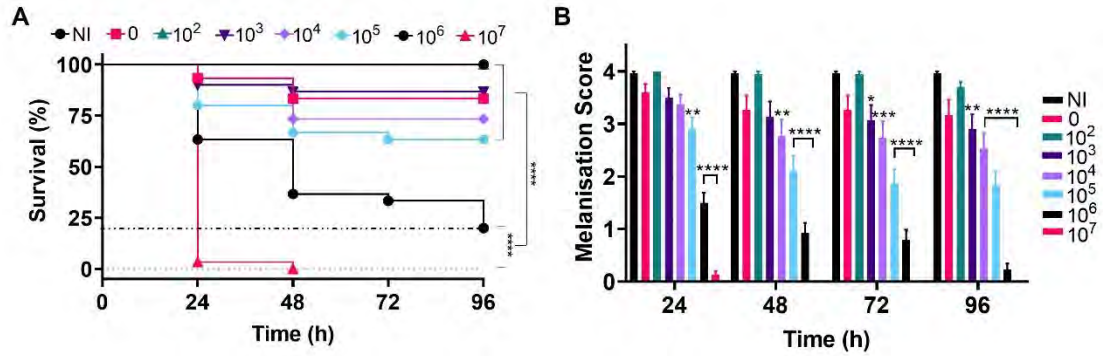


**Figure 4.5: Exposure of *Galleria mellonella* larvae to a different concentrations of *Acinetobacter baumannii* NCTC 13302 causes differing levels of immune response and lethality**

Groups of *G. mellonella* larvae were injected with 10  $\mu$ l of *A. baumannii* containing between  $1.7 \times 10^2$  to  $1.7 \times 10^7$  cells per larvae, control groups were injected with PBS or were not injected. (A) Larval survival was monitored every 24 h for 96 h post-injection. The dotted line corresponds to 80 % larval death (\*\*\*\* P < 0.0001, N = 30 larvae per condition) (B) Melanisation was recorded for all larvae every 24 h for 96 h post-injection a standard melanisation score (\*P = 0.0423, \*\*P = 0.001-0.0063, \*\*\*P = 0.0006, \*\*\*\*P < 0.0001, N = 30 larvae per concentration,  $\pm$  SEM).

#### **4.2.4.2 A range of silver acetate concentrations commonly used in antibiotic therapy shows minimal toxicity to *Galleria mellonella***

For an antimicrobial to be appropriate for therapy it should display two key features: antimicrobial activity against the target pathogen(s) and minimal toxicity towards the host. The *G. mellonella* model was used to determine the toxicity of silver acetate towards the host over a variety of clinically relevant concentrations.

Larvae were divided, treated and monitored in the same way as for the infection study (Figure 4.5) except silver acetate was administered to the larvae in concentrations ranging from 0 – 80 mg kg<sup>-1</sup> of animal weight (approximately 0 – 24 µg silver acetate per larvae). The data here demonstrated that only the 80 mg kg<sup>-1</sup> dosage caused persistent larval death of just above 10% (Figure 4.6:A). A Log rank (Mantel-cox) test showed a significant difference between the survival of larvae at 80 mg kg<sup>-1</sup> silver acetate versus the other concentrations ( $p < 0.05$ ). The melanisation scores reflected these results as only the larvae exposed to the highest concentration of silver acetate showed any visible melanisation and therefore a decrease in health (Figure 4.6:B). However, a multiple comparisons test of the melanisation scores showed that there were no significant differences between the melanisation scores until hour 72 when significant differences developed between the 80 mg kg<sup>-1</sup> concentration and the other concentrations.

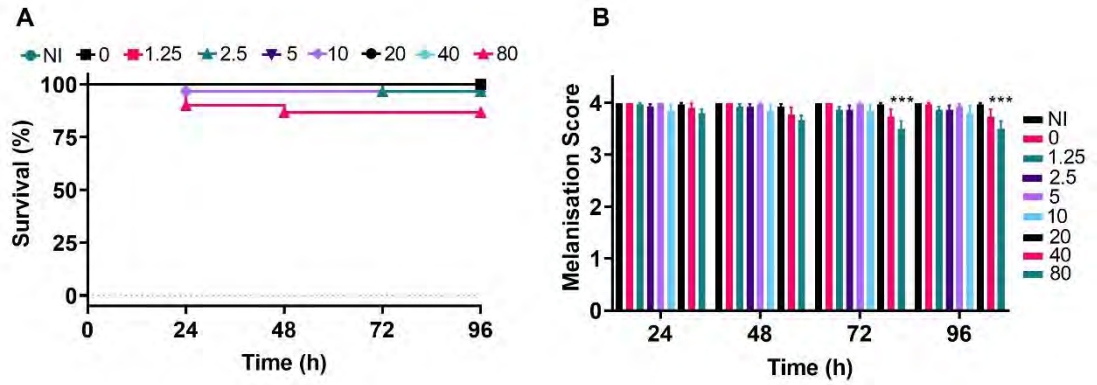


**Figure 4.6: A range of medically relevant silver acetate concentrations shows minimal toxicity to *Galleria mellonella***

Groups of *G. mellonella* larvae were injected with 10  $\mu$ l of silver acetate between 0 – 80 mg kg<sup>-1</sup> animal weight. (A) Larval survival was monitored every 24 h for 96 h post-injection (N = 30 larvae per condition). (B) Melanisation was recorded for all larvae every 24 h for 96 h post-injection and assigned a standard melanisation score (\*\*P = 0.0006, N = 30 larvae per condition,  $\pm$  SEM).

#### **4.2.4.3 Treatment of *Galleria mellonella* larvae infected with *Acinetobacter baumannii* NCTC 13302 with silver acetate increased the survival and health of the larvae**

To address whether silver acetate is an effective antimicrobial against infection in a *Galleria mellonella* infection model, larvae were injected with concentrations that would cause significant larval death within 96 hours without intervention (Figure 4.5,  $1.7 \times 10^5$  and  $1.7 \times 10^6$  cells per larvae). Thirty minutes post-infection, the larvae were administered with 10 or 20 mg kg<sup>-1</sup> silver acetate, both concentrations having demonstrated minimal toxicity to galleria (Figure 4.6).

As expected, larvae injected with the  $1.7 \times 10^5$  bacterial cells per larvae were better able to survive than larvae injected with the  $1.7 \times 10^6$  bacterial cells per larvae both in the absence and presence of silver acetate (Figure 4.7). Larvae infected with the lower infectious dose showed an increase in survival of 20% at both doses of silver acetate (Figure 4.7:A). For larvae receiving the higher infectious dose, 10 mg kg<sup>-1</sup> silver acetate treatment caused an increase in larval survival of 31% and 20 mg kg<sup>-1</sup> increased survival by 27% (Figure 4.7:B). This difference in survival between the two doses of antimicrobial was not statistically significant.

Correlating with the increased survival, improved larval health was also observed (Figure 4.7:C+D). As with the infection studies (Figure 4.5) the melanisation score of untreated larvae injected with both  $1.7 \times 10^5$  and  $1.7 \times 10^6$  bacterial cells per larvae showed a significant reduction in health between 48 and 72 hours. Larvae that were treated with silver acetate began to show significant differences in health by 72 hours (larvae injected with  $\sim 10^5$  bacteria) and 96 hours (larvae injected with  $\sim 10^6$  bacteria) ( $P < 0.042$  and  $< 0.009$  respectively).

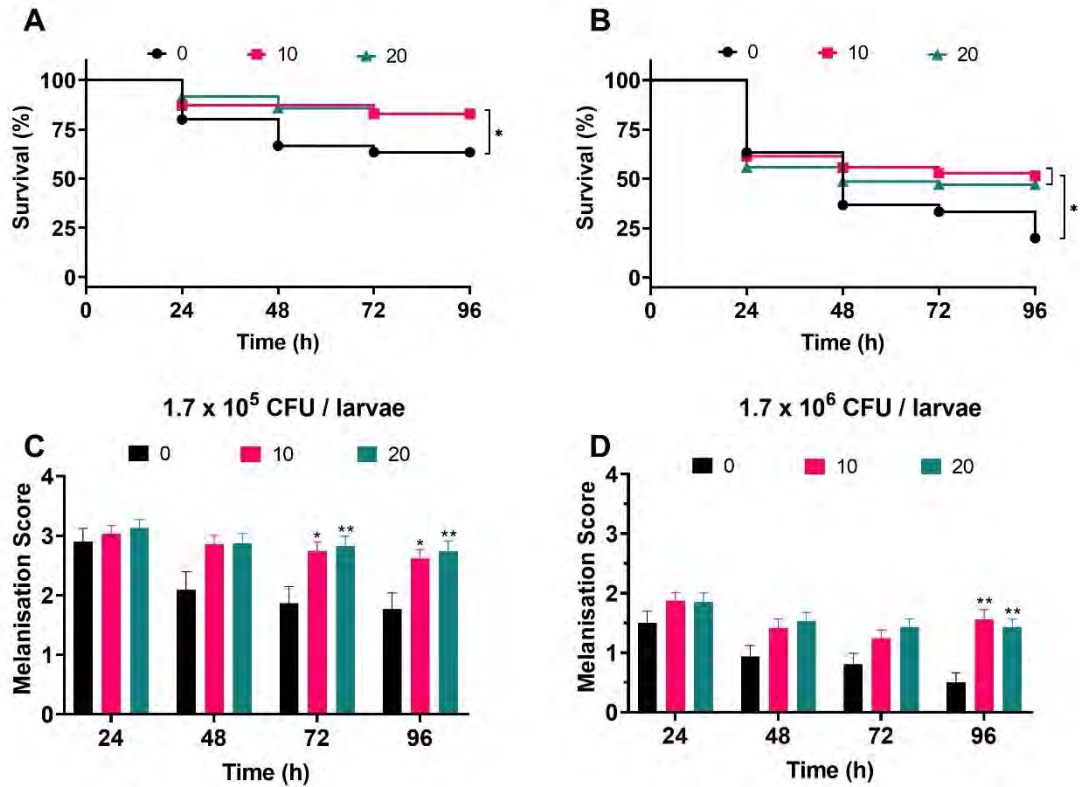


**Figure 4.7: Treatment of *Galleria mellonella* larvae infected with *A. baumannii* NCTC 13302 with silver acetate reduced lethality and improved overall health of the larvae**

Groups of *Galleria mellonella* larvae were injected with 10  $\mu$ l of *A. baumannii* containing either  $1.7 \times 10^5$  or  $1.7 \times 10^6$  cells per larvae, 30 min post-infection groups of larvae were administered either 10 or 20 mg kg<sup>-1</sup> silver acetate as treatment. N = 70 larvae per condition. (A + B) Survival and (C + D) melanisation were recorded every 24 h for 96 h post-injection. (A + B) \*P < 0.05. (C + D) Error bars show SEM, \*P = 0.0168-0.0235, \*\*P = 0.0015-0.0089.

### 4.3 Discussion

Silver salts are incorporated into many commercially available, indwelling medical devices to provide antimicrobial protection against infection during insertion when the risk of infection is highest<sup>219</sup>. Similarly, silver is also incorporated into wound dressings to provide antimicrobial activity against infected wounds<sup>220,221</sup>. This chapter sought to gain a better understanding of the antimicrobial efficacy and toxicity of silver acetate to provide further insight into its potential value in infection control using the *Galleria mellonella in vivo* model.

Silver acetate proved to be an effective antimicrobial against *A. baumannii in vitro* with minimal inhibitory and bactericidal concentrations in the range of many clinically relevant antibiotics as assessed using standardised methods for determination of MIC and MBC values<sup>222</sup>. These values were broadly similar for all strains of *A. baumannii* tested, including strains with limited antibiotic resistance and those with multiple resistances suggesting that existing antibiotic resistance mechanisms do not cause increased resistance to silver. This is expected due to the multiple biological mechanisms and pathways that silver ions can target. The MIC values also fall in line with what is shown in other pathogens such as *S. aureus* (0.08 – 32 mg L<sup>-1</sup>), *P. aeruginosa* (0.04 – 8 mg L<sup>-1</sup>) and *E. coli* (0.5 – 2.5 mg L<sup>-1</sup>)<sup>215–218</sup>. Interestingly, when exponentially growing bacteria were exposed to silver acetate at the MIC, there was an initial decrease in the turbidity of the solution until around 10 hours, after which there was an increase. The decreases in turbidity during the death of the bacteria at the 3.91, 7.81 and 15.6 mg L<sup>-1</sup> point towards silver acetate having a bactericidal effect and causing the cells to rupture. The increase in turbidity after so many hours is potentially due to the way silver ions bind to the bacterial molecules and are therefore, less available in the solution. Once all the silver ions are bound, there will no longer be any bactericidal effect and any remaining bacteria are able to continue growing.

The issue of the development of resistance to silver compounds due to widespread use has been a topic of much debate. Whilst much research has suggested that resistance to silver is slow to emerge and mild due to the requirement of the bacterium to develop resistances that nullify all of the previously mentioned mechanisms of action<sup>105</sup>, others have described various mechanisms of silver resistance that is emerging across the globe. One such mechanism is the production of redox active metabolites, for example the production of pyocyanin by *Pseudomonas aeruginosa* has been demonstrated to not

only protect itself but also other species of bacteria in close proximity to the phenazine compound<sup>223</sup>. This is a concern as *P. aeruginosa* is frequently isolated from polymicrobial infections. Another mechanism of silver resistance described in the literature is the increased expression or acquisition via horizontal gene transfer of the *sil* system<sup>125</sup>. This collection of genes primarily reduces intracellular accumulation of silver inside the cell by expressing periplasmic proteins that bind silver preventing further penetration into the cell and by expressing silver efflux pumps. This and the data provided in this chapter highlights the importance of strict monitoring of silver use as an antimicrobial and administration of the appropriate dosages when used.

Besides antimicrobial activity, a key factor in the determination of whether silver acetate is suitable as an effective treatment for infection or prophylaxis, is its toxicity to the host. In this study toxicity testing in the *G. mellonella* model revealed that only the highest concentration of silver acetate used (80 mg kg<sup>-1</sup>) caused significant death of the larvae. Therapeutic ranges of antimicrobials can be as low as 5 mg kg<sup>-1</sup> daily to up to 85 mg kg<sup>-1</sup> for urinary tract infections caused by indwelling catheters<sup>224</sup>. The dose depends on the administration method and the severity of the infection; however, most doses administered are less than 20 mg kg<sup>-1</sup>. As 10 - 20 mg kg<sup>-1</sup> silver acetate showed no negative effect on the larvae here, it can be concluded that these are safe therapeutic doses in this model. Additionally, these low doses were able to significantly improve survival of the larvae after infection with a carbapenem-resistant strain of *A. baumannii* providing promising data for the clearance of drug-resistant bacterial pathogens.

The inoculum study revealed that 1.7 x 10<sup>6</sup> bacterial cells per larvae was able to cause 80% larval death (20% survival), which is an appropriate amount of mortality for subsequent treatment studies<sup>202</sup>. For comparison, a 10-fold lower infectious dose was also tested. The survival of larvae injected with 1.7 x 10<sup>5</sup> bacteria cells increased by 20% at both concentrations of silver acetate used to treat the infection, while for the 10-fold higher infectious dose, survival increased by 27% and 31% for treatment with 20 and 10 mg kg<sup>-1</sup> doses respectively but these results were not significantly different from each other. Future research could utilise this statistically significant improvement in survival upon administration of both concentrations of silver acetate in combination with antibiotic treatment to look for increased antimicrobial activity. Previous studies have demonstrated the potential synergy of silver ions with established antibiotics of the  $\beta$ -lactam, quinolone and aminoglycoside groups<sup>109</sup>. Further study of the adjuvant effects of silver acetate against drug resistant bacterial pathogens when administered alongside

antibiotics currently on the market, could provide a new route to antimicrobial treatment of these pathogens.

In conclusion the data presented in this chapter demonstrates the efficacy of silver acetate as an antimicrobial against carbapenem resistant *A. baumannii*. This is the first known work that demonstrated silver acetate as non-toxic to *G. mellonella* at concentrations able to cause antimicrobial activity and improve survival of infected larvae. However, *Galleria* have been used to test other silver compounds such as silver nanoparticles, where *Pseudomonas aeruginosa* infections were treated with silver nanoparticles at a concentration of 25 mg/kg and were found to greatly increase larval survival<sup>225</sup>.

Silver acetate is unlikely to be administered systemically for treatment of infection due to the potential for complications, however, silver salts can and are used in some indwelling devices such as catheters and in wound dressings and antimicrobial creams. Upon introduction of these antimicrobial materials to the host, there may be leeching of the compound into the system. Identifying that silver acetate was non-toxic in an *in vivo* model and was an effective treatment against infection, suggests that silver acetate would be a suitable silver salt candidate for antimicrobial therapy when administered in medical device materials or topical applications at an appropriate concentration.

## 5 The development of a catheter-associated urinary tract infection model with a modified drip flow biofilm reactor®

### **5.1 Introduction**

The ability of *Acinetobacter baumannii* to form biofilms is thought to be one of this bacterium's main virulence mechanisms<sup>226</sup> and contributes to its ability to cause nosocomial infections via growth on medical devices<sup>18</sup>. *A. baumannii* is a pathogen frequently found to colonise tubing used in intensive care units most commonly causing ventilator associated pneumonia but also catheter-associated urinary tract infections (CAUTIs)<sup>15</sup>.

Catheters are an invasive medical device used when a patient is incapable of carrying out normal bladder functions and urinating normally<sup>62,227</sup>. Approximately 12-16% of adult patients in hospital are likely to be catheterised and catheters are the most common cause of hospital acquired urinary tract infections<sup>227</sup>. The biggest risk factor for acquiring a CAUTI is the length of time the catheter is in place<sup>51,228</sup>, as catheters may become colonised via extraluminal (contamination upon insertion or contamination of the tube) or intraluminal (contamination via a failed closed draining system) methods<sup>63</sup>.

*A. baumannii* is only recently becoming recognised as a cause for concern in CAUTIs. Several studies have found the bacterium to be among the top three causes of CAUTIs in various hospitals<sup>15,229,230</sup>, with a systematic review including studies from 1995 through to August 2017 finding *A. baumannii* to be isolated from 17% of urinary sources<sup>15</sup>.

To cause a medical tubing infection, bacteria must first adhere to the surface and once adhered biofilm formation can occur. Biofilms are said to be one of the biggest challenges to catheter use, as given time, biofilms will form on and in the catheter causing a need for frequent replacement<sup>62</sup> and significant risk to the patients health. To tackle the problem of biofilm formation in medical settings we must understand how biofilms form in these environments. Therefore much research is focused on the development of biofilm models that better replicate the natural environment where biofilms form<sup>132</sup>. In the case of bladder catheter models there are a few that exist for different purposes with the most common being models that utilise a "glass bladder" that allows the researcher to analyse biofilms formed on catheter tubing and also the bacterial cell numbers in

standing urine<sup>155,231,232</sup>. The glass bladder model was initially developed by Stickler *et. al.* (1999) and utilised a double walled glass vessel as the 'bladder'<sup>155</sup> (Figure 5.1). This study aimed to utilise the mDFR a standardised and commercially available reactor, to mimic a urinary catheter biofilm without the use of a glass bladder as these are not commercially available or standardised. Glass bladders for these models are bespoke creations that may lead to differences in size and shape between studies<sup>233</sup>.

**This image has been removed due to third party copyright.**



**Figure 5.1: The glass bladder used to study catheter associated urinary tract infections *in vitro***

The glass bladder is a double walled glass vessel which allows for the study of catheter associated urinary tract infections and biofilm formation. The model allows for the collection of urine below the opening of the foley catheter and sterile urine is fed in from the top. When urine reaches the opening of the foley catheter, it will drain down into the collection bag attached to the catheter. The black arrows point to the opening ports of the double wall which allows for the circulation of 37°C water which maintains the temperature of the model<sup>155,233</sup>. Image adapted from Nzakizwanayo *et. al.* (2019)<sup>233</sup>.



The DFR is a commercially available reactor that allows for the growth of four separate biofilms under low shear/laminar flow<sup>134</sup>. The reactor is used in a variety of studies as it allows for the analysis of biofilms formed with different species on various materials and coatings including coatings of an antimicrobial nature although these are usually flat surfaces<sup>157-159</sup>. The mDFR is based on the original DFR, however it is modified to include influent and effluent ports that can hold sections of tubing within the chambers<sup>160,161</sup>. When running the mDFR the flow of liquid can be through the tubing or dripped around the outer surface and allowed to fill the chamber. This allows for biofilm formation within, and on the outer surface of the tubing when inoculated with bacteria and bacteria are fed via flow of nutrient media. The tubes can be harvested and biofilms analysed

quantitatively by viable counts and live/dead staining or qualitatively via SEM and CLSM<sup>160</sup>. This chapter aimed to develop a clinically relevant biofilm model for a catheter associated urinary tract infection caused by *A. baumannii*.

## 5.2 Results

### 5.2.1 Development of a biofilm tubing model

The Drip Flow Biofilm Reactor<sup>®</sup> (Figure 5.2) system was initially developed utilising the Montana State University Drip Flow Biofilm Reactor instructional videos as a reference guide<sup>234</sup> but with the bespoke modifications that included fittings to allow tubing to run through the centre of the chamber. As shown in Figure 5.3, sterile media and inoculum were connected to one tube per channel that ran into the peristaltic pump. From the pump, either media or inoculum was fed into the mDFR, through the tubing attached within the channel and out to a waste vessel. To switch between media and bacterial culture clamps were attached at positions indicated in Figure 5.3 and glass flow breaks were attached to the tubing coming from the sterile media to prevent backflow and contamination.

**This image has been removed due to third party copyright.**

#### **Figure 5.2: Schematic diagrams of the Drip Flow Biofilm Reactor<sup>®</sup>**

Above is the standard commercially available biofilm reactor from BioSurface Technologies Corporation with four channels. This reactor is available with six channels and is made from black Polyethylene Terephthalate (PET). This is an example of the reactor without the modifications used in this thesis. Image from BioSurface Technologies Corporation<sup>156</sup>

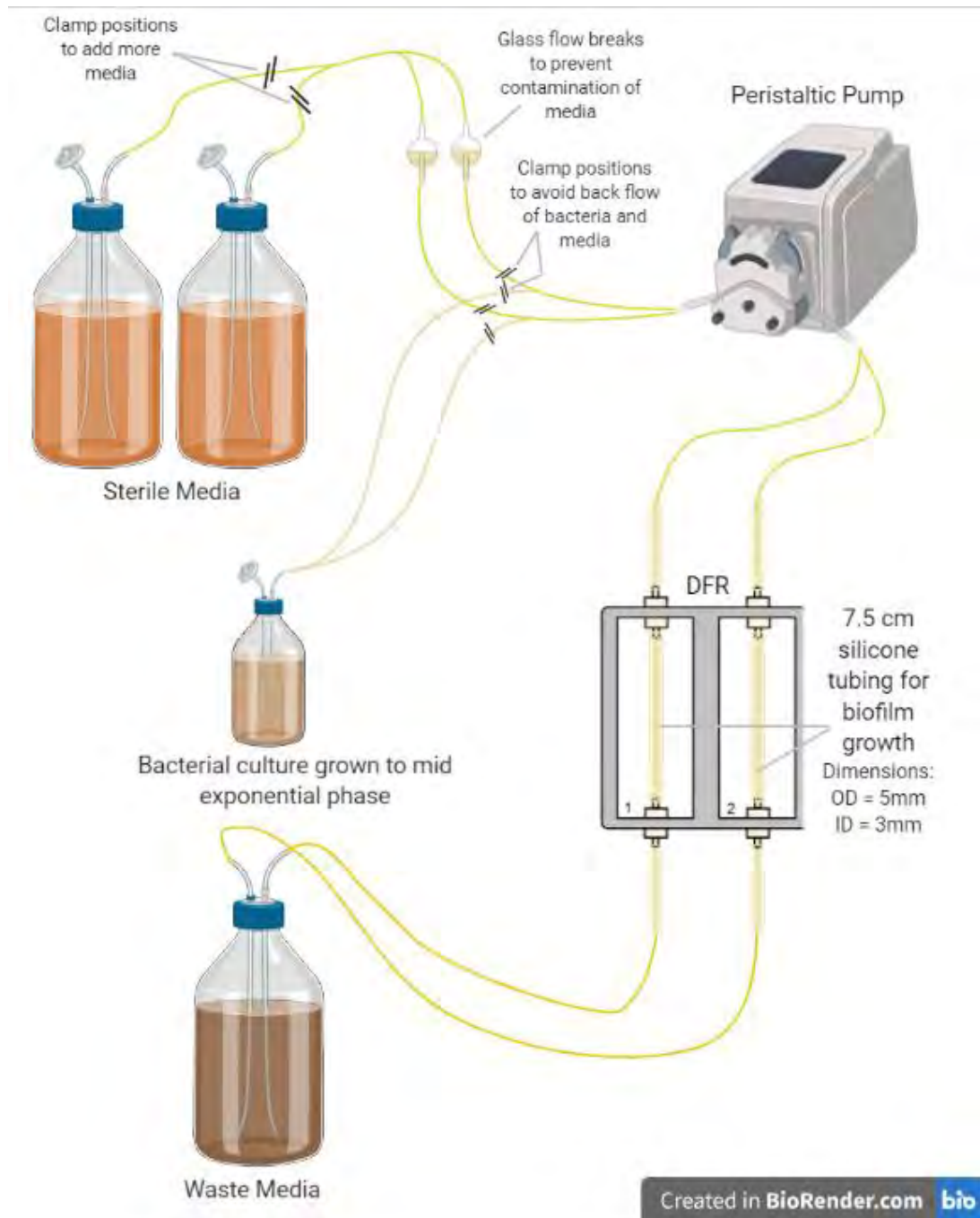


**Figure 5.3: Schematic diagram of modified Drip Flow Biofilm Reactor®**

Schematic shows how sterile media and bacterial culture tubing was joined together before entry into the peristaltic pump. Also visible are the glass flow breaks that prevent backflow and potential contamination of the sterile media and the clamps that allow for switching between media and bacterial culture during the inoculation period. In this model individual channels are run by independent lengths of tube and do not mix. Image created in BioRender.com.

Prior to inoculation with bacteria, the equivalent flow rate for each channel was established in the mDFR, and pump speeds were adjusted accordingly to ensure equivalent flow through each channel. The flow rate of media was tested and ultimately a speed of  $0.5 \text{ ml min}^{-1}$  was utilised for the model as this is in line with the media output for catheterised patients and within the accepted range in the literature<sup>155,233</sup>. To set the pump speed accurately, a standard curve was produced by measuring the volume of water over a set period at different speeds on the pump. Once the standard curve was created, the equation of the line was used to select the correct pump speed and the volume of water was recorded at the specific speed to ensure accuracy of the flow rate.

After selecting the appropriate flow speed for the model, the mDFR was run with one channel for five days, half the time used in the glass bladder model by Stickler *et. al.* (1999)<sup>155</sup> to test biofilm formation in 50% MHB and provide a focused exploration of how the mDFR ran (Figure 5.4). 50% MHB was used for the initial model development because most studies that utilised the mDFR also used this concentration of MHB<sup>160,161</sup>, possibly because MHB is a rich media.



**Figure 5.4: Six channel modified Drip Flow Biofilm Reactor® set up with only one channel**

Only one channel was used when working out how many days the reactor would be run for to produce a mature biofilm. Image shown is the channel after removal of the lid before the silicone tube is disconnected.

As biofilm growth was possible with only 50% MHB the decision was made to continue with the same strength media. In the initial tests, a mature biofilm was characterised as a biofilm that could be visibly seen within the silicone tube after growth and would withstand an initial wash step of 3 ml PBS directly injected down the lumen of the tube. Analysis of the biofilms determined that five-day old biofilms were the appropriate size for study and showed classic biofilm characteristics such as cell stacks and channels for nutrient flow (Figure 5.5). Initial characterisation utilised a static incubator to maintain growth, however it was determined that the use of a warm room to handle the size of the media and waste vessels was the easiest method of incubation for the mDFR tubing colonisation model.

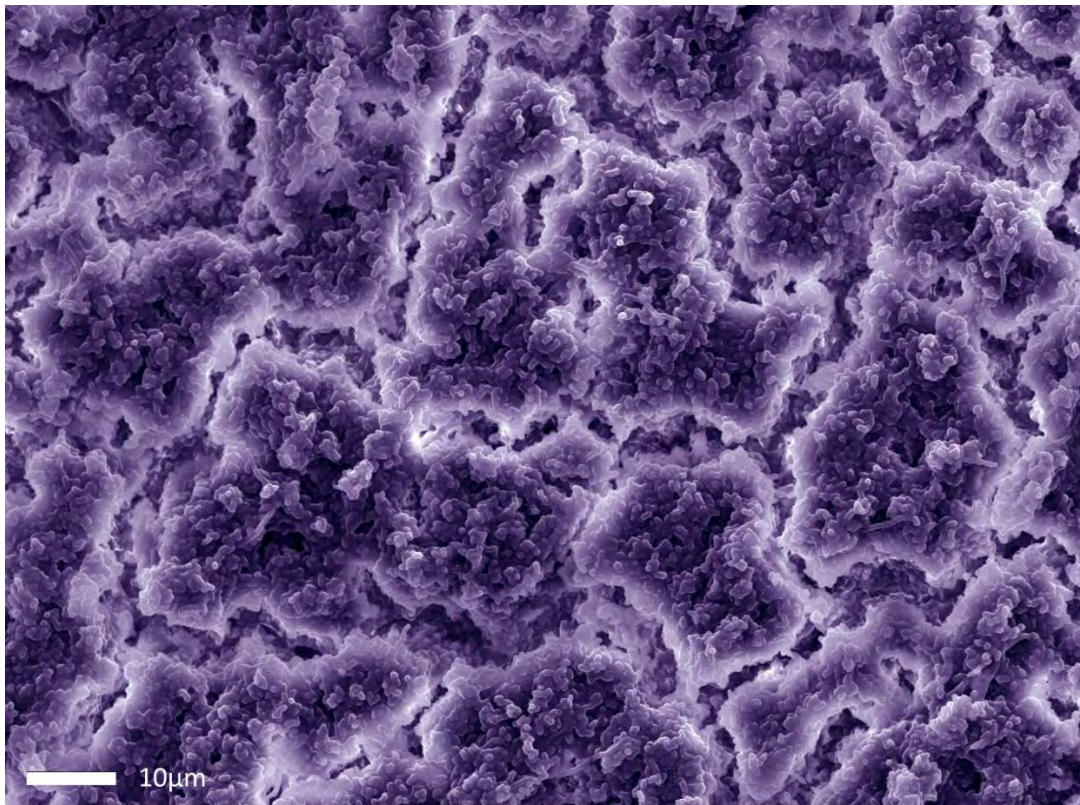


**Figure 5.5: False colour SEM image of *Acinetobacter baumannii* biofilm**

*A. baumannii* biofilms formed in MHB within the mDFR tubing colonisation model, show multilayer cell stacks with clear channels which allow for the flow of nutrients throughout the biofilm. Image taken using SEM at 15kv under 1000X Magnification.

Following is a description of the final developed methodology for the mDFR tubing colonisation model. The mDFR was set up with two media vessels connected, providing 8.5 L of 50% MHB in total. One vessel was always clamped so the system only used one vessel at any given time and this system allowed changeover of media supply without a risk of contamination. Before inoculation, media was flushed through from both vessels to prime the lines and remove large air bubbles. This short burst of media was also used to check that all connections were secure, as if the mDFR system had a break then the pump would not pull through media and the system would no longer be sterile. After checking everything was correctly connected, the bacterial culture vessel containing a magnetic flea was inoculated with 5 ml overnight culture then placed on a magnetic stirrer. The whole system was moved into the warm room, the magnetic stirrer was turned on and the bacteria were grown for three hours, which was the required time for *A. baumannii* NCTC 13302 to enter mid-exponential phase (Figure 5.6). Once the culture reached mid-exponential phase, the peristaltic pump for the system was turned on and the bacterial culture was passed through the mDFR for two hours at a flow rate of 0.5 ml min<sup>-1</sup> before bacterial culture was stopped and clamped off and sterile media flow resumed.

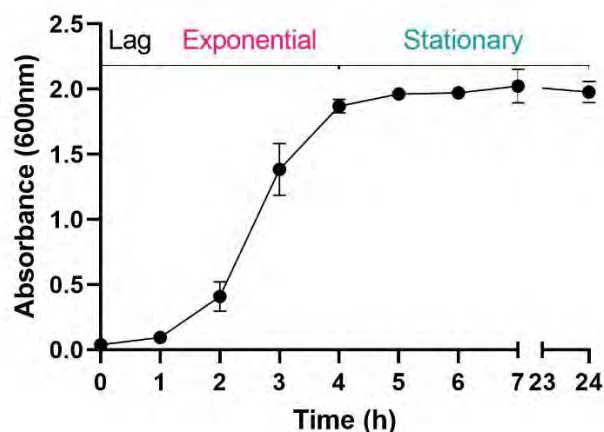


**Figure 5.6: Growth curve in MHB for *Acinetobacter baumannii* NCTC 13302**

*Acinetobacter baumannii* was incubated at 37 °C in a 20 ml MHB in a 250 ml flask, shaking at 150 rpm. Absorbance readings were taken hourly until seven hours had passed with a final reading at 24 hours. The resulting absorbances provided a 'stereotypical' growth curve with lag, exponential and stationary phases of growth. N=3±SEM.

## 5.2.2 Preparation of biofilms obtained from the mDFR for characterisation studies

As the biofilm was grown within a silicone tube (Figure 5.7), it was necessary to consider how to analyse the biofilms to compare the effects that media would have as the model was adapted towards a more clinical representation. To quantify the viability of the biofilm, viable counts were performed to calculate the number of live cells, however biofilms are not made up solely of live cells and contain multiple components including dead cells. This prompted the use of the LIVE/DEAD® BacLight™ Bacterial Viability Kit by Invitrogen to check the 'health' of the biofilm. The health of the biofilm in this study refers to how many cells remaining in the biofilm are still viable in comparison to how many cells are dead.

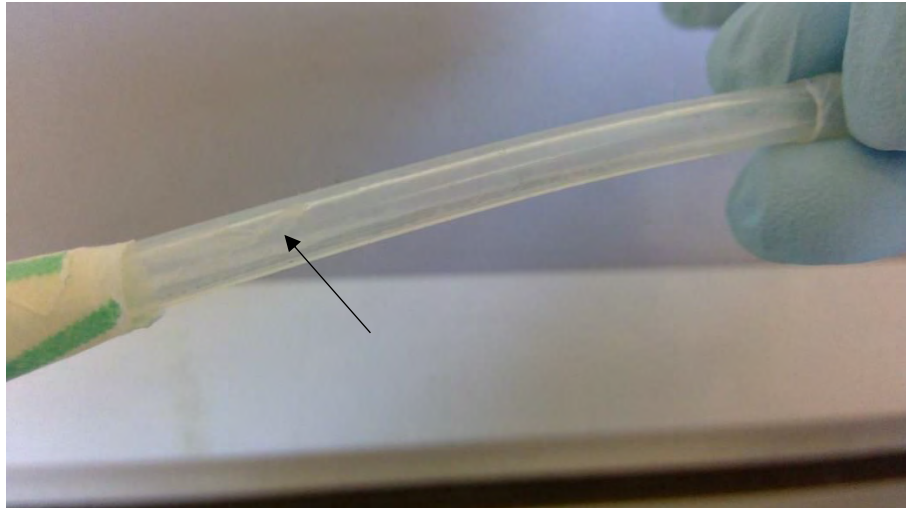


**Figure 5.7: Silicone tubing used for growth of biofilms.**

Silicone tubing used for growth of biofilms had an outer diameter of 5 mm with a 3 mm internal diameter and 1 mm thick walls. Arrow points to visible biofilm left within the tube after draining.

To carry out the viability and live/dead staining tests of the biofilms, the silicone tube growing biofilm in channel two of the mDFR was recovered and washed with 3 ml sterile PBS to remove unbound cells. The tube was then transferred to a fresh 15 ml centrifuge and 10 ml sterile PBS was washed down the centre of the tube vigorously to remove as much of the biofilm as possible. Manual washing was not sufficient to completely detach the biofilm from the surface of the silicone, so the tube was vortex mixed for one minute, followed by a two-minute sonication in an Ultrawave Q series sonicating machine, followed by another vortexing step. If subsequently biofilm was still visible on the inside of the silicone tubing, the process was repeated.

Scanning Electron Microscopy was used to qualitatively examine the biofilm at the cellular level. To view the biofilm via SEM, the silicone tube was cut into 1 mm sections using a scalpel and tweezers were used to stabilise the shape of the silicone ring as it was cut to avoid damage to the biofilm. This produced small rings with the biofilm intact on the inner lumen of the tube (Figure 5.8). The rings were fixed using the protocol in Table 2.7 before they were sliced in half to be sputter coated with 5 nm of gold and viewed with a Jeol JSM-7100F LV FEG-Scanning electron microscope with high vacuum

at 15 kV. The SEM provided images of the biofilm that allowed qualitative comparisons of the biofilm structures and thickness in different media.

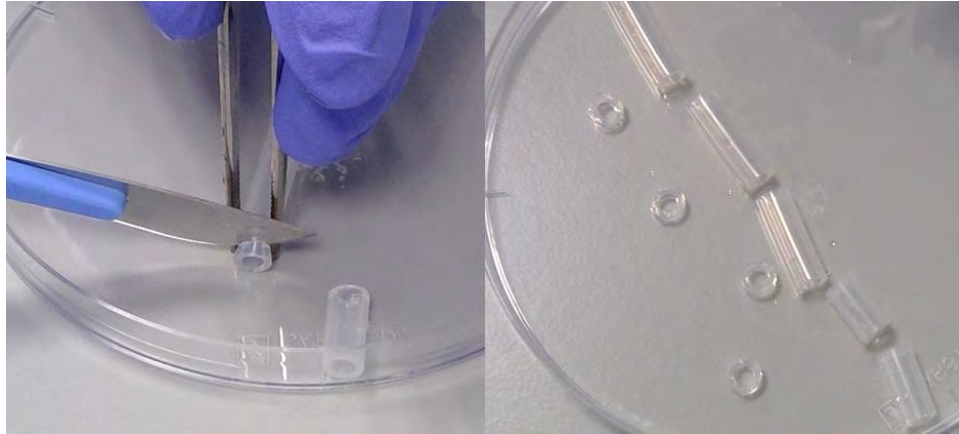


**Figure 5.8: Slicing the silicone tube into 1 mm discs for SEM.**

1 mm discs were sliced from the tube to be fixed and stained for SEM. A sterile scalpel was used to slice the tube and sterile tweezers were used to stabilise the sides of the tube to avoid squashing and damaging the biofilm within the tube.

### **5.2.3 Development and testing of clinically relevant media for a urinary catheter infection model**

To move the model closer to a catheter infection, it was necessary to analyse the biofilm in urine. Ethical approval is required to work with human urine and the components and make up of urine varies depending on sex, age, ethnicity, presence of disease, activity levels and many other environmental factors<sup>235–238</sup>. For this reason, the mAUM by Liang *et. al.* (2020)<sup>184</sup>, which is adapted from the artificial urine media in Brooks and Keevil (1997)<sup>183</sup> was used as a clinically relevant substitute.

To test the effectiveness of this media, growth curves with and without silver acetate, static biofilm assays with and without silver acetate and minimum inhibitory / bactericidal concentration assays were carried out (section 5.2.3.1) before the media was utilised within the mDFR.

### 5.2.3.1 *A. baumannii* growth in modified Artificial Urine media show significantly lower growth than in Mueller Hinton Broth

*A. baumannii* cultures were grown in 20 ml mAUM in 250 ml flasks over the course of 24 hours with turbidity readings taken every hour for 7 hours. The growth curve that this produced was compared to the growth curve produced by cultures grown in MHB and it was seen that turbidity was up to four-fold lower than when grown in rich media, however exponential phase appears to begin at the same time in both media (Figure 5.9).

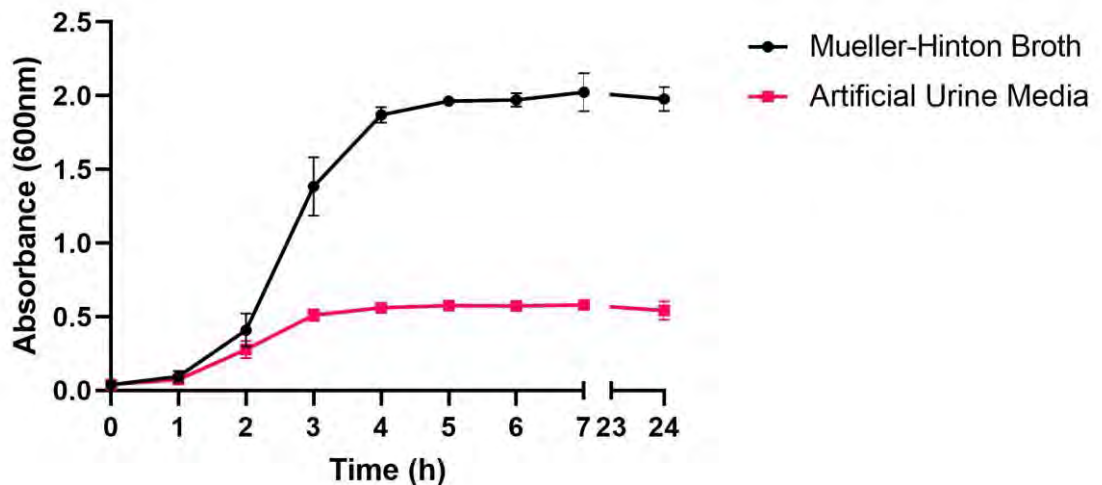


**Figure 5.9: Growth of *A. baumannii* is reduced in modified Artificial Urine Medium compared with growth in Mueller-Hinton Broth**

Overnight cultures of bacteria were diluted 1:100 in 20 ml within 250 ml flasks containing mAUM (square) or MHB (circle). Flasks were incubated at 37°C shaking at 150 rpm for 24 hours with OD<sub>600nm</sub> absorbance readings carried out hourly for the first 7 hours. N = 3 ± SEM

### 5.2.3.2 *A. baumannii* biofilm formation is not significantly altered by growth medium

A 96-well biofilm formation assay was carried out in mAUM to analyse whether the biofilm forming capabilities of *A. baumannii* NCTC 13302 were affected by the use of different media. The mean absorbance of crystal violet recovered from the resulting biofilm in

mAUM was 0.234 (SD  $\pm$  0.00813) while for MHB it was 0.249 (SD  $\pm$  0.0384). An unpaired t-test produced a P-value of 0.5346, therefore there was no significant difference in biofilm formation between MHB and mAUM.

### 5.2.3.3 Minimum inhibitory / bactericidal concentration assays reveal silver acetate to be more effective against *A. baumannii* grown in modified artificial urine medium compared with Mueller-Hinton broth

One of the possible uses of the drip flow reactor would be to test the effectiveness of a silver acetate coating on sections of silicone tubing used for catheters. To carry out such an experiment, the MIC and MBC of silver acetate in the mAUM would need to be known to ensure that a sufficiently high concentration of silver acetate was used in the coating. The results of a minimum inhibitory/bactericidal concentration assay (Table 5.1) show that the MIC and MBC of silver acetate against *A. baumannii* NCTC 13302 in mAUM approximately 3.58-fold less than the MIC and 7.1-fold less than the MBC in MHB.

**Table 5.1: MIC and MBC results for silver acetate tested in mAUM are lower than MIC and MBC results for MHB**

Media	MIC mg L <sup>-1</sup> (±SD)	MBC mg L <sup>-1</sup> (±SD)
Modified Artificial Urine Media	1.09 (0.187)	1.09 (0.187)
Mueller-Hinton Broth	3.91 (0)	7.81 (0)
P value	0.002	0.002

To determine whether the MIC of *A. baumannii* in MHB was 3.91 mg L<sup>-1</sup> or whether it was in the range between 3.91 and 7.81 mg L<sup>-1</sup> a second MIC assay was performed where the concentrations decreased in increments of 1 mg L<sup>-1</sup> (rather than two-fold as previously). It was found that the MIC in MHB was 5.73 mg L<sup>-1</sup> (SD ± 1.22) and the MBC was 6.4 mg L<sup>-1</sup> (SD ± 1.68) and a Wilcoxon matched pairs signed rank test provided a P value of 0.0078 indicating significant differences between the MIC and the MBC in Mueller-Hinton Broth.

#### **5.2.3.4 Exponentially growing *A. baumannii* is inhibited by the presence of silver acetate at close to or above the MIC for silver acetate in mAUM**

As stated in section 4.2.3 an infection is usually well established before antimicrobial intervention occurs and so when using a media that can represent urine it was necessary to reassess the effect of silver acetate on the growth of *A. baumannii* in the presence of the mAUM as the growth medium. Growth curves (Figure 5.10) revealed that at the sub-MIC concentration of 0.488 mg L<sup>-1</sup>, there was a slight decrease in turbidity ( $P < 0.05$ ), however after 6 hours growth recovered and there was no statistical significance in growth compared with non-treated cultures. For all other concentrations of silver acetate (0.977, 1.95, 3.91, 7.81 mg L<sup>-1</sup>) there was a significant difference ( $P < 0.05$ ) in growth from 30 minutes after addition of silver acetate.

Viable counts were performed hourly from the addition of silver acetate to enumerate the number of live cells throughout the experiments. Figure 5.11 shows that the viability reflects the trends seen with growth, where the lowest concentration of silver acetate showed viability similar to the control and no significance evident between this concentration and the control. The highest concentrations of silver acetate (1.95, 3.91 and 7.81 mg L<sup>-1</sup>) showed significant differences in viability ( $P < 0.0158$ ) from one-hour post-addition of silver acetate and complete cell death at 24-hours, whilst the 0.977 mg L<sup>-1</sup> concentration allowed for viable cells at the end point of the experiment and did not show any statistically significant variation in comparison to the control.

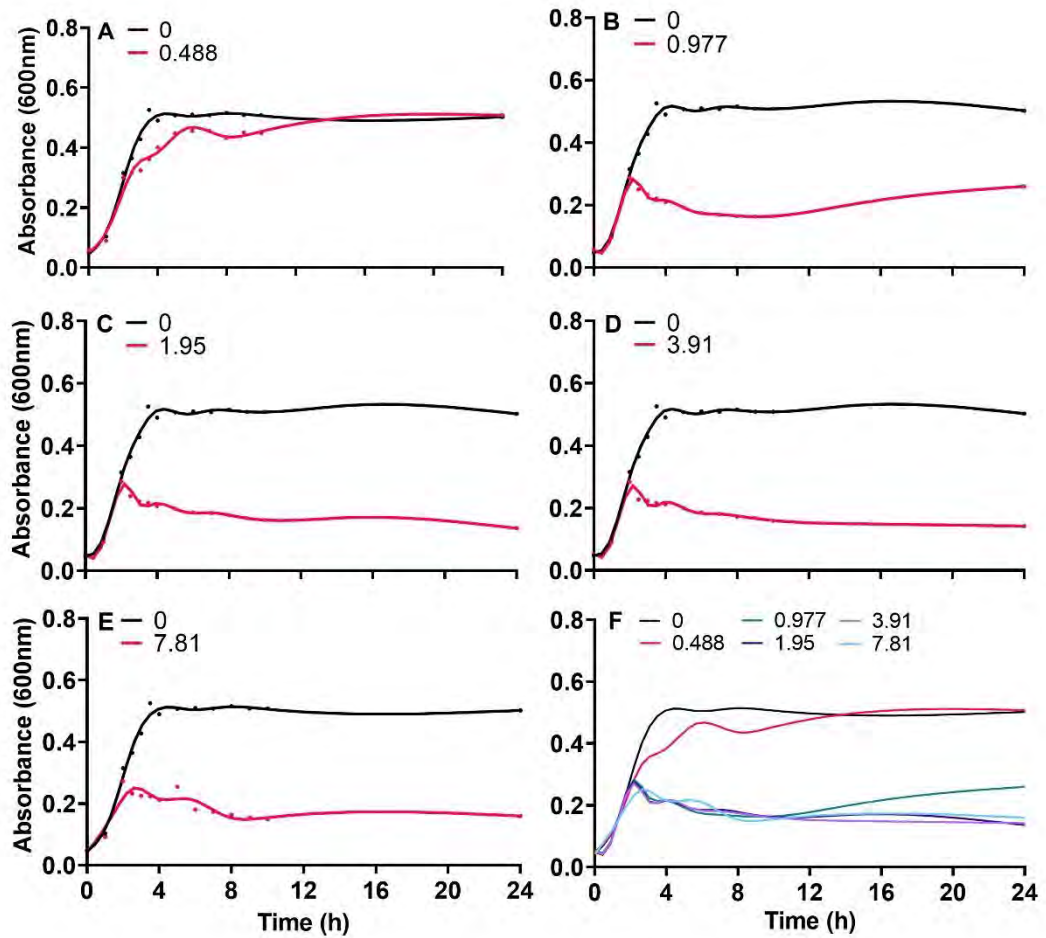


**Figure 5.10: The inhibition of exponentially growing *Acinetobacter baumannii* is dependent on the concentration of silver acetate in mAUM**

Silver acetate was added to exponentially growing cultures at the 2 h time point at final concentrations of (A) 0.488, (B) 0.977, (C) 1.95, (D) 3.91 and (E) 7.81. Cultures were incubated at 37 °C with shaking and growth monitored via absorbance (OD<sub>600</sub>) every 30 min for 4 h, followed by every hour for a further 6 h with a final reading at the 24 h time point. (F) Panel shows growth in the presence of all concentrations of silver acetate for comparison (Black = 0, Pink = 0.488, Dark blue = 0.977, **clarify the remaining lines**). N = 3, error bars are omitted for clarity, but standard deviations were all within the range 0.0008 – 0.207.

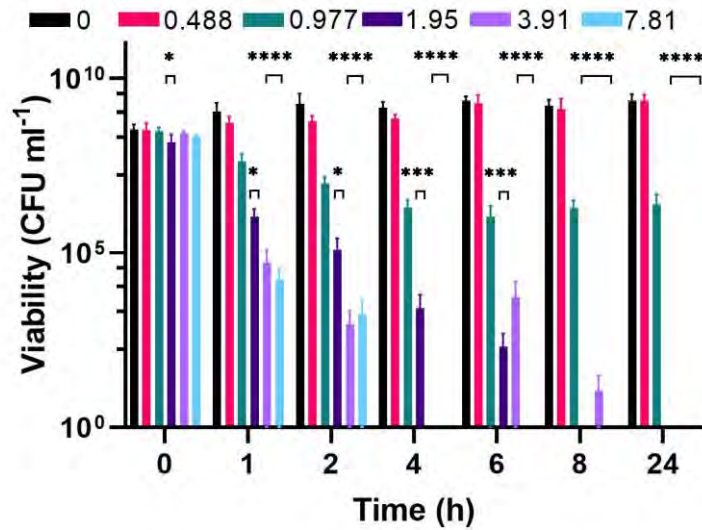


**Figure 5.11: The bactericidal effect of silver acetate on *Acinetobacter baumannii* in mAUM is concentration dependent**

Silver acetate was added to exponentially growing cultures of *A. baumannii* at final concentrations of 7.81, 3.91, 1.95, 0.977 and 0.488 mg L<sup>-1</sup>. The cultures were incubated at 37°C with shaking at 150 rpm and samples were taken at hourly intervals for the first two hours, followed by two-hour intervals for 8 hours with a final reading taken at 24 hours. The highest concentrations of silver acetate produce statistically significant variation in viability in comparison to the control and asterisks highlight these results. N= 3 ± SD (\* = P < 0.0158, \*\*\* = P < 0.0008, \*\*\*\* = P < 0.0001)

### 5.2.3.5 Less biofilm is formed in mAUM than in MHB in response to the presence of silver acetate

As the aim of the drip flow reactor model was to grow a biofilm within a media that represented urine with a view to possibly coat silicone tubing with silver acetate, it was important to understand whether the presence of the mAUM changed the effects of silver acetate on the ability of *A. baumannii* to form biofilms. Figure 5.12 shows that the presence of silver acetate, regardless of concentration, significantly reduced both the absorbance of crystal violet recovered from bacterial biofilms (Figure 5.12:A) and the number of viable cells (Figure 5.12:B) in comparison to the no silver acetate controls ( $P < 0.05$ ,  $N = 3 \pm SD$ ).

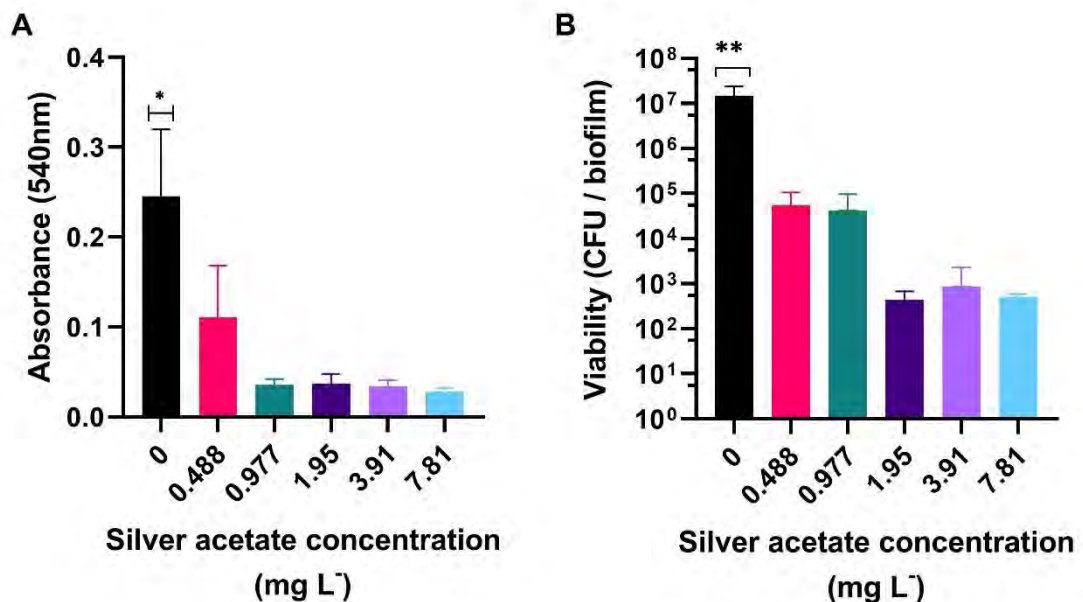


**Figure 5.12: Crystal violet staining, and biofilm viability is reduced in the presence of silver acetate regardless of concentration**

Silver acetate made up in mAUM was added to wells of a 24 well plate to concentrations of 7.81, 3.91, 1.95, 0.977, 0.488 and 0 mg/L. To each well, 100  $\mu$ l of *A. baumannii* diluted to 0.5 OD<sub>600nm</sub> was added and plates were incubated statically overnight at 37°C. (A) Biofilms were washed and stained with crystal violet and absorbance of recovered crystal violet was read at 540nm (\* =  $P < 0.0238$ ,  $N = 3 \pm SD$ ). (B) Biofilms were washed and recovered from wells in PBS. Viable counts were carried out on recovered suspension and recorded, (\*\* =  $P < 0.0036$ ,  $N = 3 \pm SD$ ).

Figure 5.13: C shows that silver acetate decreases biofilm viability and volume more when the media used is mAUM versus MHB. Figure 5.13: C:A shows that significant differences exist between biofilm formation in different media at low and no concentrations of silver acetate (0 and 0.5 MIC). When comparing the viability from the biofilms formed in different media, there was no significant difference in the 0 mg L<sup>-1</sup> silver acetate controls. At the 0.5 MIC and 1 MIC concentrations of silver acetate, the mAUM gave significantly lower numbers of viable cells than MHB while at twice the concentration of the MIC (2 MIC) there was no significant difference between media (Figure 5.13: C:B). According to this *A. baumannii* NCTC 13302 biofilms have a lower biovolume in the presence of silver acetate when grown in mAUM as opposed to MHB.

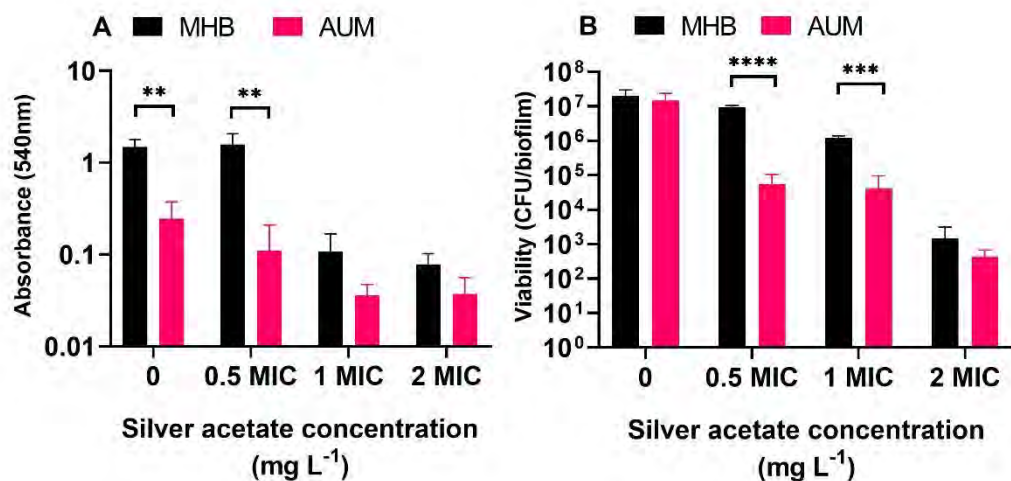


**Figure 5.13: Comparison of crystal violet staining and biofilm viability suggests biofilm formation is negatively impacted to a greater degree by silver acetate in mAUM**

Silver acetate made up in MHB or mAUM was added to wells of a 24 well plate to concentrations of 0, 0.5, 1 and 2X MIC in the relevant media. To each well, 100  $\mu$ l of *A. baumannii* diluted to 0.5 OD<sub>600nm</sub> was added, and plates were incubated statically overnight at 37°C. (A) Biofilms were washed and stained with crystal violet and absorbance of recovered crystal violet was read at 540nm. (B) Biofilms were washed and recovered from wells in PBS. Viable counts were carried out on recovered suspension and recorded. (N = 3  $\pm$  SD, \*\* = P < 0.007, \*\*\* = P < 0.0005 \*\*\*\* = P < 0.0001).

## **5.2.4 Infection of silicone tubing with *Acinetobacter baumannii* within the modified Drip Flow Biofilm Reactor**

With the mDFR successfully developed for use (section: 5.2.1) and the preliminary experiments with the mAUM obtained (section: 5.2.3), the next step was to infect silicone tubing with *A. baumannii* in MHB. Running the model with a standard medium was a cost-effective, easily reproducible way to optimise the protocol, whilst also providing a useful control. After obtaining three repeats with MHB as the media, the medium was changed to mAUM to bring the model closer to a clinical representation of a catheter biofilm. In the following sections a comparison is presented of the appearance, viability, and 'health' of the resulting biofilms in MHB and mAUM.

### **5.2.4.1 Scanning electron microscopy images of biofilms obtained from mDFR show that biofilms grown in MHB are thicker and more mature than biofilms grown in mAUM**

To compare the effect of media on biofilm formation, the mDFR was set up as described in 5.2.1 and biofilms were allowed to develop on silicone tubing over five days at 37 °C. To view the appearance of the biofilm formed within the silicone tube, the tube was sliced into 1mm sections and four sections from random points along the tube were fixed, sliced in half, gold coated and viewed under a Jeol JSM-7100F LV FEG-Scanning electron microscope with high vacuum at 15 kV. Biofilms formed in MHB were seen to be thicker and more mature than those formed in mAUM when observing the surface of the biofilm (Figure 5.14). When the tubes were turned on their side it was possible to view the thickness and profile of the biofilm. Although it is impossible to quantify the exact thickness of individual biofilms via this method, it is possible to see qualitatively that biofilms formed in MHB protrude further from the tube more than biofilms formed in mAUM (Figure 5.15).

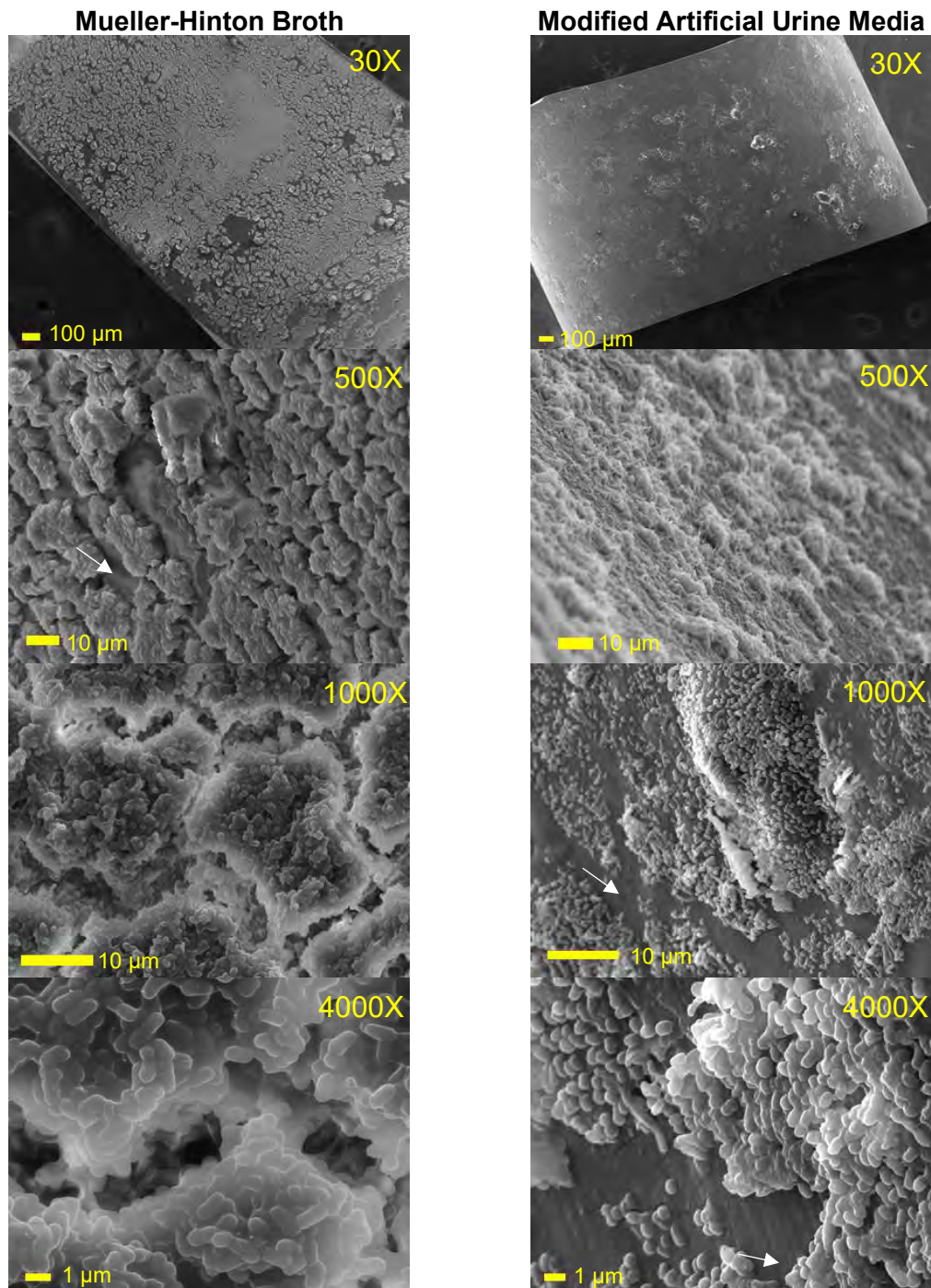


**Figure 5.14: SEM images of biofilm surface taken at 15 kV**

Images show examples of the biofilm grown on the inner lumen of a silicone tube after growth of a biofilm for five days with the mDFR in MHB (Left) or mAUM (right). White arrows point out the surfaces of the silicone tubes.

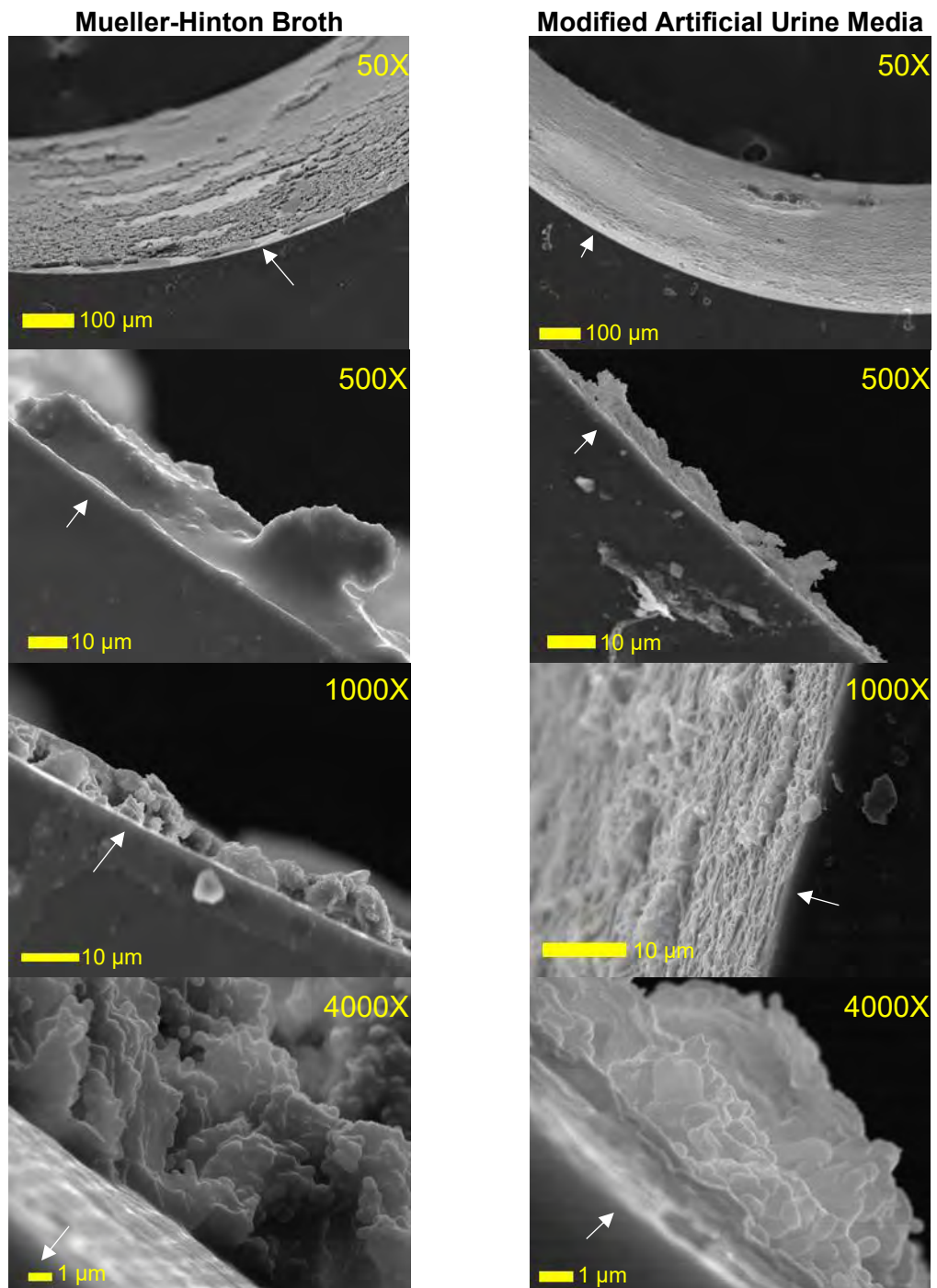


**Figure 5.15: SEM images of biofilm thickness taken at 15 kV**

Images show examples of the thickness of a biofilm grown on the inner lumen of a silicone tube after growth of a biofilm for five days with the mDFR in MHB (Left) or mAUM (Right). White arrows point out the surface edge of the silicone tube.

#### **5.2.4.2 Live / dead staining and fluorescent imaging indicates that biofilms formed in mAUM may contain more dead cells than those formed in MHB**

The LIVE/DEAD® BacLight™ Bacterial Viability Kit \*for microscopy\* by Invitrogen was used to stain biofilm cells recovered and resuspended from tubing by sonication and vortex mixing at the end of the mDFR run to understand the overall health of the biofilm by comparing the percentages of live and dead cells. The percentage of live and dead cells was calculated by counting cells that were stained green (SYTO 9 stained live cells) and red (propidium iodide stained dead cells) across four fields of view for three repeats of the mDFR run. Figure 5.16 shows the spread of the data for live/dead percentages in MHB versus mAUM. There was no statistical significance seen although there is a trend towards MHB biofilms having more live cells, with one mDFR biofilm formed in mAUM containing a very high number of dead cells in comparison to the others. When observing the images taken under the Green fluorescent protein and Texas red settings it's possible to see that biofilms grown in MHB (Figure 5.17:A) had consistently more cells in a single field of view in comparison to biofilms grown in mAUM (Figure 5.17:B). There is also a higher ratio of live to dead cells in MHB versus in mAUM.

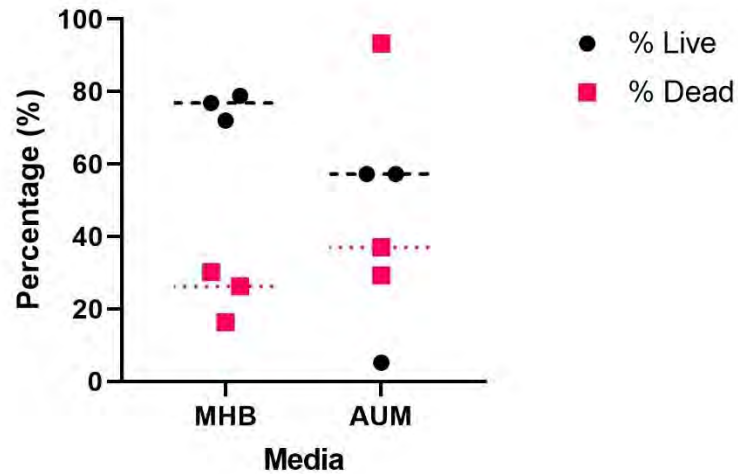


**Figure 5.16: Biofilms formed in MHB and AUM have no statistically significant differences in the percentages of live to dead cells**

Images of live (circles) and dead (squares) cells stained with the LIVE/DEAD® BacLight™ Bacterial Viability Kit \*for microscopy\* by Invitrogen were taken on a Leica DMI8 Microscope and the percentages of live to dead cells for different media was calculated by counting the live and dead cells. No statistical significance was seen between different media however one set of results from the biofilms formed in mAUM is very different.

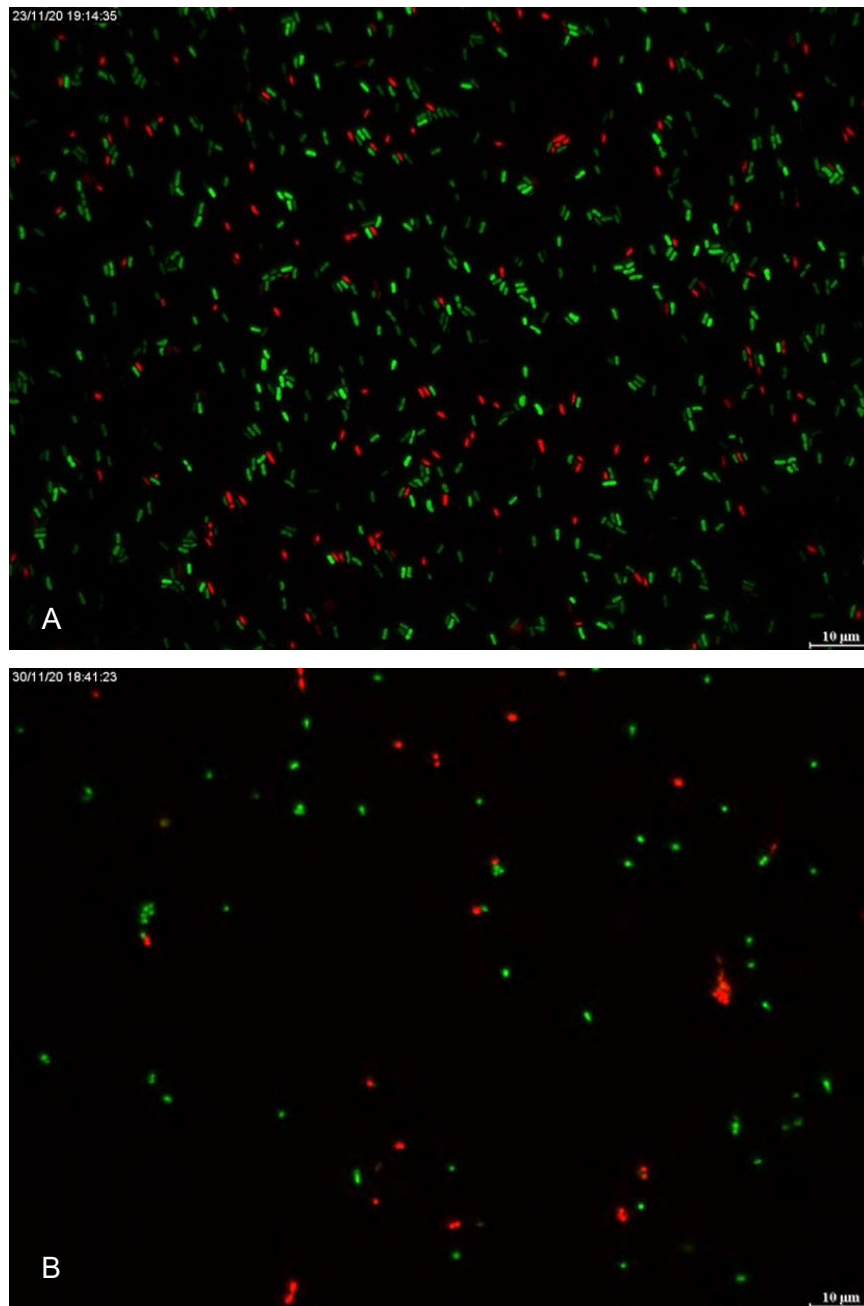


**Figure 5.17: Live/Dead staining fluorescent microscopy images of *A. baumannii* recovered from mDFR biofilms grown in MHB (A) and mAUM (B)**

Images taken under the 100X oil immersion lens of a Leica DMI8 fluorescent microscope. Red = dead cells stained with propidium iodide and viewed under Texas red settings, green cell = live cells stained with SYTO 9 and viewed under Green Fluorescent Protein settings. Staining kit used was the LIVE/DEAD® BacLight™ Bacterial Viability Kit \*for microscopy\* by Invitrogen.

#### **5.2.4.3 Viability counts of biofilms obtained from the mDFR reveal there is no significant difference between cells grown in MHB versus mAUM**

The final experiment analysing the biofilms obtained from the mDFR runs was a viable count performed on the resuspended biofilms recovered from the silicone tubing. There was an average of  $1.93 \times 10^{10}$  (SD  $\pm 1.95 \times 10^{10}$ ) viable cells recovered from biofilms grown in MHB (N = 3) while there was an average of  $3.23 \times 10^7$  (SD  $\pm 3.90 \times 10^7$ ) viable cells recovered from the biofilms grown in mAUM (N = 3). A Mann-Whitney U test determined that despite the large difference in values, there was no significant difference between the numbers of viable cells in each media.

### 5.3 Discussion

The aim of this chapter was to develop a catheter tubing infection model using the mDFR that could ultimately be used to create a model that imitates a catheter-associated urinary tract infection (CAUTI). Herein, the mDFR infection model was developed to contain tubing within the chamber and allow biofilm formation along the internal surface of the tubing as the bacteria were fed with 50% MHB, which is consistent with other methods within the literature<sup>160,161</sup>. The length of time the model would be run for was also of interest as patients are at higher risk of biofilm formation on a catheter the longer the device is in place<sup>51,227,228</sup>. The current models that utilise an mDFR with the same modification only allow biofilms to form for up to 48 hr, however their models were utilised for different types of infections<sup>160,161</sup> and biofilm formation within a catheter is often detected around five days after the insertion of the catheter<sup>239</sup>.

Another factor of high importance was what media to use in the model. MHB is a very rich medium containing beef extract, hydrolysed casein, and starch, which can be broken down easily by bacteria to provide amino acids, carbon, vitamins, nitrogen, and other important nutrients. Therefore, it is a very unrealistic media to use in a clinically relevant CAUTI model as all these nutrients will not be available in human urine which would be the best media to use. Unfortunately, due to the length of time which this experiment is run for, it requires 8.5 L of media, for one biological repeat. To accurately draw conclusions about biofilm formation in this model more than three repeats are needed, which amounts to more than 25 L of media. Human urine is therefore not an ideal media at this point of development as it requires ethical approval to work with and will incur an extra cost to acquire. To tackle this issue, a modified Artificial Urine Medium (mAUM) by Liang *et. al.* (2020) was found that supported the growth of common urinary pathogens and better replicated the *in vivo* conditions<sup>184</sup>.

To use the mAUM it was necessary to first understand how *A. baumannii* grew and formed biofilms within it. Additionally, as there are antimicrobial catheters commercially available that coat with silver compounds, the efficacy of silver acetate as an antimicrobial in mAUM, rather than a rich microbiological growth medium was also investigated. From the experiments carried out in this chapter it was firstly noted that *A. baumannii* is unable to grow to the same cell density in mAUM as it can in MHB. This is seen in the growth curve with MHB vs mAUM where there is an approximate 4-fold

difference in the final turbidity, however, the bacterium enters the exponential growth phase at the same time regardless of the media, which is important to note as mid-exponential phase bacteria were required to inoculate the biofilm model.

The trend of *A. baumannii* growing more in MHB than in mAUM continued throughout the experiments to investigate biofilm formation and silver acetate antimicrobial efficacy, with one potential anomaly. The initial test for biofilm formation in the mAUM versus MHB in a 96 well plate, showed there to be no significant differences between the biovolume in either medium. However, when tested in a 24 well plate, MHB produced a higher absorbance and therefore significantly more biovolume than mAUM even though the viable counts were not significantly different. To clarify this, further tests could be carried out in 96 well plates and 24 well plates to evaluate whether this was an anomalous result, or if the size of the wells had an impact on the biofilm biomass. It may also be of interest to repeat the experiment and measure the viability of the biofilm. This would allow exploration of if there was a significant difference in viability in the 96 well plate as with no significant difference in the absorbance, if there were differences in viability, this could potentially point the one of the mediums used having more of an impact on bacterial biofilm formation.

The MIC of silver acetate in mAUM was approximately 3.5-fold lower than in MHB and with the biofilm tests, bacteria grown in mAUM were more susceptible to silver acetate at low concentrations than in MHB. These differences between the growth in different media and how the bacteria react to silver acetate are suspected to be due to the rich nature of MHB and the presence of high levels of protein and therefore amino acids as opposed to the defined nature of mAUM which did not contain protein. MHB may have protected *A. baumannii* from the effects of silver acetate as it contains a large amount of protein in the form of casein and beef extract which silver ions may bind to. Moreover, these are also products which aren't present in normal human urine<sup>238</sup>. Interestingly, the urine of a patient with certain diseases and conditions such as cancer or pregnancy, can contain high levels of protein which is not seen in the mAUM<sup>238</sup>. However, in the interest of standardisation, the mAUM is an ideal media that provides growth of bacteria.

When MHB was replaced with mAUM in the mDFR tubing colonisation model, the viability, live/dead staining and appearance of the biofilms was compared with the biofilms formed in MHB. The mDFR tubing colonisation model was run in triplicate for each media type, however this was not enough repeats to see significant differences in the quantitative results. All that can be said is that a trend exists where more biofilm is

formed in MHB with more live cells present in samples than dead, however further repeats are needed to confirm whether these are significant differences between the two media types. The qualitative SEM images reflect that MHB appeared to produce more biofilm and these biofilms were more developed. This was observed in the way the cells had formed more compact cell aggregates and mushroom like structures with channels that allow for nutrient acquisition as seen in the literature in healthy, established biofilms<sup>55,69</sup>.

The mDFR tubing colonisation model developed here is the foundation for not only a clinically relevant CAUTI model, but also models that may imitate infections of endotracheal tubes and vascular access grafts. This model allows for the initial analysis of biofilm formation in clinically relevant media on clinically relevant surfaces and from the perspective of CAUTIs the mDFR tubing colonisation model could be adapted to resemble the schematic in Figure 5.18.

In the mDFR CAUTI biofilm model, the inside of the mDFR chamber would represent the bladder and the model would imitate an infection via extraluminal catheter colonisation where contamination occurs on insertion and begins from the opening of the catheter<sup>63</sup>. A set number of bacterial cells would be injected onto the outside of the catheter segment after sterilisation via the needle syringe. After inoculation mAUM would flow in and fill the chamber. When the chamber became full enough to just cover the opening of the catheter segment the second peristaltic pump would be switched on to pull media from the 'bladder' through the catheter segment at a flow rate of  $0.5 \text{ ml min}^{-1}$  equal to 0.72 L a day. Urine production varies from person to person but averages between 0.6 – 2.6 L a day<sup>236</sup>. It is hoped that this would allow for biofilm formation on the outside and inside of the catheter segment, which more accurately represents a clinical catheter associated urinary tract infection<sup>63</sup>.

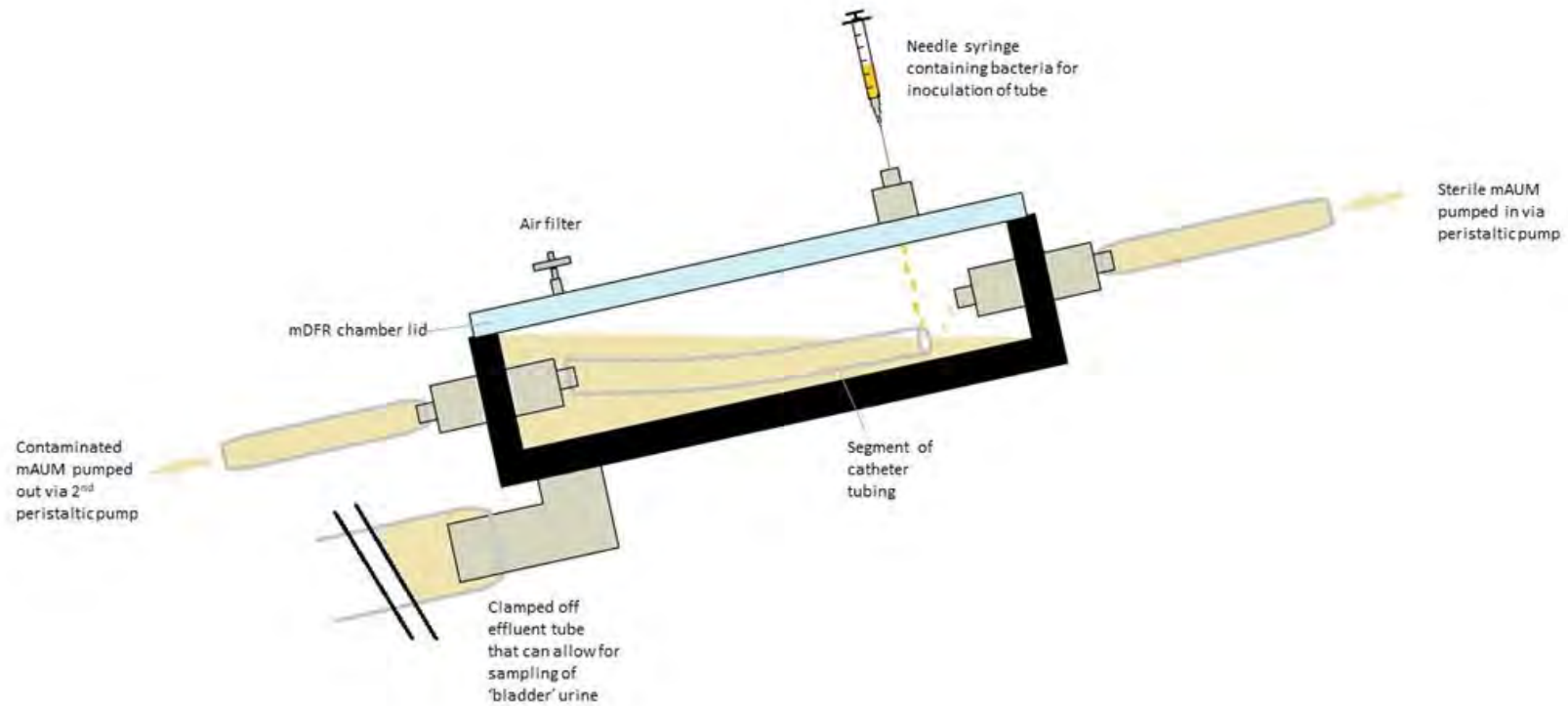


**Figure 5.18: Schematic diagram of proposed mDFR CAUTI biofilm model**

The schematic depicts the cross section of a channel of the mDFR when set up to run as the bladder catheter infection model. A catheter segment would sit within the chamber and would be inoculated on the outside of the tube via the needle syringe port in the chamber lid. Modified AUM would then be flowed into the system via one peristaltic pump and pulled out of the system through the catheter segment by a second pump. The effluent tube at the base of the chamber would allow for testing of the standing urine within the 'bladder'.

Analysis of this model would incorporate the same methods used for the basic biofilm model with the addition of analysing the numbers of viable bacteria within the remaining urine in the bladder via the effluent port at the base of the mDFR. This data would be interesting as catheters do not allow for complete drainage of the bladder and bacteria would inevitably colonise the bladder<sup>232</sup>. Another further experiment that could be carried out with this model would be to coat catheter segments with silver acetate and analyse differences in biofilm formation with and without silver whilst also analysing how much silver acetate leeches out of the coating and into the surrounding urine over the course of the experiment.

In conclusion, the mDFR tubing colonisation model is an efficient model to study biofilm formation within tubing over an extended period. With the current set up, it would be possible to run this model for longer than five days as the daily consumption of media is approximately 1.5 L. To fully analyse the differences in biofilm formation within different media, more repeats would be needed of the mDFR tubing colonisation model but the initial work with the mAUM outside of the biofilm model shows that is a sufficient media for biofilm work. Development of this model paves the way for future development of biofilm infection models that could lead to a better understanding of how CAUTI develop *in vitro* and allow for testing of antimicrobial catheter materials like silver acetate, in a clinically relevant model, reducing the number of materials that are sent forward for animal testing and ultimately reducing the incidence and severity of biofilm catheter infections.

## 6 Discussion

The work completed in this thesis was focussed upon two main aims. The first aim was to determine whether silver acetate is an effective antimicrobial against *Acinetobacter baumannii* and the second was to develop a clinically relevant tubing infection model for an *A. baumannii* infection. With the development of a clinically relevant model to replicate an infection caused by tubing colonisation, with further time and resources, silver acetate could have been tested as a tubing coating to evaluate the efficacy of the compound as a preventative measure to infection.

Chapter 4 shows that silver acetate can be used *in vitro* as an effective antimicrobial against *A. baumannii* providing raw data for this antimicrobial that did not previously exist for this bacterium. As silver is an ancient therapy and silver salts have been used in medicine for years, there appears to be an assumption that silver acetate is entirely effective, when there are very few studies which include raw data of the efficacy of this silver salt. This has led to the use of silver acetate coatings in commercially available tubing which is particularly concerning when considering the emergence of antimicrobial resistance and the emergence of bacteria which are multi-drug, pan-drug and extremely-drug resistant, such as *A. baumannii*. *A. baumannii* has only become known as a concerning pathogen in the last 40 years and so it has not been tested against silver acetate, especially as the recent focus of silver therapy is in silver nanoparticles. So, this chapter sought to fill this gap and provide raw data about the efficacy of silver acetate against *A. baumannii*

To provide further evidence of the efficacy of silver acetate against *A. baumannii* an *in vivo* *G. mellonella* larvae infection model was used. Here the larvae were treated with silver acetate after prior infection with *A. baumannii* and a significant improvement in survival was observed with this treatment. However, in modern medicine, it is highly unlikely that silver acetate would ever be injected as a form of treatment as silver is known to have levels of toxicity to human cells when in high concentrations. The most common uses of this compound would be in wound dressings and coatings of medical device materials to prevent infection and silver acetate is already used as a commercially available coating for vascular access grafts<sup>219</sup>. If silver acetate is used as a coating for indwelling medical devices or as a dressing, it is contained to the medium it is in, thus reducing the toxicity to the patient which they could otherwise face if they were to ingest silver acetate or take it via injection. However, there is a possibility that silver acetate

may come into contact with the patient's cells if it is in a graft or a catheter. On this basis the larvae were an excellent test for *in vivo* toxicity of silver acetate.

With more time, this work would have been expanded to incorporate human tissue culture methodologies. In the proposed study, HTB9 uroepithelial cells would have been exposed to concentrations of silver acetate to test toxicity of the compound *in vitro*. The choice to use bladder cells stems from the second aim of this thesis where development of a tubing infection model focussed upon urinary catheter infections. An initial aim for development of this model was to test the efficacy of silicone tubing impregnated with silver acetate, however due to time and logistical issues this was not possible. Human cell line cytotoxicity assays against silver acetate would have been implemented to determine the effect, if any, of the antimicrobial leeching from the coating into standing urine, where it would come into contact with the uroepithelial cells of the bladder and therefore it would be necessary to know the toxicity of silver acetate against human uroepithelial cells.

Chapter 5 focused on the development of a mDFR tubing colonisation model as the progenitor to a catheter-associated urinary tract infection (CAUTI) biofilm model using the modified Drip Flow Biofilm Reactor<sup>®</sup>. After development of the mDFR tubing colonisation model there were two aims, to develop the model further into the model shown in Section 5.3, Figure 5.18 and to coat sections of tubing with silver acetate and analyse the biofilm formation with and without silver acetate to determine its efficacy in preventing biofilm formation.

The work achieved provides raw data for the effectiveness of silver acetate against an ESKAPE pathogen less researched than its counterparts, utilising some newer methods to do so in the form of the *G. mellonella* larvae model. Alongside this, a protocol for growing and analysing a biofilm with the mDFR tubing colonisation model was developed. This model has the potential for adaptation to imitate other models such as endotracheal tube and vascular access graft models as infections in these medical devices involve media flowing within the tubing and around it. Adapting the model to contain flow around the outside of the tubing would better replicate these environments the model could be run for longer periods of time should the study call for it.

## **The impact of COVID-19 on my PhD: overcoming and adaptation**

The COVID-19 pandemic provided a unique challenge to overcome during a PhD and the choice to discuss it here is to highlight this challenge in a way that is deserved. Firstly, the lockdown arrived in the last six months of my third year, which forced a rapid adaptation of the proposed experiments carried out. This is apparent in the fact I was no longer able to carry out the tissue culture experiments I had planned, and I was unable to progress the mDFR tubing colonisation model to the final mDFR CAUTI biofilm model. With time and funding cut short, I had to work with my supervisor to assess what experiments were still feasible to complete this thesis.

A second challenge to this pandemic was more personal as I am quite a sociable person and used my time on campus to not only work but socialise with members of my team and other PhD's across campus. The people I interacted with on campus were occasionally sounding boards and emotional support and alongside this I played Lacrosse, and this was then suspended. The lockdown meant that I was suddenly facing the challenge of writing my PhD thesis but without the face-to-face support of my colleagues, friends and supervisor, and the necessary unwinding provided by my sport and my team.

Despite the challenges faced, I managed to overcome and turn the lockdown in my favour and wrote Chapters 3 and 4 and then produced a paper from Chapter 4 which was published in April 2021. I learned to become more flexible with my research, learning when to accept that a different route needed to be taken and found an alternate way to complete experiments I wanted to do by applying for and securing a research fellowship.

## 7 References

1. Meumann, E. M. *et al.* Genomic epidemiology of severe community-onset *Acinetobacter baumannii* infection. *Microb. Genomics* **5**, 1–13 (2019).
2. Peleg, A. Y., Seifert, H. & Paterson, D. L. *Acinetobacter baumannii*: Emergence of a successful pathogen. *Clin. Microbiol. Rev.* **21**, 538–582 (2008).
3. Maragakis, L. L. *et al.* An Outbreak of Multidrug-Resistant *Acinetobacter baumannii* Associated With Pulsatile Lavage Wound Treatment. *JAMA* **292**, 3006–3011 (2004).
4. Bouvet, P. J. M. & Grimont, P. A. D. Taxonomy of the genus *Acinetobacter* with the recognition of *Acinetobacter baumannii* sp. nov., *Acinetobacter haemolyticus* sp. nov., *Acinetobacter johnsonii* sp. nov., and *Acinetobacter junii* sp. nov. and emended descriptio. *Int. J. Syst. Bacteriol.* **36**, 228–240 (1986).
5. McConnell, M. J., Actis, L. & Pachón, J. *Acinetobacter baumannii*: Human infections, factors contributing to pathogenesis and animal models. *FEMS Microbiol. Rev.* **37**, 130–155 (2013).
6. Howard, A., O'Donoghue, M., Feeney, A. & Sleator, R. D. *Acinetobacter baumannii* An emerging opportunistic pathogen. *Virulence* **3**, 5 (2012).
7. Scott, P. *et al.* An outbreak of multidrug-resistant *Acinetobacter baumannii-calcoaceticus* complex infection in the US military health care system associated with military operations in Iraq. *Clin. Infect. Dis.* **44**, 1577–1584 (2007).
8. Elston, J. W. T., Bannan, C. L., Chih, D. T. & Boutlis, C. S. *Acinetobacter spp* in gunshot injuries. *Emerg. Infect. Dis.* **14**, 178–180 (2008).
9. Murray, C. K., Yun, H. C., Griffith, M. E., Hospenthal, D. R. & Tong, M. J. *Acinetobacter* Infection: What Was the True Impact during the Vietnam Conflict? *Clin. Infect. Dis.* **43**, 383–384 (2006).
10. Tong, M. J. Septic Complications of War Wounds. *JAMA* **219**, 1044–47 (1972).
11. Sebeny, P. J., Riddle, M. S. & Petersen, K. *Acinetobacter baumannii* skin and soft-tissue infection associated with war trauma. *Clinical Infectious Diseases* vol. 47 444–449 (2008).
12. Santajit, S. & Indrawattana, N. Mechanisms of Antimicrobial Resistance in ESKAPE Pathogens. *Biomed Res. Int.* **2016**, (2016).
13. Mulani, M. S., Kamble, E. E., Kumkar, S. N., Tawre, M. S. & Pardesi, K. R. Emerging strategies to combat ESKAPE pathogens in the era of antimicrobial resistance: A review. *Front. Microbiol.* **10**, (2019).
14. Gulen, T. A., Guner, R., Celikbilek, N., Keske, S. & Tasyaran, M. Clinical

- importance and cost of bacteremia caused by nosocomial multi drug resistant *Acinetobacter baumannii*. *Int. J. Infect. Dis.* **38**, 32–35 (2015).
15. Di Venanzio, G. *et al.* Urinary tract colonization is enhanced by a plasmid that regulates uropathogenic *Acinetobacter baumannii* chromosomal genes. *Nat. Commun.* **10**, 1–13 (2019).
  16. World Health Organisation. Global action plan on antimicrobial resistance. *WHO Press* (2015).
  17. Antunes, L. C. S., Imperi, F., Carattoli, A. & Visca, P. Deciphering the multifactorial nature of *Acinetobacter baumannii* pathogenicity. *PLoS One* **6**, (2011).
  18. Harding, C. M., Hennon, S. W. & Feldman, M. F. Uncovering the mechanisms of *Acinetobacter baumannii* virulence. *Nat. Rev. Microbiol.* **16**, 91–102 (2018).
  19. Aliramezani, A., Soleimani, M., Mazaheri, R., Fard, N. & Nojoomi, F. Virulence determinants and biofilm formation of *Acinetobacter baumannii* isolated from hospitalized patients. *Germs* **9**, 148–153 (2019).
  20. Ali, H. M. *et al.* Investigation of the virulence factors and molecular characterization of the clonal relations of multidrug-resistant *Acinetobacter baumannii* isolates. *J. AOAC Int.* **100**, 152–158 (2017).
  21. Espinal, P., Martí, S. & Vila, J. Effect of biofilm formation on the survival of *Acinetobacter baumannii* on dry surfaces. *J. Hosp. Infect.* **80**, 56–60 (2012).
  22. Gaiarsa, S. *et al.* Can Insertion Sequences Proliferation Influence Genomic Plasticity? Comparative Analysis of *Acinetobacter baumannii* Sequence Type 78, a Persistent Clone in Italian Hospitals. *Front. Microbiol.* **10**, (2019).
  23. Kyriakidis, I., Vasileiou, E., Pana, Z. D. & Tragiannidis, A. *Acinetobacter baumannii* antibiotic resistance mechanisms. *Pathogens* **10**, 1–31 (2021).
  24. Markley, J. L. & Wencewicz, T. A. Tetracycline-inactivating enzymes. *Front. Microbiol.* **9**, 1–22 (2018).
  25. Miyachiro, M. ., Contreras-Martel, C. & Dessen, A. Penicillin-Binding Proteins (PBPs) and Bacterial Cell Wall Elongation Complexes. in *Macromolecular Protein Complexes II: Structure and Function* (eds. Harris, J. & Marles-Wright, J.) 273–289 (Springer, Cham, 2019).
  26. Tooke, C. L. *et al.*  $\beta$ -Lactamases and  $\beta$ -Lactamase Inhibitors in the 21st Century. *J. Mol. Biol.* **431**, 3472–3500 (2019).
  27. Yong, D. *et al.* Characterization of a new metallo- $\beta$ -lactamase gene, *bla*<sub>N<sub>DM</sub>-1</sub>, and a novel erythromycin esterase gene carried on a unique genetic structure in *Klebsiella pneumoniae* sequence type 14 from India. *Antimicrob. Agents Chemother.* **53**, 5046–5054 (2009).
  28. Hujer, K. M. *et al.* Identification of a new allelic variant of the *Acinetobacter*

- baumannii* cephalosporinase, ADC-7  $\beta$ -lactamase: Defining a unique family of class C enzymes. *Antimicrob. Agents Chemother.* **49**, 2941–2948 (2005).
29. Turton, J. F. *et al.* Identification of *Acinetobacter baumannii* by detection of the bla OXA-51-like carbapenemase gene intrinsic to this species. *J. Clin. Microbiol.* **44**, 2974–2976 (2006).
  30. Woodford, N. *et al.* Multiplex PCR for genes encoding prevalent OXA carbapenemases in *Acinetobacter* spp. *Int. J. Antimicrob. Agents* **27**, 351–353 (2006).
  31. Turton, J. F. *et al.* The role of ISAba1 in expression of OXA carbapenemase genes in *Acinetobacter baumannii*. *FEMS Microbiol. Lett.* **258**, 72–77 (2006).
  32. Magnet, S., Courvalin, P. & Lambert, T. Resistance-Nodulation-Cell Division-Type Efflux Pump Involved in Aminoglycoside Resistance in *Acinetobacter baumannii* Strain BM4454. *Society* **45**, 3375–3380 (2001).
  33. Ramirez, M. S. & Tolmasky, M. E. Aminoglycoside modifying enzymes. *Drug Resist. Updat.* **13**, 151–171 (2010).
  34. Zavascki, A. P., Carvalhaes, C. G., Picão, R. C. & Gales, A. C. Multidrug-resistant *Pseudomonas aeruginosa* and *Acinetobacter baumannii*: Resistance mechanisms and implications for therapy. *Expert Rev. Anti. Infect. Ther.* **8**, 71–93 (2010).
  35. Garneau-Tsodikova, S. & Labby, K. J. Mechanisms of resistance to aminoglycoside antibiotics: Overview and perspectives. *Med. Chem. Commun.* **7**, 11–27 (2016).
  36. Vila, J., Martí, S. & Sánchez-Céspedes, J. Porins, efflux pumps and multidrug resistance in *Acinetobacter baumannii*. *J. Antimicrob. Chemother.* **59**, 1210–1215 (2007).
  37. Sugawara, E. & Nikaido, H. OmpA is the principal nonspecific slow porin of *Acinetobacter baumannii*. *J. Bacteriol.* **194**, 4089–4096 (2012).
  38. Smani, Y. *et al.* Role of OmpA in the Multidrug Resistance Phenotype of *Acinetobacter baumannii*. *Antimicrob. Agents Chemother.* **58**, 1806–1808 (2014).
  39. Mussi, M. A., Limansky, A. S. & Viale, A. M. Acquisition of resistance to carbapenems in multidrug-resistant clinical strains of *Acinetobacter baumannii*: Natural insertional inactivation of a gene encoding a member of a novel family of  $\beta$ -barrel outer membrane proteins. *Antimicrob. Agents Chemother.* **49**, 1432–1440 (2005).
  40. Coyne, S., Courvalin, P. & Périchon, B. Efflux-mediated antibiotic resistance in *Acinetobacter* spp. *Antimicrob. Agents Chemother.* **55**, 947–953 (2011).
  41. Putman, M., Van Veen, H. W. & Konings, W. N. Molecular Properties of Bacterial

- Multidrug Transporters. *Microbiol. Mol. Biol. Rev.* **64**, 672–693 (2000).
42. Guardabassi, L., Dijkshoorn, L., Collard, J. M., Olsen, J. E. & Dalsgaard, A. Distribution and in-vitro transfer of tetracycline resistance determinants in clinical and aquatic *Acinetobacter* strains. *J. Med. Microbiol.* **49**, 929–936 (2000).
  43. Almasaudi, S. B. *Acinetobacter spp.* as nosocomial pathogens: Epidemiology and resistance features. *Saudi J. Biol. Sci.* **25**, (2018).
  44. Lari, A. R., Ardebili, A. & Hashemi, A. AdeR-AdeS mutations & overexpression of the AdeABC efflux system in ciprofloxacin-resistant *Acinetobacter baumannii* clinical isolates. *Indian J. Med. Res.* **147**, 413–421 (2018).
  45. Héritier, C., Poirel, L., Lambert, T. & Nordmann, P. Contribution of acquired carbapenem-hydrolyzing oxacillinases to carbapenem resistance in *Acinetobacter baumannii*. *Antimicrob. Agents Chemother.* **49**, 3198–3202 (2005).
  46. Ardebili, A., Lari, A. R., Beheshti, M. & Lari, E. R. Association between mutations in *gyrA* and *parC* genes of *Acinetobacter baumannii* clinical isolates and ciprofloxacin resistance. *Iran. J. Basic Med. Sci.* **18**, 623–626 (2015).
  47. Chin, C. Y., Gregg, K. A., Napier, B. A., Ernst, R. K. & Weiss, D. S. A PmrB-regulated deacetylase required for lipid A modification and polymyxin resistance in *Acinetobacter baumannii*. *Antimicrob. Agents Chemother.* **59**, 7911–7914 (2015).
  48. Sun, B. *et al.* New Mutations Involved in Colistin Resistance in *Acinetobacter baumannii*. *mSphere* **5**, (2020).
  49. Aldred, K. J., Kerns, R. J. & Osheroff, N. Mechanism of quinolone action and resistance. *Biochemistry* **53**, 1565–1574 (2014).
  50. Inchai, J. *et al.* Risk factors of multidrug-resistant, extensively drug-resistant and pandrug-resistant *Acinetobacter baumannii* ventilator-associated pneumonia in a Medical Intensive Care Unit of University Hospital in Thailand. *J. Infect. Chemother.* **21**, 570–574 (2015).
  51. Michalopoulos, A. & Falagas, M. E. Treatment of *Acinetobacter* infections. *Expert Opin. Pharmacother.* **11**, 779–788 (2010).
  52. O’Toole, G., Kaplan, H. B. & Kolter, R. Biofilm Formation as Microbial Development. *Annu. Rev. Microbiol.* **54**, 49–79 (2000).
  53. Diaconu, O., Siriopol, I., Poloşanu, L. I. & Grigoraş, I. Endotracheal Tube Biofilm and its Impact on the Pathogenesis of Ventilator-Associated Pneumonia. *J. Crit. Care Med.* **4**, 50–55 (2018).
  54. Hall-Stoodley, L. *et al.* Towards diagnostic guidelines for biofilm-associated infections. *FEMS Immunol. Med. Microbiol.* **65**, 127–145 (2012).
  55. Tomaras, A. P., Dorsey, C. W., Edelman, R. E. & Actis, L. A. Attachment to and

- biofilm formation on abiotic surfaces by *Acinetobacter baumannii*: involvement of a novel chaperone-usher pili assembly system Printed in Great Britain. *Microbiology* **149**, 3473–3484 (2003).
56. Kaplan, H. B. & Greenberg, E. P. Diffusion of autoinducer is involved in regulation of the *Vibrio fischeri* luminescence system. *J. Bacteriol.* **163**, 1210–1214 (1985).
  57. Rutherford, S. T. & Bassler, B. L. Bacterial quorum sensing: Its role in virulence and possibilities for its control. *Cold Spring Harb. Perspect. Med.* **2**, 1–25 (2012).
  58. Niu, C., Clemmer, K. M., Bonomo, R. A. & Rather, P. N. Isolation and characterization of an autoinducer synthase from *Acinetobacter baumannii*. *J. Bacteriol.* **190**, 3386–3392 (2008).
  59. López-Martín, M., Dubern, J. F., Alexander, M. R. & Williams, P. AbaM regulates Quorum sensing, Biofilm Formation, and Virulence in *Acinetobacter baumannii*. *J. Bacteriol.* **203**, 1–13 (2021).
  60. Fernández-barat, L. & Torres, A. Biofilms in ventilator-associated pneumonia. *Future Microbiol.* **11**, 1599–1610 (2016).
  61. Raad, I. I. *et al.* The prevention of biofilm colonization by multidrug-resistant pathogens that cause ventilator-associated pneumonia with antimicrobial-coated endotracheal tubes. *Biomaterials* **32**, 2689–94 (2011).
  62. Cortese, Y. J., Wagner, V. E., Tierney, M., Devine, D. & Fogarty, A. Review of Catheter-Associated Urinary Tract Infections and In vitro Urinary Tract Models. *J. Healthc. Eng.* **2018**, 2986742 (2018).
  63. Mandakhalikar, K. D., Chua, R. R. & Tambyah, P. A. New Technologies for Prevention of Catheter Associated Urinary Tract Infection. *Curr. Treat. Options Infect. Dis.* **8**, 24–41 (2016).
  64. Colquhoun, J. M. & Rather, P. N. Insights Into Mechanisms of Biofilm Formation in *Acinetobacter baumannii* and Implications for Uropathogenesis. *Front. Cell. Infect. Microbiol.* **10**, (2020).
  65. de Breij, A. *et al.* CsuA/BABCDE-dependent pili are not involved in the adherence of *Acinetobacter baumannii* ATCC19606<sup>T</sup> to human airway epithelial cells and their inflammatory response. *Res. Microbiol.* **160**, 213–218 (2009).
  66. Loehfelm, T. W., Luke, N. R. & Campagnari, A. A. Identification and characterization of an *Acinetobacter baumannii* biofilm-associated protein. *J. Bacteriol.* **190**, 1036–1044 (2008).
  67. Gaddy, J. A., Tomaras, A. P. & Actis, L. A. The *Acinetobacter baumannii* 19606 OmpA Protein Plays a Role in Biofilm Formation on Abiotic Surfaces and in the Interaction of This Pathogen with Eukaryotic Cells. *Infect. Immun.* **77**, 3150–3160 (2009).

68. Choi, A. H. K., Slamti, L., Avci, F. Y., Pier, G. B. & Maira-Litrán, T. The *pgaABCD* locus of *Acinetobacter baumannii* encodes the production of poly- $\beta$ -1-6-N-acetylglucosamine, which is critical for biofilm formation. *J. Bacteriol.* **191**, 5953–5963 (2009).
69. Greene, C., Wu, J., Rickard, A. H. & Xi, C. Evaluation of the ability of *Acinetobacter baumannii* to form biofilms on six different biomedical relevant surfaces. *Lett. Appl. Microbiol.* **63**, 233–239 (2016).
70. Ishii, S., Koki, J., Unno, H. & Hori, K. Two Morphological Types of Cell Appendages on a Strongly Adhesive Bacterium, *Acinetobacter* sp. Strain Tol 5. *Appl. Environ. Microbiol.* **70**, 5026–5029 (2004).
71. Gaddy, J. A. & Actis, L. A. Regulation of *Acinetobacter baumannii* biofilm formation. *Future Microbiol.* **4**, 273–278 (2009).
72. Tomaras, A. P., Flagler, M. J., Dorsey, C. W., Gaddy, J. A. & Actis, L. A. Characterization of a two-component regulatory system from *Acinetobacter baumannii* that controls biofilm formation and cellular morphology. *Microbiology* **154**, 3398–3409 (2008).
73. De Gregorio, E. *et al.* Biofilm-associated proteins: News from *Acinetobacter*. *BMC Genomics* **16**, 1–14 (2015).
74. Sharon Goh, H. M. *et al.* Molecular analysis of the *Acinetobacter baumannii* biofilm-associated protein. *Appl. Environ. Microbiol.* **79**, 6535–6543 (2013).
75. Cucarella, C. *et al.* Bap, a *Staphylococcus aureus* Surface Protein involved in Biofilm Formation. *J. Bacteriol.* **183**, 2888–2896 (2001).
76. Brossard, K. A. & Campagnari, A. A. The *Acinetobacter baumannii* biofilm-associated protein plays a role in adherence to human epithelial cells. *Infect. Immun.* **80**, 228–233 (2012).
77. He, X. *et al.* Biofilm formation caused by clinical *Acinetobacter baumannii* isolates is associated with overexpression of the AdeFGH efflux pump. *Antimicrob. Agents Chemother.* **59**, 4817–25 (2015).
78. Smani, Y. *et al.* Role of Fbronectin in the Adhesion of *Acinetobacter baumannii* to Host Cells. *PLoS One* **7**, 1806–1808 (2012).
79. Nie, D. *et al.* Outer membrane protein A (OmpA) as a potential therapeutic target for *Acinetobacter baumannii* infection. *J. Biomed. Sci.* **27**, 1–8 (2020).
80. Maira-Litrán, T. *et al.* Immunochemical properties of the Staphylococcal Poly-N-acetylglucosamine surface polysaccharide. *Infect. Immun.* **70**, 4433–4440 (2002).
81. Wang, X., Preston, J. F. & Romeo, T. The *pgaABCD* Locus of *Escherichia coli* Promotes the Synthesis of a Polysaccharide Adhesin Required for Biofilm Formation. *J. Bacteriol.* **186**, 2724–2734 (2004).

82. Flannery, A., Le Berre, M., Pier, G. B., O'gara, J. P. & Kilcoyne, M. Glycomics Microarrays Reveal Differential *In Situ* Presentation of the Biofilm Polysaccharide Poly-*N*-Acetylglucosamine on *Acinetobacter baumannii* and *Staphylococcus aureus* Cell Surfaces. *Int. J. Mol. Sci.* **21**, (2020).
83. J. Wesley, A. History of the Medical Use of Silver. *Surg. Infect. (Larchmt)*. **10**, 289–292 (2009).
84. Russell, A. D. & Hugo, W. B. Antimicrobial Activity and Action of Silver. *Prog. Med. Chem.* **31**, 351–370 (1994).
85. Lansdown, A. B. Silver. I: Its antibacterial properties and mechanism of action. *J. Wound Care* **11**, 125–130 (2002).
86. Sims, J. M. & Marion-Sims, H. *The Story of My Life*. (D. Appleton and Company 1884, 1884).
87. Schneider, G. Silver nitrate prophylaxis. *Can. Med. Assoc. J.* **131**, 193–196 (1984).
88. Halsted, W. S. Operative Treatment of Hernia. *Am. J. Med. Sci.* **110**, 13–17 (1895).
89. Legge Roe, A. Collosol Argentum and Its Ophthalmic Uses. *Br. Med. J.* **1**, 104 (1915).
90. Lansdown, A. B. G. G. Silver in Healthcare: antimicrobial Effects and safety in use. *Curr. Probl. Dermatol.* **33**, 17–34 (2006).
91. Maitre, S., Jaber, K., Perrot, J. L., Guy, C. & Cambazard, F. [Increased serum and urinary levels of silver during treatment with topical silver sulfadiazine]. *Ann. Dermatol. Venereol.* **129**, 217–219 (2002).
92. Witkop, B. Paul Ehrlich and His Magic Bullets , Revisited Published by : American Philosophical Society Paul Ehrlich and His Magic Bullets-Revisited. *Proc. Am. Phil. Soc.* **143**, 540–557 (1999).
93. Fox, C. L. Silver Sulfadiazine - A new topical. *Arch. Surg.* **96**, 4–8 (1968).
94. Carr, H. S., Wlodkowski, T. J. & Rosenkranz, H. S. Silver sulfadiazine: in vitro antibacterial activity. *Antimicrob. Agents Chemother.* **4**, 585–587 (1973).
95. Hohl, D. H. *et al.* Comparison Between Two Strategies of Topical Treatment in Tar Burn: A Case Report. *J. Burn Care Res.* **42**, 590–593 (2021).
96. Politano, A. D., Campbell, K. T., Rosenberger, L. H. & Sawyer, R. G. Use of silver in the prevention and treatment of infections: Silver review. *Surg. Infect. (Larchmt)*. **14**, 8–20 (2013).
97. Wasef, L. G. *et al.* Effects of Silver Nanoparticles on Burn Wound Healing in a Mouse Model. *Biol. Trace Elem. Res.* **193**, 456–465 (2020).
98. Chaloupka, K., Malam, Y. & Seifalian, A. M. Nanosilver as a new generation of

- nanoproduct in biomedical applications. *Trends Biotechnol.* **28**, 580–588 (2010).
99. Siddiqi, K. S., Husen, A. & Rao, R. A. K. A review on biosynthesis of silver nanoparticles and their biocidal properties. *J. Nanobiotechnology* **16**, 1–28 (2018).
  100. Aymonier, C. *et al.* Hybrids of silver nanoparticles with amphiphilic hyperbranched macromolecules exhibiting antimicrobial properties. *Chem. Commun.* **24**, 3018–3019 (2002).
  101. Sondi, I. & Salopek-Sondi, B. Silver nanoparticles as antimicrobial agent: A case study on *E. coli* as a model for Gram-negative bacteria. *J. Colloid Interface Sci.* **275**, 177–182 (2004).
  102. Van Der Zande, M. *et al.* Distribution, elimination, and toxicity of silver nanoparticles and silver ions in rats after 28-day oral exposure. *ACS Nano* **6**, 7427–7442 (2012).
  103. Kim, S. & Ryu, D. Y. Silver nanoparticle-induced oxidative stress, genotoxicity and apoptosis in cultured cells and animal tissues. *J. Appl. Toxicol.* **33**, 78–89 (2013).
  104. Hackenberg, S. *et al.* Silver nanoparticles: Evaluation of DNA damage, toxicity and functional impairment in human mesenchymal stem cells. *Toxicol. Lett.* **201**, 27–33 (2011).
  105. Marx, D. E. & Barillo, D. J. Silver in medicine: The basic science. *Burns* **40**, S9–S18 (2014).
  106. Modak, S. M. & Fox, C. L. Binding of silver sulfadiazine to the cellular components of *Pseudomonas aeruginosa*. *Biochem. Pharmacol.* **22**, 2391–2404 (1973).
  107. Bovenkamp, G. L., Zanzen, U., Krishna, K. S., Hormes, J. & Prange, A. X-Ray absorption near-edge structure (XANES) spectroscopy study of the interaction of silver ions with *Staphylococcus aureus*, *Listeria monocytogenes*, and *Escherichia coli*. *Appl. Environ. Microbiol.* **79**, 6385–6390 (2013).
  108. Xu, F. F. & Imlay, J. A. Silver(I), mercury(II), cadmium(II), and zinc(II) target exposed enzymic iron-sulfur clusters when they toxify *Escherichia coli*. *Appl. Environ. Microbiol.* **78**, 3614–3621 (2012).
  109. Morones-Ramirez, J. R., Winkler, J. A., Spina, C. S. & Collins, J. J. Silver Enhances Antibiotic Activity Against Gram-negative Bacteria. *Sci. Transl. Med.* **5**, 1–21 (2013).
  110. Arakawa, H., Neault, J. F. & Tajmir-Riahi, H. A. Silver(I) Complexes with DNA and RNA Studied by Fourier Transform Infrared Spectroscopy and Capillary Electrophoresis. *Biophys. J.* **81**, 1580–1587 (2001).
  111. Starodub, M. E. & Trevors, J. T. Silver accumulation and resistance in *Escherichia coli* R1. *J. Inorg. Biochem.* **39**, 317–325 (1990).
  112. Percival, S. L., Bowler, P. G. & Russell, D. Bacterial resistance to silver in wound

- care. *J. Hosp. Infect.* **60**, 1–7 (2005).
113. Mchugh, G. L., Moellering, R. C., Hopkins, C. C. & Swartz, M. N. *Salmonella typhimurium* Resistant to Silver Nitrate, Chloramphenicol and Ampicillin. A new threat in burn units? *Lancet* **305**, 235–240 (1975).
  114. Finley, P. J. *et al.* Unprecedented silver resistance in clinically isolated Enterobacteriaceae: Major implications for burn and wound management. *Antimicrob. Agents Chemother.* **59**, 4734–4741 (2015).
  115. Hendry, A. T. & Stewart, I. O. Silver-resistant Enterobacteriaceae from hospital patients. *Can. J. Microbiol.* **25**, 915–921 (1979).
  116. Haefeli, C., Franklin, C. & Hardy, K. Plasmid-determined silver resistance in *Pseudomonas stutzeri* isolated from a silver mine. *J. Bacteriol.* **158**, 389–392 (1984).
  117. Deshpande, L. . & Chopade, B. A. Plasmid Mediated Silver Resistance in *A. baumannii*. *Biometals* **7**, 49–56 (1994).
  118. Klaus, T., Joerger, R., Olsson, E. & Granqvist, C. G. Silver-based crystalline nanoparticles, microbially fabricated. *Proc. Natl. Acad. Sci. U. S. A.* **96**, 13611–13614 (1999).
  119. Li, X. Z., Nikaido, H. & Williams, K. E. Silver-resistant mutants of *Escherichia coli* display active efflux of Ag<sup>+</sup> and are deficient in porins. *J. Bacteriol.* **179**, 6127–6132 (1997).
  120. McNeilly, O., Mann, R., Hamidian, M. & Gunawan, C. Emerging Concern for Silver Nanoparticle Resistance in *Acinetobacter baumannii* and Other Bacteria. *Front. Microbiol.* **12**, (2021).
  121. Randall, C. P., Gupta, A., Jackson, N., Busse, D. & O'Neill, A. J. Silver resistance in Gram-negative bacteria: A dissection of endogenous and exogenous mechanisms. *J. Antimicrob. Chemother.* **70**, 1037–1046 (2015).
  122. Gupta, A., Matsui, K., Lo, J. F. & Silver, S. Molecular basis for resistance to silver cations in *Salmonella*. *Nat. Med.* **5**, 183–188 (1999).
  123. Andrade, L. N., Siqueira, T. E. S., Martinez, R. & Darini, A. L. C. Multidrug-resistant CTX-M-(15, 9, 2)- and KPC-2-producing *Enterobacter hormaechei* and *Enterobacter asburiae* isolates possessed a set of acquired heavy metal tolerance genes including a chromosomal sil operon (for acquired silver resistance). *Front. Microbiol.* **9**, 1–6 (2018).
  124. Loh, J. V., Percival, S. L., Woods, E. J., Williams, N. J. & Cochrane, C. A. Silver resistance in MRSA isolated from wound and nasal sources in humans and animals. *Int. Wound J.* **6**, 32–38 (2009).
  125. Hosny, A. E. D. M. S., Rasmy, S. A., Aboul-Magd, D. S., Kashef, M. T. & El-Bazza,

- Z. E. The increasing threat of silver-resistance in clinical isolates from wounds and burns. *Infect. Drug Resist.* **12**, 1985–2001 (2019).
126. Fang, L. *et al.* Co-spread of metal and antibiotic resistance within ST3-IncHI2 plasmids from *E. coli* isolates of food-producing animals. *Sci. Rep.* **6**, 1–8 (2016).
  127. Sütterlin, S. *et al.* Silver resistance genes are overrepresented among *Escherichia coli* isolates with CTX-M production. *Appl. Environ. Microbiol.* **80**, 6863–6869 (2014).
  128. Percival, S. L., Salisbury, A. M. & Chen, R. Silver, biofilms and wounds: resistance revisited. *Crit. Rev. Microbiol.* **45**, 223–237 (2019).
  129. Bjarnsholt, T. *et al.* The in vivo biofilm. *Trends Microbiol.* **21**, 466–474 (2013).
  130. Coenye, T. & Nelis, H. J. In vitro and in vivo model systems to study microbial biofilm formation. *J. Microbiol. Methods* **83**, 89–105 (2010).
  131. Roberts, A. E. L., Kragh, K. N., Bjarnsholt, T. & Diggle, S. P. The Limitations of in Vitro Experimentation in Understanding Biofilms and Chronic Infection. *J. Mol. Biol.* **427**, 3646–3661 (2015).
  132. Azeredo, J. *et al.* Critical review on biofilm methods. *Crit. Rev. Microbiol.* **43**, 313–351 (2017).
  133. Gomes, I. B. *et al.* Standardized reactors for the study of medical biofilms: a review of the principles and latest modifications. *Crit. Rev. Biotechnol.* **38**, 657–670 (2018).
  134. Goeres, D. M. *et al.* A method for growing a biofilm under low shear at the air-liquid interface using the drip flow biofilm reactor. *Nat. Protoc.* **4**, 783–788 (2009).
  135. Stepanović, S. *et al.* Quantification of biofilm in microtiter plates: Overview of testing conditions and practical recommendations for assessment of biofilm production by *Staphylococci*. *Apmis* **115**, 891–899 (2007).
  136. O'Toole, G. A. & Kolter, R. Initiation of biofilm formation in *Pseudomonas fluorescens* WCS365 proceeds via multiple, convergent signalling pathways: A genetic analysis. *Mol. Microbiol.* **28**, 449–461 (1998).
  137. Sandberg, M., Määttä, A., Peltonen, J., Vuorela, P. M. & Fallarero, A. Automating a 96-well microtitre plate model for *Staphylococcus aureus* biofilms: an approach to screening of natural antimicrobial compounds. *Int. J. Antimicrob. Agents* **32**, 233–240 (2008).
  138. Macià, M. D., Rojo-Moliner, E. & Oliver, A. Antimicrobial susceptibility testing in biofilm-growing bacteria. *Clin. Microbiol. Infect.* **20**, 981–990 (2014).
  139. Peeters, E., Nelis, H. J. & Coenye, T. Comparison of multiple methods for quantification of microbial biofilms grown in microtiter plates. *J. Microbiol. Methods* **72**, 157–165 (2008).

140. Ceri, H., Olson, M. E., Stremick, C., Read, R. R. & Morck, D. The Calgary Biofilm Device. *J. Clin. Microbiol.* **37**, 1771–1776 (1999).
141. Innovotech Canada. MBEC Assay<sup>®</sup>. <https://www.innovotech.ca/products/mbec-assays/> (2021).
142. Harrison, J. J. *et al.* The use of microscopy and three-dimensional visualization to evaluate the structure of microbial biofilms cultivated in the Calgary biofilm device. *Biol. Proced. Online* **8**, 194–213 (2006).
143. Moskowitz, S. M., Foster, J. M., Emerson, J. & Burns, J. L. Clinically Feasible Biofilm Susceptibility Assay for Isolates of *Pseudomonas aeruginosa* from Patients with Cystic Fibrosis. *J. Clin. Microbiol.* **42**, 1915–1922 (2004).
144. Mulet, X. *et al.* Azithromycin in *Pseudomonas aeruginosa* biofilms: Bactericidal activity and selection of *nfxB* mutants. *Antimicrob. Agents Chemother.* **53**, 1552–1560 (2009).
145. Salek, M. M., Jones, S. M. & Martinuzzi, R. J. Methicillin resistant *Staphylococcus aureus* biofilm susceptibility in response to increased level of shear stresses and flow agitation. *Proc. IEEE Annu. Northeast Bioeng. Conf. NEBEC* (2009) doi:10.1109/NEBC.2009.4967769.
146. McCoy, W. F., Bryers, J. D., Robbins, J. & Costerton, J. W. Observations of fouling biofilm formation. *Can. J. Microbiol.* **27**, 910–917 (1981).
147. Nickel, J. C., Ruseska, I., Wright, J. B. & Costerton, A. J. W. Tobramycin Resistance of *Pseudomonas aeruginosa* Cells Growing as a Biofilm on Urinary Catheter Material. *Antimicrob. Agents Chemother.* **27**, 619–624 (1985).
148. BioSurface Technologies Corporation. Bio-inLine Biofilm Reactor - BioSurface Technologies. <https://biofilms.biz/products/biofilm-reactors/bio-inline-biofilm-reactor/>.
149. Kharazmi, A., Giwercman, B. & Hoiby, N. Robbins Device in Biofilm Research. *Methods Enzymol.* **310**, 207–215 (1999).
150. Coenye, T., De Prijck, K., De Wever, B. & Nelis, H. J. Use of the modified Robbins device to study the *in vitro* biofilm removal efficacy of NitrAdine<sup>™</sup>, a novel disinfecting formula for the maintenance of oral medical devices. *J. Appl. Microbiol.* **105**, 733–740 (2008).
151. Yassin, S. A., German, M. J., Rolland, S. L., Rickard, A. H. & Jakubovics, N. S. Inhibition of multispecies biofilms by a fluoride-releasing dental prosthesis copolymer. *J. Dent.* **48**, 62–70 (2016).
152. Blanc, V. *et al.* Characterization and application of a flow system for *in vitro* multispecies oral biofilm formation. *J. Periodontal Res.* **49**, 323–332 (2014).
153. Linton, C. J., Sherriff, A. & Millar, M. R. Use of a modified robbins device to directly

- compare the adhesion of *Staphylococcus epidermidis* RP62A to surfaces. *J. Appl. Microbiol.* **86**, 194–202 (1999).
154. Magana, M. *et al.* Options and limitations in clinical investigation of bacterial biofilms. *Clin. Microbiol. Rev.* **31**, 1–49 (2018).
  155. Stickler, D. J., Morris, N. S. & Winters, C. Simple physical model to study formation and physiology of biofilms on urethral catheters. *Methods Enzymol.* **310**, 463–494 (1999).
  156. BioSurface Technologies Corporation. Drip Flow Biofilm Reactor. <https://biofilms.biz/products/biofilm-reactors/drip-flow-biofilm-reactor/>.
  157. Schwartz, K., Stephenson, R., Hernandez, M., Jambang, N. & Boles, B. The Use of Drip Flow and Rotating Disk Reactors for *Staphylococcus aureus* Biofilm Analysis. *J. Vis. Exp.* **27**, 1–5 (2010).
  158. Chen, X., Hirt, H., Li, Y., Gorr, S. U. & Aparicio, C. Antimicrobial GL13K peptide coatings killed and ruptured the wall of *Streptococcus gordonii* and prevented formation and growth of biofilms. *PLoS One* **9**, 111579 (2014).
  159. Williams, D. L. *et al.* Effect of silver-loaded PMMA on *Streptococcus mutans* in a drip flow reactor. *J. Biomed. Mater. Res. - Part A* **105**, 2632–39 (2017).
  160. Curtin, J. J. & Donlan, R. M. Using bacteriophages to reduce formation of catheter-associated biofilms by *Staphylococcus epidermidis*. *Antimicrob. Agents Chemother.* **50**, 1268–1275 (2006).
  161. Fu, W. *et al.* Bacteriophage cocktail for the prevention of biofilm formation by *Pseudomonas aeruginosa* on catheters in an *in vitro* model system. *Antimicrob. Agents Chemother.* **54**, 397–404 (2010).
  162. Ionescu, A. C. *et al.* Silver-polysaccharide antimicrobial nanocomposite coating for methacrylic surfaces reduces *Streptococcus mutans* biofilm formation *in vitro*. *J. Dent.* **43**, 1483–90 (2015).
  163. Thermofisher Scientific. LIVE/DEAD™ BacLight™ Bacterial Viability Kit, for microscopy & quantitative assays. <https://www.thermofisher.com/order/catalog/product/L7012#/L7012>.
  164. Korber, D. R., Lawrence, J. R., Zhang, L. & Caldwell, D. E. Effect of gravity on bacterial deposition and orientation in laminar flow environments. *Biofouling* **2**, 335–350 (1990).
  165. Rutter, P. & Leech, R. The Deposition of *Streptococcus sanguis* NCTC 7868 from a flowing suspension. *J. Gen. Microbiol.* **120**, 301–307 (1980).
  166. Wolfaardt, G. M., Lawrence, J. R., Robarts, R. D., Caldwell, S. J. & Caldwell, D. E. Multicellular organization in a degradative biofilm community. *Appl. Environ. Microbiol.* **60**, 434–446 (1994).

167. Sternberg, C. & Tolker-Nielsen, T. Growing and Analyzing Biofilms in Flow Cells. in *Current Protocols in Microbiology* 1–15 (2006). doi:10.1002/9780471729259.mc01b02s00.
168. Tolker-Nielsen, T. & Sternberg, C. Methods for Studying Biofilm Formation: flow cells and confocal laser scanning microscopy. in *Pseudomonas Methods and Protocols* (eds. Filloux, A. & Ramos, J. L.) 615–629 (Humana Press, 2014).
169. David, C., Heuschkel, I., Buher, K. & Karande, R. Cultivation of Productive Biofilms in flow reactors and their characterisation by CLSM. in *Immobilisation of Enzymes and Cells* (eds. Guisan, J., Bolivar, J., Lopez-Gallango, F. & Rocha-Martin, J.) 437–452 (Humana Press, 2020).
170. Møller, S. *et al.* In situ gene expression in mixed-culture biofilms: Evidence of metabolic interactions between community members. *Appl. Environ. Microbiol.* **64**, 721–732 (1998).
171. Haagensen, J. A. J. *et al.* Differentiation and distribution of colistin- and sodium dodecyl sulfate-tolerant cells in *Pseudomonas aeruginosa* biofilms. *J. Bacteriol.* **189**, 28–37 (2007).
172. Gómez-Suárez, C., Busscher, H. J. & Van Der Mei, H. C. Analysis of Bacterial Detachment from Substratum Surfaces by the Passage of Air-Liquid Interfaces. *Appl. Environ. Microbiol.* **67**, 2531–2537 (2001).
173. BioSurface Technologies Corporation. Capillary Flow Cells - BioSurface Technologies Corporation. <https://biofilms.biz/products/microscopy-flow-cells/capillary-flow-cells/>.
174. Pitts, B. *et al.* A repeatable laboratory method for testing the efficacy of biocides against toilet bowl biofilms. *J. Appl. Microbiol.* **91**, 110–117 (2001).
175. Donlan, R. M. *et al.* Monochloramine disinfection of biofilm-associated. *Legionella* 406–410 (2002).
176. Biosurface Technologies Corporation. CDC Biofilm Reactor - BioSurface Technologies Corporation. <https://biofilms.biz/products/biofilm-reactors/cdc-biofilm-reactor/>.
177. Garo, E. *et al.* Asiatic acid and corosolic acid enhance the susceptibility of *Pseudomonas aeruginosa* biofilms to tobramycin. *Antimicrob. Agents Chemother.* **51**, 1813–1817 (2007).
178. Donlan, R. M. *et al.* Model system for growing and quantifying *Streptococcus pneumoniae* biofilms *in situ* and in real time. *Appl. Environ. Microbiol.* **70**, 4980–4988 (2004).
179. Buckingham-Meyer, K., Goeres, D. M. & Hamilton, M. A. Comparative evaluation of biofilm disinfectant efficacy tests. *J. Microbiol. Methods* **70**, 236–244 (2007).

180. Parra-Ruiz, J., Vidailiac, C., Rose, W. E. & Rybak, M. J. Activities of high-dose daptomycin, vancomycin, and moxifloxacin alone or in combination with clarithromycin or rifampin in a novel in vitro model of *Staphylococcus aureus* biofilm. *Antimicrob. Agents Chemother.* **54**, 4329–4334 (2010).
181. Jin, Y. *et al.* The use of new probes and stains for improved assessment of cell viability and extracellular polymeric substances in *Candida albicans* biofilms. *Mycopathologia* **159**, 353–360 (2005).
182. Goeres, D. M. *et al.* Statistical assessment of a laboratory method for growing biofilms. *Microbiology* **151**, 757–762 (2005).
183. Brooks, T. & Keevil, C. W. A simple artificial urine for the growth of urinary pathogens. *Lett. Appl. Microbiol.* **24**, 203–206 (1997).
184. Liang, P. *et al.* The aerobic respiratory chain of *Pseudomonas aeruginosa* cultured in artificial urine media: Role of NQR and terminal oxidases. *PLoS One* **15**, 1–20 (2020).
185. Miles, A. A., Misra, S. S. & Irwin, J. O. The estimation of the bactericidal power of the blood. *J. Hyg. (Lond)*. **38**, 732–749 (1938).
186. Merritt, J. H., Kadouri, D. E. & O'Toole, G. A. Growing and analyzing static biofilms. *Curr. Protoc. Microbiol.* **Chapter 1**, (2011).
187. Higgins, P. G., Dammhayn, C., Hackel, M. & Seifert, H. Global spread of carbapenem-resistant *Acinetobacter baumannii*. *J. Antimicrob. Chemother.* **65**, 233–238 (2009).
188. Smith, C. A. *et al.* Structural basis for carbapenemase activity of the OXA-23  $\beta$ -Lactamase from *Acinetobacter baumannii*. *Chem. Biol.* **20**, 1107–1115 (2013).
189. El-Gamal, M. I. *et al.* Recent updates of carbapenem antibiotics. *Eur. J. Med. Chem.* **131**, 185–195 (2017).
190. Papp-Wallace, K. M., Endimiani, A., Taracila, M. A. & Bonomo, R. A. Carbapenems: Past, present, and future. *Antimicrob. Agents Chemother.* **55**, 4943–4960 (2011).
191. El-Shazly, S., Dashti, A., Vali, L., Bolaris, M. & Ibrahim, A. S. Molecular epidemiology and characterization of multiple drug-resistant (MDR) clinical isolates of *Acinetobacter baumannii*. *Int. J. Infect. Dis.* **41**, 42–49 (2015).
192. Evans, B. A. & Amyes, S. G. B. OXA  $\beta$ -lactamases. *Clin. Microbiol. Rev.* **27**, 241–263 (2014).
193. Tehrani, S., Saffarfar, V., Hashemi, A. & Abolghasemi, S. A survey of genotype and resistance patterns of ventilator-associated pneumonia organisms in ICU patients. *Tanaffos* **18**, 215–222 (2019).
194. Rezaei, A., Fazeli, H., Moghadampour, M., Halaji, M. & Faghri, J. Determination

- of antibiotic resistance pattern and prevalence of OXA-type carbapenemases among *Acinetobacter baumannii* clinical isolates from inpatients in Isfahan, central Iran. *Le Infez. Med.* **1**, 61–66 (2018).
195. Wang, C., Wang, B. & Li, B. Bioavailability of peptides from casein hydrolysate *in vitro*: Amino acid compositions of peptides affect the antioxidant efficacy and resistance to intestinal peptidases. *Food Res. Int.* **81**, 188–196 (2016).
  196. American Type Culture Collection. ATCC® 17978™ | *Acinetobacter baumannii* | ATCC Genome Portal. <https://genomes.atcc.org/genomes/e1d18ea4273549a0?tab=overview-tab>.
  197. Tafreshi, N., Babaeekhou, L. & Ghane, M. Antibiotic resistance pattern of *Acinetobacter baumannii* from burns patients: Increase in prevalence of *bla*<sub>oxa-24-like</sub> and *bla*<sub>oxa-58-like</sub> genes. *Iran. J. Microbiol.* **11**, 502–509 (2019).
  198. Azizi, O., Shakibaie, M. R., Modarresi, F. & Shahcheraghi, F. Molecular detection of class-D OXA carbapenemase genes in biofilm and non-biofilm forming clinical isolates of *Acinetobacter baumannii*. *Jundishapur J. Microbiol.* **8**, 1–6 (2015).
  199. Kappaun, K., Piovesan, A. R., Carlini, C. R. & Ligabue-Braun, R. Ureases: Historical aspects, catalytic, and non-catalytic properties – A review. *J. Adv. Res.* **13**, 3–17 (2018).
  200. Zweiker, D. *et al.* Semi-permanent skin staining associated with silver-coated wound dressing Acticoat®. *Ann. Burns Fire Disasters* **27**, 197–200 (2014).
  201. Getinge AB. Intergard Silver. <https://www.getinge.com/int/product-catalog/intergard-silver/> (2019).
  202. Ignasiak, K. & Maxwell, A. *Galleria mellonella* (greater wax moth) larvae as a model for antibiotic susceptibility testing and acute toxicity trials. *BMC Res. Notes* **10**, 1–8 (2017).
  203. Frankel, G. & Schroeder, G. N. *The Galleria mellonella infection Model for Investigating the Molecular Mechanisms of Legionella Virulence. Methods in Molecular Biology vol. 1921* (Humana Press, 2019).
  204. Brennan, M., Thomas, D. Y., Whiteway, M. & Kavanagh, K. Correlation between virulence of *Candida albicans* mutants in mice and *Galleria mellonella* larvae. *FEMS Immunol. Med. Microbiol.* **34**, 153–157 (2002).
  205. Wojda, I. Immunity of the greater wax moth *Galleria mellonella*. *Insect Sci.* **24**, 342–357 (2017).
  206. Cook, S. M. & McArthur, J. D. Developing *Galleria mellonella* as a model host for human pathogens. *Virulence* **4**, 350–353 (2013).
  207. Hernandez, R. J. *et al.* Using the wax moth larva *Galleria mellonella* infection model to detect emerging bacterial pathogens. *PeerJ* **6**, e6150 (2019).

208. Cruz, L. I. B. *et al.* Anti-*Candida albicans* activity of thiazolyhydrazone derivatives in invertebrate and murine models. *J. Fungi* **4**, 1–14 (2018).
209. Lazarini, J. G. *et al.* Bioprospection of *Eugenia brasiliensis*, a Brazilian native fruit, as a source of anti-inflammatory and antibiofilm compounds. *Biomed. Pharmacother.* **102**, 132–139 (2018).
210. Aneja, B. *et al.* Natural Product-Based 1,2,3-Triazole/Sulfonate Analogues as Potential Chemotherapeutic Agents for Bacterial Infections. *ACS Omega* **3**, 6912–6930 (2018).
211. Dolan, N. *et al.* Synthesis, antibacterial and anti-MRSA activity, in vivo toxicity and a structure-activity relationship study of a quinoline thiourea. *Bioorganic Med. Chem. Lett.* **26**, 630–635 (2016).
212. Maguire, R., Duggan, O. & Kavanagh, K. Evaluation of *Galleria mellonella* larvae as an in vivo model for assessing the relative toxicity of food preservative agents. *Cell Biol. Toxicol.* **32**, 209–216 (2016).
213. Dubovskiy, I. M. *et al.* More than a colour change: Insect melanism, disease resistance and fecundity. *Proc. R. Soc. B Biol. Sci.* **280**, (2013).
214. Li, D. *et al.* Insect hemolymph clotting: Evidence for interaction between the coagulation system and the prophenoloxidase activating cascade. *Insect Biochem. Mol. Biol.* **32**, 919–928 (2002).
215. Peetsch, A. *et al.* Silver-doped calcium phosphate nanoparticles: Synthesis, characterization, and toxic effects toward mammalian and prokaryotic cells. *Colloids Surfaces B Biointerfaces* **102**, 724–729 (2013).
216. Zhang, F. *et al.* Degradable polyphosphoester-based silver-loaded nanoparticles as therapeutics for bacterial lung infections. *Nanoscale* **7**, 2265–2270 (2015).
217. Oates, A., Lindsay, S., Mistry, H., Ortega, F. & McBain, A. J. Modelling antisepsis using defined populations of facultative and anaerobic wound pathogens grown in a basally perfused biofilm model. *Biofouling* **34**, 507–518 (2018).
218. Shah, K. N. *et al.* N-Acetyl cysteine abrogates silver-induced reactive oxygen species in human cells without altering silver-based antimicrobial activity. *Toxicol. Lett.* **332**, 118–129 (2020).
219. Jeanmonod, P. *et al.* Silver acetate coating promotes early vascularization of Dacron vascular grafts without inducing host tissue inflammation. *J. Vasc. Surg.* **58**, 1637–1643 (2013).
220. Leaper, D., Ayello, E. A., Carville, K., Fletcher, J. & Keast, D. H. Appropriate Use of Silver. *Wounds Int.* 2–24 (2012).
221. National Institute for Health and Care Excellence. Silver dressings. (2020).
222. The European Committee on Antimicrobial Susceptibility Testing. Breakpoint

- tables for interpretation of MICs and zone diameters, version 9.0. (2019).
223. Muller, M. Bacterial Silver Resistance Gained by Cooperative Interspecies Redox Behavior. *Antimicrob. Agents Chemother.* **62**, 1–10 (2018).
  224. National Institute for Health and Care Excellence. *Urinary tract infection (lower): antimicrobial prescribing*. Nice (2018).
  225. Thomaz, L. *et al.* In vivo Activity of Silver Nanoparticles Against *Pseudomonas aeruginosa* Infection in *Galleria mellonella*. *Front. Microbiol.* **11**, (2020).
  226. Longo, F., Vuotto, C. & Donelli, G. Biofilm formation in *Acinetobacter baumannii*. *New Microbiol.* **37**, 119–127 (2014).
  227. Lo, E. *et al.* Strategies to Prevent Catheter-Associated Urinary Tract Infections in Acute Care Hospitals: 2014 Update. *Infect. Control Hosp. Epidemiol.* **35**, 464–479 (2014).
  228. Donlan, R. M. Biofilms and device-associated infections. *Emerg. Infect. Dis.* **7**, 277–281 (2001).
  229. Ding, R., Li, X., Zhang, X., Zhang, Z. & Ma, X. The Epidemiology of Symptomatic Catheter-associated Urinary Tract Infections in the Intensive Care Unit: A 4-year Single Centre Retrospective Study. *Urol. J.* **16**, 312–317 (2019).
  230. Duszynska, W. *et al.* Device associated –health care associated infections monitoring, prevention and cost assessment at intensive care unit of University Hospital in Poland (2015–2017). *BMC Infect. Dis.* **20**, 1–10 (2020).
  231. Barford, J. M. T., Anson, K., Hu, Y. & Coates, A. R. M. A model of catheter-associated urinary tract infection initiated by bacterial contamination of the catheter tip. *BJU Int.* **102**, 67–74 (2008).
  232. Jordan, R. P., Malic, S., Waters, M. G., Stickler, D. J. & Williams, D. W. Development of an antimicrobial urinary catheter to inhibit urinary catheter encrustation. *Microbiol. Discov.* **3**, 1 (2015).
  233. Nzakizwanayo, J., Pelling, H., Milo, S. & Jones, B. . An *in vitro* bladder model for studying catheter-associated urinary tract infection and associated analysis of Biofilms. in *Proteus Mirabilis* (ed. Pearson, M.) 139–158 (Humana Press, 2019).
  234. Goeres, D. M. & Montana State University. Standardized Biofilm Methods Training Videos - Center for Biofilm Engineering | <https://biofilm.montana.edu/standardized-biofilm-methods-training-videos.html>.
  235. Fan, S. *et al.* Sex-associated differences in baseline urinary metabolites of healthy adults. *Sci. Rep.* **8**, 1–11 (2018).
  236. Rose, C., Parker, A., Jefferson, B. & Cartmell, E. The Characterization of Feces and Urine: A Review of the Literature to Inform Advanced Treatment Technology. *Crit. Rev. Environ. Sci. Technol.* **45**, 1827–1879 (2015).

237. Bankir, L., Perucca, J. & Weinberger, M. H. Ethnic differences in urine concentration: Possible relationship to blood pressure. *Clin. J. Am. Soc. Nephrol.* **2**, 304–312 (2007).
238. Shearman, E. J. On the Changes in the Urine Effected by Disease; and the Tests to Distinguish them. *Prov. Med. Surg. J.* **9**, 333–338 (1845).
239. Sabir, N. *et al.* Bacterial biofilm-based catheter-associated urinary tract infections: Causative pathogens and antibiotic resistance. *Am. J. Infect. Control* **45**, 1101–1105 (2017).